

THESIS FOR THE DEGREE OF DOCTOR OF PHILOSOPHY

Power Quality Disturbances and Protective Relays

Component Switching and Frequency Deviation

by

Fan Wang



Department of Electric Power Engineering

Chalmers University of Technology

Göteborg, Sweden

2003

Power Quality Disturbances and Protective Relays
— Component Switching and Frequency Deviation

Fan Wang
ISBN 91-7291-324-X

Copyright © Fan Wang, 2003
All rights reserved

Doktorsavhandlingar vid Chalmers tekniska högskola
Ny serie nr 2006
ISSN 0346-718X

School of Electrical Engineering
Chalmers University of Technology
Technical Report No. 457
ISSN 1651-498X

CHALMERS UNIVERSITY OF TECHNOLOGY

Department of Electric Power Engineering

S-412 96 Göteborg, Sweden

Telephone: +46 (0) 31 – 772 1660

Facsimile: +46 (0) 31 – 772 1633

Chalmers Bibliotek, Reproservice
Göteborg, 2003

博士學位論文

電能質量擾動與保護繼電器

元件投切及頻率偏差

王凡



查爾默斯理工大學 電力工程系

瑞典 哥德堡

二〇〇三

Abstract

This thesis combines knowledge from two areas: power quality and power system protection. Power quality concerns the effect of voltage disturbances on end-user equipment and of current disturbances on network components. Power system protection concerns the detection of faults in the system from measured voltages and currents. However, non-fault voltage and current disturbances may lead to the inadvertent detection of a fault in the same way as voltage disturbances may lead to the tripping of end-user equipment.

The aim of the research presented in this thesis is to quantify non-fault voltage and current disturbances at the terminals of protective relays; in other words: to define power quality from the viewpoint of a protective relay.

Starting from the principles (algorithms) of the relays, a quantification approach is developed to assess the disturbance impact on the relays. The quantification is based on the relay response after processing the disturbance signals by relay filters. This makes it possible to quantify the disturbance impact by the consequences caused by the disturbances, other than by the signal waveforms of the disturbances.

For component switching disturbances, the so-called “impact severity curve” is developed to quantify the disturbance impact on a relay. It is a measure of the potential risks that a relay faces in case of a particular power system disturbance. It also facilitates the relative comparison among different disturbance cases. For frequency deviation disturbances, the resulting errors in relay outputs are estimated, which is helpful in determining whether an accurate frequency measurement is needed.

The proposed approach in the project can be applied in testing the disturbance immunity of any future fast relay algorithm. The test results, which are in the form of impact severity curves, can be adopted as the basis of disturbance classification in the viewpoint of protective relays and further lead to the setup of immunity test database.

Keywords: power quality, power system disturbance, digital protective relays, protection algorithms, component switching, frequency deviation, overcurrent relays, impedance relays.

Acknowledgement

I hereby express my deepest gratitude to my supervisor and examiner, Professor Math H. J. Bollen, for his constructive guidance, valuable comments and inspiring advice during my research work in this project. I have benefited a lot from not only the fruitful discussions with him, but also his insight into the research direction and his creative thinking in simplifying complicated problems.

Energimyndigheten, Elforsk and ABB Automation Products are acknowledged for funding this project. I would like to sincerely thank all my steering group members, Murari Mohan Saha (ABB Automation Products), Helge Seljeseth (SINTEF Energy Research, Norway), Christian Roxenius (Göteborg Energi Nät AB) and Robert Olofsson (Unipower AB), for their valuable suggestions on my research work throughout the duration of this project.

Special thanks to SINTEF Energy Research, Göteborg Energi Nät AB, Scottish Power and STRI, for providing large amount of field measurement data, which are crucial in this project. I am also much grateful to Gunilla le Dous from Göteborg Energi Nät AB for providing equipment data, which are vital in simulating the operation of practical power system.

I would like to sincerely thank Dr. Philip Moore at University of Bath for his guidance and help when I had the short-term overseas study there. Many thanks to Dr. Miles Redfern for the valuable technical discussions. Also thanks to Mr. Brian Ross for his help in running relay testing experiment, and Mrs. Jacqui Matthews for her help in fixing the administrative procedures for my visit at Bath.

Thanks to Martin Adiels at the Department of Mathematics, for providing consultation that verifies my mathematic deductions in this thesis.

Many thanks to all the present and former staff and colleagues at the Department of Electric Power Engineering, who are always willing to help, for creating a pleasant working atmosphere that helped me carry out my research smoothly.

I am greatly indebted to my family and especially my parents and my wife Ying, for all the love, understanding, care and selfless support.

Finally, I wish to thank all the others, who in one way or the other, have contributed to the successful completion of this project.

List of Relevant Publications

This thesis is based on work contained in the following technical papers.

Publications since the conferment of the Degree of Licentiate of Engineering

- I **F. Wang, M. H. J. Bollen**, "Frequency response characteristics and error estimation in RMS measurement", accepted for publication in *IEEE Transactions on Power Delivery*, in print
- II **F. Wang, M. H. J. Bollen**, "Quantification of transient current signals in the viewpoint of overcurrent relays", *Proceedings of IEEE PES Annual Meeting 2003*, July 2003, Toronto, Canada
- III **F. Wang, M. H. J. Bollen**, "Classification of component switching transients in the viewpoint of protective relays", *Electric Power Systems Research*, Vol. 64, Issue 3, pp. 197-207, March 2003.
- IV **F. Wang, M. H. J. Bollen**, "Simulating the propagation of power system voltage events", *Proceedings of Nordic and Baltic Workshop on Power Systems*, February 2002, Tampere, Finland
- V **F. Wang, M. H. J. Bollen** and **P. J. Moore**, "Impact of transmission line switching transients on digital impedance relays and evaluation of relay algorithms", in communication with Dr. P. J. Moore at Dept of Electronic and Electrical Engineering, University of Bath, UK

Publications up to the conferment of the Degree of Licentiate of Engineering

- VI **F. Wang, M. H. J. Bollen**, "Quantifying the potential impacts of disturbances on power system protection", *Proceedings of the Seventh International Conference on Developments in Power System Protection*, pp. 262-265, April 2001, Amsterdam, Netherlands
- VII **F. Wang, M. H. J. Bollen**, "Disturbance database setup for protective relay testing", *Proceedings of 9th International Conference on Harmonics and Quality of Power (ICHQP)*, Vol. 3, pp. 1059-1064, 2000, Orlando, USA

- VIII **F. Wang, M. H. J. Bollen**, “Measurement of 182 Hz interharmonics and their impact on relay operation”, *Proceedings of 9th International Conference on Harmonics and Quality of Power (ICHQP)*, Vol. 1, pp. 55-60, 2000, Orlando, USA
- IX **F. Wang, M. H. J. Bollen**, “Evaluating the effect of measured power disturbances on protective relay operation”, *Proceeding of International Conference on Electric Utility Deregulation and Restructuring, and Power Technologies 2000 (DRPT 2000)*, pp. 232-237, 2000, London, UK

Table of Contents

Abstract		I
Acknowledgement		II
List of Relevant Publications		III
Table of Contents		V
Chapter1	Introduction	1
1.1	Background of the project	3
1.2	Objective of the project	4
1.3	Chapter outline	5
Chapter 2	Structure of the Study	8
2.1	Disturbance types studied in this thesis	8
2.1.1	Steady-state disturbances	8
2.1.2	Transient disturbances	9
2.1.3	Impact of disturbances on relay operation	11
2.2	Research work done in the areas	13
2.2.1	Impact of harmonics on protective relays	13
2.2.2	Impact of frequency deviation on protective relays	15
2.2.3	Impact of component switching on protective relays	17
2.3	Relay types studied in this thesis	19
2.4	Protection types studied in this thesis	20
2.5	Research focus in this thesis	21
2.6	Research procedures in this thesis	22
2.6.1	Principles of impact quantification for steady-state and transient disturbances	22
2.6.2	The new quantification approach step by step	23
2.6.3	Implementation of the new approach for disturbance classification	24
2.6.4	Application of the new approach for disturbance classification	25

Chapter 3	Principles of Digital Relays in Power Systems	26
3.1	Structure of digital relays	26
3.2	Digital algorithms for single-input relays	29
3.2.1	Discrete Fourier algorithm (DFT)	29
3.2.2	Least Square algorithm (LS)	32
3.2.3	Root Mean Square algorithm (RMS)	34
3.2.4	Walsh algorithm	34
3.2.5	Kalman algorithm	37
3.2.6	Advantages and disadvantages of the above algorithms	42
3.3	Digital algorithms for dual-input relays	43
3.3.1	Discrete Fourier algorithm (DFT)	43
3.3.2	Differential Equation algorithm (DEA)	44
3.3.3	Traveling wave based algorithm	45
3.3.4	Advantages and disadvantages of the above algorithms	47
3.4	Existing relay algorithms and future fast relay algorithms	49
Chapter 4	Classification of Component Switching Transients	51
4.1	Way to quantify component switching impact	51
4.2	How to test relays under component switchings	53
4.3	Component switching analysis	58
4.3.1	Generator-transformer group switching	59
4.3.2	Unloaded transmission line/cable switching	59
4.3.3	Transformer switching (with/without load)	60
4.3.4	Shunt capacitor/inductor switching	60
4.3.5	Tap-changer operation	61
4.4	Detection of switching sources	63
4.5	Quantification of component switchings	68
4.5.1	Overcurrent relays	69
4.5.2	Impedance relays	72
Chapter 5	Impact of Component Switching on Overcurrent Relays	75
5.1	Operation principles of overcurrent relays	76
5.1.1	Definite-time-delayed overcurrent relays	76
5.1.2	Inverse-time-delayed overcurrent relays	77
5.1.3	Thermal overcurrent relays	79
5.2	Determination of the constants for different types of overcurrent relay	80
5.3	Impact severity curve	83
5.3.1	Current after relay filtering	83
5.3.2	Impact severity curve — way to interpret the processed current	84

5.4	Case studies of impact severity curves	90
Chapter 6	Impact of Component Switching on Impedance Relays	100
6.1	Component switching at transmission level	100
6.2	Impedance relay operation principles	101
6.3	Analysis of switching transients for unloaded transmission lines	108
6.4	Impact of switching transients on impedance relays	111
6.5	Simulation test of switching transients on impedance relays	112
6.6	Impact severity curve	116
6.7	Case studies of impact severity curve	122
Chapter 7	Impact of Frequency Deviation on RMS-based Relays	125
7.1	RMS expression in general form	125
7.2	RMS output for an arbitrary signal	127
7.3	Frequency response for single frequency signals	129
7.3.1	Impact of sampling rate on RMS output	132
7.3.2	Impact of point-on-wave on RMS output	136
7.3.3	Impact of sampling window size on RMS output	137
7.4	RMS output error for single frequency signals	139
7.5	Frequency response for mixed frequency signals	140
7.5.1	Impact of sampling rate on total RMS output	141
7.5.2	Impact of point-on-wave on total RMS output	142
7.5.3	Impact of sampling window size on total RMS output	142
7.6	RMS output error for mixed frequency signals	147
7.7	RMS error of single frequency signals due to frequency deviation	150
7.8	RMS error of mixed frequency signals due to frequency deviation	152
Chapter 8	Impact of Frequency Deviation on DFT/DEA-based Relays	155
8.1	Response of DFT for overcurrent relays in case of frequency deviation	155
8.2	Response of DFT for impedance relays in case of frequency deviation	159
8.3	Response of DEA for impedance relays in case of frequency deviation	165

Chapter 9	Conclusions and Future Work	166
9.1	Main contributions in this work	166
9.2	Summary of conclusions in this work	167
9.3	Directions for future research	171
References		173

Chapter 1 Introduction

Power system disturbances are, in the sense of source, the result of switching or operation of power system components; or in the sense of measurement, the transient or steady-state distortion in the waveforms of power system voltage and current; or in the sense of impact on power systems, the disturbances that degrade the performance of device, equipment or system. The presence of power system disturbances reflects the power quality in a system.

The term power quality was first introduced in late 1960's [1][2][3], almost a century after the first power system was put in service. It became in common use twenty years later. Before that time, it did not attract too much attention mainly because of two reasons. One is that in the past there were much fewer power system components that could generate power system disturbances. The other is that in the past there were much fewer power system components that were sensitive to power system disturbances. Obviously these two factors are mutually linked [4].

With the development in electronics technology, more and more power system components are equipped with electronic devices. The introduction of electronic devices enables much more flexibility for system and component operation, regulation and protection. While the improvement on the functions is enormous, its side effect is also inevitable: the presence of electronic device in the systems, together with the flexible component operation mode brought by electronic device, will lead to both transient and steady-state problems in power systems. Such power quality disturbances not only exist

locally, but also propagate to other parts of the power system. On the other hand the electronic device itself is much more vulnerable to such power quality disturbances than the classical power system components. In a word, the main source of power quality disturbances today is the application of electronic technology as well as the change of operation mode benefiting from the application of such techniques.

Of course the benefits from applying electronic techniques are huge when compared with its side effect. What one can do is to reduce the side effect. With the trend of deregulation of power market, more attention has been paid on the power system disturbances because:

- In a deregulated market, anything that might affect the normal operation of power systems or their components can be, in one way or the other, directly expressed as economic losses. So power system disturbance becomes an important issue.
- In a deregulated market, the agreement between the utilities and customers is to ensure normal operation and reduce the effects of power system disturbances. Such an agreement depends on the definition of the responsibilities for each party, as each party can be the source of power system disturbances. Also the effects can be due to ill-designed equipment on either side.

There are two ways to deal with power system disturbances, from the viewpoints of utilities and from the viewpoint of customers. What the utilities can do is to locate the source of the disturbances and take necessary measures to limit the severity and occurrence frequency of such disturbances, so as to ensure the stable and safe operation of power systems. For the customers, it is necessary to study the impact of power system disturbances on the

equipment. Applying a particular device or control mode may migrate such disturbance effect. Generally speaking, system stability and component performance are the main issues to be studied whenever there are power system disturbances.

Whatever the sources are, power system disturbances are, according to the “observation” by the system and by end-user equipment, the transient and steady state distortion in voltage and current waveforms. Therefore study of the disturbance impact should start from analysis of voltage and current waveforms during power system disturbances.

1.1 Background of the project

Power system disturbances are of various types related to their different sources. Disturbances can be due to steady-state load currents, dynamic operations as well as faults. The components that suffer from such disturbances are also of various types. Among the affected components, the protective relay is an important device for the safe and reliable operation of power systems.

Protective relays play no role when the operation of power systems is stable and normal. They are designed to operate when there are faults involved in the systems. The direct consequence of relay operation is system component cutoff, which definitely affect the operation of the system. Therefore either a fail-to-trip or a mal-trip can lead to considerable economic losses. In the former case, a fail-to-trip makes the fault-involved components remain at critical conditions too long, damaging the components either in short-term or in long-term. In the latter case, a mal-trip cuts off components that are under healthy operation, possibly causing direct economic losses to customers.

Therefore two characteristics are important for protective relays: sensibility (or dependability in a more formal way) when there is a fault, and immunity (or security in a more formal way) when there is anything other than faults. The former tells how reliable a relay is when it should operate, while the latter tells how robust a relay is when it should not operate.

In this sense, protective relays should not react to any power system disturbance. However, most protective relays are designed to deal with the situation when the voltage and current signals are steady-state sinusoidal waveforms. In case of power system disturbances, whether protective relays will experience a mal-trip is dependent on the type of the disturbance as well as the structure of the relay. Although some new generation relays possess ability to be adaptive to some of the external changes, this cannot guarantee complete immunity from the disturbances because the disturbance conditions are far more than one can expect. Also with the possible higher requirement on fault-clearing time in the future, faster relays will be needed. A faster relay means a shorter decision-making time, which implies a higher possibility of mal-trip due to inadequate information obtained by the relay within such short time.

To study the impact of power system disturbances on protective relays, it is necessary to apply some typical disturbances in protective relay testing. The applied disturbances can be either obtained from practical measurements, or from reasonable simulation of practical power system structures and events.

1.2 Objective of the project

The aim of this project is the creation of a set of general procedures for the testing of protection relays under non-fault disturbances. Such procedures

should be applicable to both the relay algorithms that are currently in use as well as possible new algorithms developed in the future. By applying these procedures, a disturbance database can be set up. Such a database will consist mainly of voltages and currents recorded in the power system during actual disturbances.

Simply speaking, the disturbance data are obtained at the user-terminal in the viewpoint of relays, and then ranked and designated for different applications in the future.

The project is divided into two stages. In the first stage, the power system disturbances are classified based on their characteristic values such as peak value and duration. The first stage includes discussions on the possible way of disturbance quantification in the viewpoints of both relay manufacturers and customers. The study results are presented in author's thesis for Licentiate of engineering degree [5]. The second stage focuses on the analysis of relay algorithms as well as quantification of typical power system disturbances for different relay algorithms. The results of the second stage are the main contents in this thesis.

1.3 Chapter outline

Chapter 2 introduces the main structure of study in this thesis. Power system disturbances are treated as two types: steady state disturbances and transient disturbances. Research results obtained by others in this field are introduced. The study focus in this thesis is proposed. Also the research procedures used are briefly summarized.

Chapter 3 discusses in detail the principles of solid-state and digital relays as well as their algorithms. The main algorithms that have commercial application are introduced and both their advantages and disadvantages are described.

A general evaluation of transient disturbance impact on relay algorithms is made in Chapter 4. The focus of the study is on transients due to component switching. Detailed analysis of component switching transients is made. The way to quantify switching severity in the viewpoints of both overcurrent and impedance relays is proposed. Based on the quantification technique it is possible to structure transient disturbance database for switching impact assessment.

Impact assessment of component switching on overcurrent relays is discussed in Chapter 5. The concept of “impact severity curve” is developed to demonstrate the relative impact severity for different disturbances on identical overcurrent relays.

Impact assessment of unloaded line switching on impedance relays is discussed in Chapter 6. Theoretical analysis of unloaded line switching is presented. Simulation results in various case studies are illustrated. Impact severity of mal-trip by impedance relays due to unloaded line switching is evaluated.

Chapter 7 studies the impact on RMS-based relay algorithm by a typical steady state disturbance — frequency deviation. RMS frequency characteristics are deducted for both single frequency and mixed frequency signals. The errors in RMS response in different conditions are estimated

mathematically. The impact on RMS output due to frequency deviation is assessed.

Chapter 8 studies the impact on Fourier and DEA relay algorithms by frequency deviation. The frequency response for Fourier algorithm is demonstrated for the cases of both single-element relay algorithm and two-element relay algorithm. The output error of Fourier algorithm due to frequency deviation is estimated mathematically. The impact of frequency deviation on DEA algorithm is discussed.

Chapter 9 gives the summary and generalization of the work implemented in this project. The main contribution of the author in this project is highlighted. The direction and prospects of further research work are presented and discussed.

Chapter 2 Structure of the Study

In the sense of detrimental impact on protective relays, power system disturbances can be classified into two main categories: steady-state disturbances and transient disturbances. The impact on protective relays can be described as two types of mal-function: fail-to-trip and mal-trip, which correspond to the two factors of relay reliability: dependability and security [6]. According to the definition of disturbance in Chapter 1, the relay mal-function that might be caused by such phenomena is relay mal-trip. The main emphasis of this thesis is on relay mal-trip immunity from disturbances.

2.1 Disturbance types studied in this thesis

2.1.1 Steady-state disturbances

The main steady-state disturbances that can affect the performance of protective relays are harmonics and frequency deviation. The former results in distortion of the voltage or current waveform while the latter causes a variation in their period.

Harmonics are a consequence of the presence of non-linear loads in power systems. The nonlinearity of such loads makes the waveforms of voltage and current distorted, thus generating various harmonics. Harmonics may also be interpreted as a way of describing the undesired changes in the waveform by referring the actual signal to the fundamental component of the signal.

Frequency deviation is due to an unbalance between generation and consumption in power systems. Lack of generation in a system will cause a

frequency drop, while a surplus of generation raises the frequency. When the frequency of the fundamental component changes, the harmonics in the system will follow accordingly.

The reason why harmonics and frequency deviation are of concern is that almost all the protective relays are designed to operate under ideal condition, i.e. the measured signal contains pure fundamental component at nominal power frequency. In case of any non-standard situation (i.e. distortion and/or frequency deviation), the reaction to a fault may become slower and the immunity from disturbances may decrease. Practically, harmonics and frequency deviation always exist in any power system. The main points that matter are how severe the harmonics and frequency deviation are and how severely they can affect the performance of protective relays.

2.1.2 Transient disturbances

The main transient disturbances that can affect the performance of protective relays are disturbances due to component switching. Such disturbances are due to the sudden change in steady state waveform in case of switching operations. Compared with long lasting disturbances such as harmonics and frequency deviation, component switching transients are of short duration but the deviation from the ideal waveform is typically larger.

Although component switching is only a short duration disturbance, the relatively high deviations in voltages and currents are a potential threat to the correct operation of protective relays. This transient has the potential to affect not only the end-user equipment at low voltage level [7], but also equally affect the correct operation of protection relays close to the component being switched at any voltage level. Mal-trips are prevented in existing equipment

by using low-pass filters and verification intervals. But this scheme will slow down the generation of a tripping signal in case of a fault. The development of future fast protection will therefore require a thorough study of switching actions and other transients.

The inrush generated by component switching is likely to considerably lessen the safety margin between the threshold and normal operating value. In case of severe component switching, the impact on protective relays is the possible relay mal-trip if the inrush reaches the threshold border.

A general classification of the sources for relay mal-function is shown in Table 2.1:

Table 2.1 Classification of relay mal-function

Mal-function	Source	Type Code	Number of component lost
Fail-to-trip	Self technical failure	I	≥ 1
	Due to voltage/current waveshape (design or setting error)	II	≥ 1
Mal-trip	Self technical failure	III	1
	Due to fault outside protection zone, Current waveshape by CT saturation during faults	IV	> 1
	Due to non-fault event (switching etc.)	V	1

In a transmission system, fail-to-trip may or may not lead to loss of more primary components than needed, depending on whether the fault is finally cleared by remote back-up protection, or just by local back-up protection. A mal-trip will always lead to loss of at least one component in the system. In such a viewpoint, a mal-trip results in more severe damage to the system than a fail-to-trip does. But when a fail-to-trip leads to tripping of the remote backup this constitutes the loss of at least two components. In transmission

systems this greatly endangers the operation of the system. The same holds for a mal-trip due to a fault elsewhere.

To deal with a fail-to-trip, a redundant protection is applied. This means that two sets of protection relays, preferable of different operation principles, are installed. The existence of two sets of protective relays generates overlapped protection and normally effectively avoids a fail-to-trip. On the other hand, the case of mal-trip is somewhat more complicated because a single mal-trip is enough to break the security of a system. The solution to mal-trips is dependent on many factors, but mainly the immunity of protective relays against the impact of any non-fault transients.

A 2-out-of-3 protection system (i.e. the operation of at least 2 out of 3 protective relays is needed to confirm a fault) can reduce both risks mentioned above. But in this case it means the protection system will be 50% more expensive.

Table 2.1 summarizes the mal-function phenomena for a protective relay. In the mal-function phenomena, types I and III are independent of any event. It is only the internal structure of a relay that matters. Types II and IV, which are related to fault events, together with type V, which is related to non-fault events, are the main concerns for the study of transient impact on relays.

2.1.3 Impact of disturbances on relay operation

Fig. 2.1.3.1 shows the basics of relay protection operation.

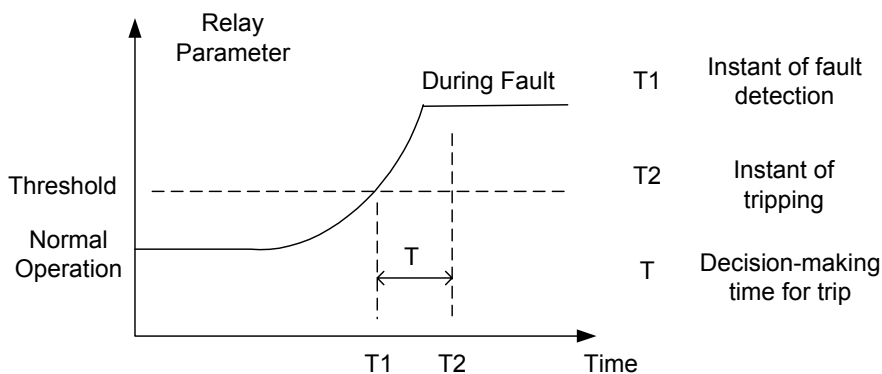


Figure 2.1.3.1 Basics of relay protection operation

Normal non-disturbed operation is based on a certain parameter crossing a threshold. Between the threshold and the normal operation status there is a safety margin, which is introduced to avoid any mal-trip in case of harmonics or overload operation. A relay trip signal is sent out only when the measured value exceeds the threshold and holds for a preset decision-making time T .

The effect of steady-state disturbances is to change the level of the measured parameter value as well as the slope of the transition, as shown in Fig. 2.1.3.2. From the diagram it can be observed that the effect can be in either direction.

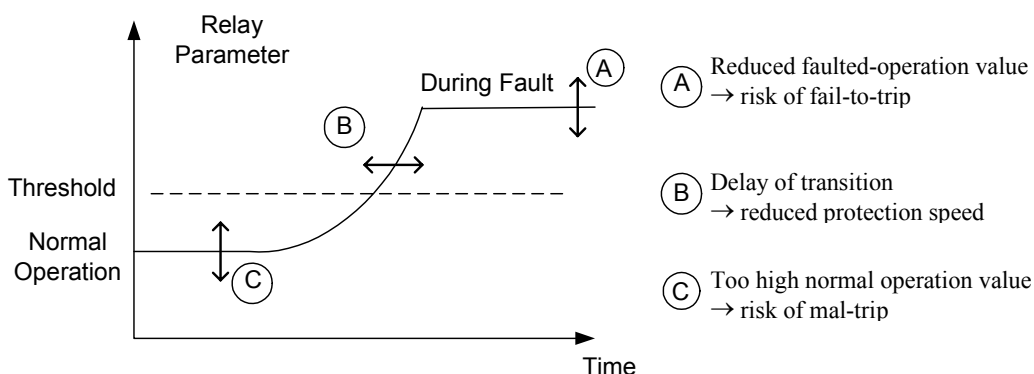


Figure 2.1.3.2 Impact of steady-state disturbances on relay operation

Summary of the effects on relay operation performance is as follows:

1. When the normal operation value is too high due to the presence of steady-state disturbances, there might be a potential risk of mal-trip
2. When the faulted-operation value is reduced due to the presence of steady-state disturbances, there might be a potential risk of fail-to-trip
3. The steady-state disturbances can also affect the transition process when there is a fault. If the transition is delayed, the relay operation speed is reduced.

As explained earlier, the study in this thesis is on the first condition, i.e. the effect of steady-state disturbances on the normal operation value measured by relays.

The effect of transient disturbances can be a temporary increase up to a value above the threshold, as shown in Fig. 2.1.3.3. To avoid mal-trip, either a higher threshold or a longer decision-making time is needed. Either case leads to slower relay operation.

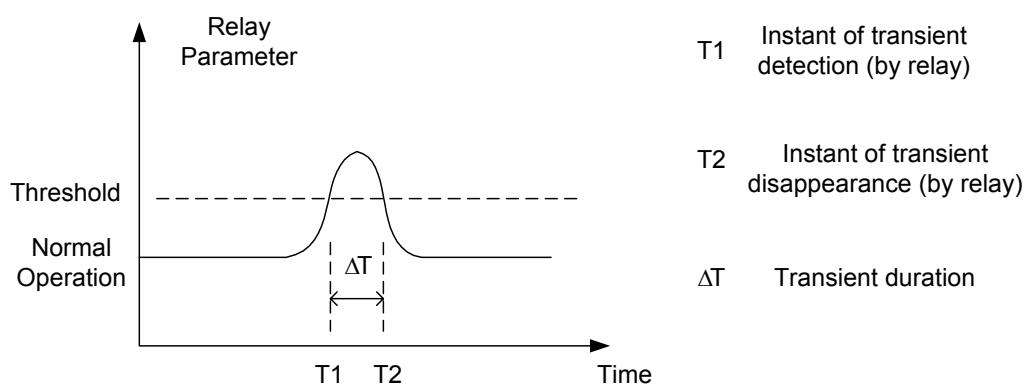


Figure 2.1.3.3 Impact of transient disturbances on relay operation

2.2 Research work done in the areas

2.2.1 Impact of harmonics on protective relays

Lots of work has been done on the impact of harmonics on protective relays. The reason for such a lasting interest in this issue is that the presence of harmonics in either voltages or currents might cause a relay to fail to trip under fault conditions, or cause mal-trip when no fault exists [8] [9].

Among these studies, some focus mainly on the waveform distortion due to the presence of harmonics [10]; some focus on the possible impact of harmonics on different types of protective relays, such as electromechanical [11][12], solid-state [13][14] and digital [15][16] relays; some focus on harmonics impact for particular types of protection [17]. Most of the existing relays use the fundamental component for protection. Harmonic distortion may deteriorate the performance of such a relay. However, some relays are making use of the harmonics for protection purposes [18][19][20].

The main research results reported in literature can be summarized as follows:

- There is obvious detrimental impact of harmonics on electromechanical and solid-state type relays, but little impact on digital type relays if the proper algorithm is selected. The impact is mainly on the relay's dependability in case of faults.
- Although digital type relays have much better immunity from harmonics, electromechanical and solid-state type relays cannot be completely replaced in the foreseen future, due to economic factors as well as different performance requirement on relays at different locations.
- Even for digital type relays, some algorithms do not completely remove all the harmonics.
- The harmonics in currents have more severe impact on protective relays than harmonics in voltages. In most cases, the harmonics in

currents are mainly determined by the characteristics of the attached load, thus being more case dependent.

In general, harmonics will cause deviation in the value of the relay parameter (i.e. the value that is compared with the threshold). harmonics will affect the during-fault performance of some types of relay, especially electromechanical and solid-state relays. However, because of the margin between normal operation values and relay tripping thresholds, the presence of harmonics will normally not lead to mal-trip when there is no fault. But a larger margin means slower fault-clearing and higher risk of a fail-to-trip. To that extend, the (potential) presence of harmonics does deteriorate the relay performance.

Also in practice various types of harmonics filters are installed in power systems to mitigate the harmonic level, both locally and throughout the system. This further reduces the potential threat of harmonics on protective relays in case of non-fault events.

The impact of harmonics on protective relays is not included in the remainder of this thesis.

2.2.2 Impact of frequency deviation on protective relays

The impact of frequency deviation involves mainly mal-trips of digital relays. Although frequency deviation does have detrimental effect on the pickup values of electromechanical and solid-state relays [13], there is little evidence that this can lead to mal-trip for such types of relays. Some work has been done in estimating the impact of frequency deviation on the performance of protective relays [21][22][23]. For some protection types that are based on

accurate frequency value, such as over/under-frequency and over-excitation relays, frequency deviation can have severe consequences. For the other protection types, the main problem that arises is that frequency deviation can shift the frequency response characteristics. This is especially a concern for algorithms based on sampling at fixed pre-set interval. Case studies have shown that this might lead to fluctuation of the relay measurement in time domain [9][21].

To solve this problem, a significant amount of work has been done on how to estimate the correct frequency [24][25][26][27]. Most of the proposed frequency measurement methods are based on finite impulse response techniques, and can yield a sufficiently accurate frequency value under steady state conditions.

The main research results for the impact of frequency deviation can be summarized as follows:

- For single-input digital type relays, the impact of frequency deviation can be estimated by studying the frequency response characteristics of the relay algorithm
- The impact severity of frequency deviation on a digital type relay depends on the algorithm used, as shown in [23], where almost all the popular algorithms are studied except for the RMS algorithm
- For the dual-input digital type relay, the algorithms that are based on Fourier theory, which is the most widely used algorithm in practice, show an error during a fault compared with other state estimation algorithms [9]. However no details are available for the size of this error.
- The frequency measurement techniques developed are for obtaining the frequency value only. In the case of parameters determined by

more than one measurement, approaches remain to be developed for yielding correct results.

As frequency deviation is a phenomenon that happens quite often, it is necessary to have a correct estimation of the possible errors due to it. Large frequency deviations especially occur during emergency states of the system. In such a case it is especially important that the protection operates correctly. Based on the research status mentioned above, the research in this thesis is focused on error estimation due to frequency deviation for RMS algorithm of one-input relays and Fourier algorithm of two-input relays.

2.2.3 Impact of component switching on protective relays

The impact of component switching on protective relays is strongly dependent on the type of relay. For electromechanical relays, component switching transient leads to irregular current flow in the induction windings, thus generating complex torque variations in the relay. For solid-state relays, the conduct and cutoff characteristics of the electronic circuit determine the relay logic output during a switching transient. For digital relays, the principle on which the relay algorithm is based does not hold during the transient process. The result is a large deviation of the value of the relay parameter from its normal-operation value. This may easily lead to fault detection but should not lead to the generation of a tripping signal. The latter will occur when the parameter value exceeds the threshold for longer than the decision-making time.

A lot of work has been done in disclosing the sources and phenomena of component switching transients [28] [29] [30] [31] [32] [33] [34] [35] [36]

[37] [38] [39]. There is even work on how to choose the proper protective relay model for such dynamic variations [40][41].

As for the impact on protective relays by switching transients such as capacitor switching, the deduction of voltage and current transients can be relatively easy, while in the cases of line/cable or transformer switching, the transients are normally available through simulation. Some work has been done in analyzing how to avoid the impact of transformer energizing on protective relays [42][43][44][45][46]. But so far not too much work is done on the impact of component switching on relays in a general sense.

The main research results on the impact of component switching on protective relays can be summarized as follows:

- The inrush peak value, duration as well as harmonics of the component switching transient are available through circuit analysis and simulation
- The component switching transients are dependent on the type of the switched component, the system structure as well as the switching point-on-wave, but mainly on the component type.
- Little work has been done on the impact of component switching transients on protective relays

Therefore in this thesis, research work is carried out to assess the impact of all the main component switchings on the main protective relays used in power systems.

2.3 Relay types studied in this thesis

All the three main types of relay, electromechanical, solid-state and digital relays, are used in practical engineering today. They represent different generations of relay technique development.

In electromechanical relays, the actuating force is created by electromagnetic interaction due to input electrical parameters. These relays contain mechanical parts such as spring, dashpot, induction disc etc. If the torque generated by the input overcomes the torque generated by the pre-stored energy in the spring, the moving part of the relay will act and generate the output signal. Electromechanical relays are in general reliable and have low requirements on operational environment. They are still in wide application today.

However, the shortcomings of these relays are also obvious: problems of maintenance, slow in action, high power consumption for auxiliary mechanisms and worst of all, incapability of implementing complex characteristics. With the advent of integrated circuits and static circuits, a new generation of devices called solid-state relays was developed. Compared with electromechanical relays, solid-state relays are faster, more accurate and can realize more complex functions. They consume much less power and require little maintenance. In practical applications solid-state relays are mainly applied in protection of transmission systems.

But there are some weak points in solid-state relays. Since solid-state relays consist of many electronic components, the overall reliability can be affected by individual components, and these electronic components are sensitive to changes in the ambient temperature. Even worse is that solid-state relays are

vulnerable to voltage transients, which may cause mal-operation. Although various approaches were explored for the amelioration of the situation, the real solution was not available until the early 70's, when computer-based relays achieved a performance at least as good as conventional relays. The relays of this third generation are called "digital relays", "numeric relays", or "microprocessor relays", alternatively.

The main advantages of digital relays over conventional relays are their reliability, functional flexibility, self-checking and somewhat self-adaptability. Digital relays are able to implement more complex functions, be more accurate and be immune from physical environment effects. Although they are relatively costly, the benefits in enhancing system security and reliability by adopting these relays can make their application worthwhile. At present, their application is mainly in transmission system protection as well as for generation unit protection. The rapid growth in computer and communication industries will alleviate their price disadvantage and explore new horizons for their wider application.

In this thesis, digital relays are adopted to study the power disturbance impact on protective devices.

2.4 Protection types studied in this thesis

The types of protection concerned in this thesis are overcurrent and impedance protection, which are the main force in relay protection throughout power systems. Compared with other protection types, these two have the widest application, as they can provide essential protection for almost all the components.

Overcurrent relays are universally used at both transmission and distribution levels. The overcurrent relays can be classified based on their principles into two different types: instantaneous and inverse time overcurrent relays. The former provides fast reaction to a fault, but only within a limited impedance from the fault location. The operation time of the latter is adaptive to the external fault conditions and can have much wider range of protection if longer time delay is permitted.

Impedance relays are mainly used at transmission levels to protect the lines/cables against faults. The types of impedance relays are classified according to their different characteristic shapes, such as Mho or quadrilateral. Compared with overcurrent relays, impedance relays have more complex algorithms, as their operation is based on both voltage and current.

2.5 Research focus in this thesis

Based on the above analysis, the research focus in this thesis can be summarized as follows:

- Disturbance types to be studied
 - frequency deviation
 - component switching
- Relay type (principle) to be studied
 - digital relay
- Protection types to be studied
 - overcurrent protection
 - impedance protection

2.6 Research procedures in this thesis

As describe in Chapter 1, the aim of the study in this thesis is to develop a set of general procedures for testing protective relays in case of non-fault disturbances, for both the relays that are currently in use and those developed in the future. To do so, it is crucial that:

- a. The relay algorithms for the existing protective relays should be studied.
- b. The characteristics of the possible algorithms developed in the future should also be studied.
- c. A proper classification of the disturbances should be proposed.

The principles of the relay algorithms (both overcurrent and impedance protection) that are adopted in practical engineering are discussed in Chapter 3.

A classification in such a case has to be based on quantifying the impact due to the presence of disturbances. Details of such classification are summarized below.

2.6.1 Principles of impact quantification for steady-state and transient disturbances

In case of frequency deviation disturbances, the quantification of the disturbance impact is available by estimating the error caused by per unit frequency deviation. Since the other parameters of a studied signal can be assumed to remain unchanged when there is frequency deviation, and since the frequency response of the relay is available from the relay algorithm, the error due to frequency deviation can be deducted mathematically. Therefore,

the classification in this case can be based on the error estimation, which is mathematically available. Details of such mathematical deduction are available in Chapters 7 and 8.

In the case of component switching disturbances, the quantification of the disturbance impact cannot be treated in the same way as in the case of frequency deviation. This is because the transients caused by component switching are not always predictable. The structure of the system, the reaction of some adaptive control devices to such switching or the operation mode can make the mathematical deduction of transient waveform almost impossible. As a consequence, the quantification in this case becomes more complex and a new approach has to be developed to fix this problem.

In the research presented in this thesis, such a new approach is proposed to quantify the impact of component switching disturbances on protective relays. Unlike the traditional methods that classify the disturbances according to the waveform characteristics (e.g. peak value, decay time constant and duration), the new approach describes these transient disturbances in the viewpoint of protective relays. The disturbance impact is assessed based on the relay responses to the studied transient disturbances, i.e. the potential risk of mal-trip due to the presence of the studied disturbances. Such an approach is proposed in Chapter 4 and further applied in Chapters 5 and 6, where case studies are presented for both overcurrent and impedance relays.

2.6.2 The new quantification approach step by step

Detailed procedures in developing the new quantification approach are presented in Chapter 4. The approach development consists of the following steps:

- a. An overview of all the disturbance phenomena in case of transient (component switching in this case) disturbances. This requires an overall consideration of all the possible operation modes for component switching.
- b. A study of the principal characteristics of the disturbance waveforms. Although these characteristics based on traditional waveform analysis are not enough in precisely describing the disturbance impact, they are helpful in recognizing the type of the studied disturbance, which is needed in the later database setup.
- d. A study of the relay response to the disturbance. The new quantification approach is based on the analysis of such relay response study. The idea is to treat the relay response output in such a way that a characteristic curve can be proposed for quantification purposes. The characteristic curve sets the boundary between mal-trip and normal operation. This is the key part in the new approach. The characteristic curves can be different for overcurrent and impedance relays.

2.6.3 Implementation of the new approach for disturbance classification

The afore-mentioned characteristic curve corresponds to a disturbance of a particular type. In practical engineering, a relay does not necessarily have to survive all the disturbances because its installation location is fixed. Therefore the characteristic curves are developed for different disturbance types independently.

In most cases, the sources of the disturbances are unknown when the disturbances are collected. However, with the help of power quality classification techniques, it is possible to recognize the disturbance type

through analyzing the disturbance signals. Such detailed procedures are described in Chapters 5 and 6.

2.6.4 Application of the new approach for disturbance classification

The application of the new approach can be summarized as in the following two aspects:

- a. Database setup of power system disturbances for the testing of relay/relay algorithm that are currently in use. By applying the proposed new approach for disturbance classification, it is possible to set up databases for different types of disturbances, on conditions that the protective relay algorithm is known. One of the advantages of this database is that it can automatically discard some less severe disturbance data while importing new disturbances of higher impact severity.
- b. Security (mal-trip) comparison among different relay algorithms, especially between the newly proposed fast relay algorithm and the existing algorithms. The newly developed characteristic curve can be used to assess the relative impact severity among different relay algorithms. This is useful in evaluating the security of the new algorithm, which in most cases gains fault detection speed at the cost of detection accuracy.

Discussions concerning the above application aspects are presented in Chapters 5 and 6.

Chapter 3 Principles of Digital Relays in Power Systems

3.1 Structure of digital relays

A digital relay consists of the following main parts:

- Processor
- Analog input system
- Digital output system
- Independent power supply

Fig. 3.1.1 shows the block diagram of a digital relay [47].

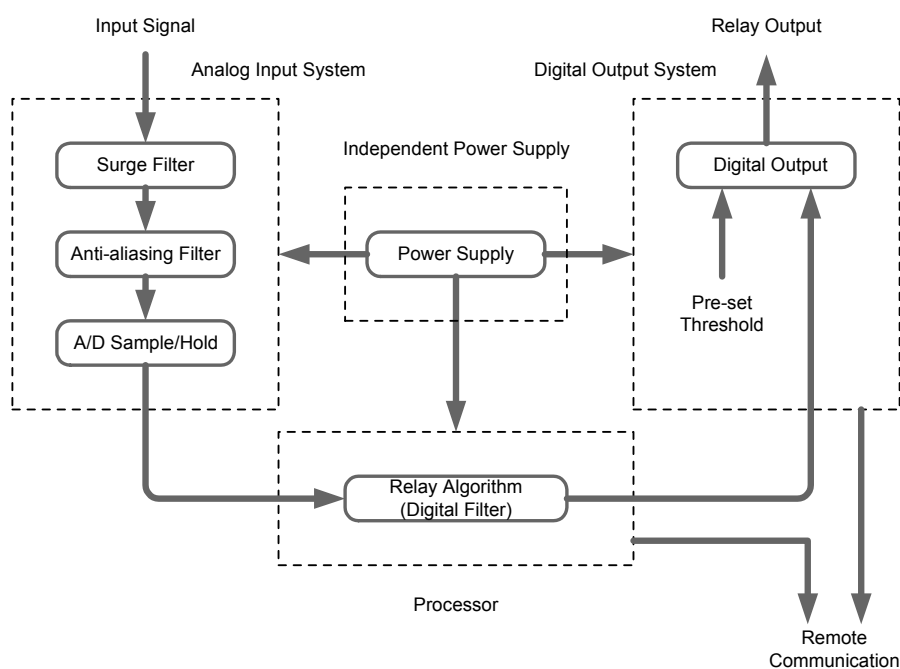


Figure 3.1.1 Block diagram of digital relay

The main difference in principle between digital relays and conventional relays is in the way of input signal processing. The input signals, which come

from CTs or PTs, are always analog signals. They are directly imposed to the electromagnetic winding or electronic circuits in conventional (electro-mechanical and static) relays. In the case of digital relays, the input signals are converted into digital signals before being processed. In the analog input system, a surge filter is used to suppress the large inrush in the input signals, for the safety of the digital relay.

An anti-aliasing filter is used to avoid possible errors in reconstructing the input signal, which is carried out after the A/D Sample/Hold section. According to the Nyquist criterion, any signal sampled at a frequency of $N \cdot f_0$ Hz (with f_0 the power system frequency, 50 or 60 Hz) can exhibit aliasing when reconstructed, if the signal contains harmonic components of order $N \pm 1$, $2N \pm 1$, ..., $xN \pm 1$. An anti-aliasing filter has to cut off all signal components above the Nyquist rate of $N/2$, i.e. the cut-off frequency for anti-aliasing filter should be set not higher than $(N/2) \cdot f_0$ Hz. In practice however, such a filter cannot remove all out of band frequencies, so the cut-off frequency for the anti-aliasing filter is typically set at about $(N/3) \cdot f_0$ Hz.

The A/D sample and hold circuit is adopted to convert the input signal from analog to digital. To scan the whole signal, a data window of limited length is applied to acquire information on part of the signal. Within the section of the signal that is scanned by the data window, a limited number of points of the waveform are sampled. With the window moving forward, more samples are obtained at different snapshots of time. In Fig. 3.1.2, it is illustrated that the input signal is frozen by the data window to achieve simultaneous sampling at each moment, when the oldest sample point is discarded and the newest one is included. These samples are held until the next sampling moment. The sampling window length, number of samples in the window as well as the shape of the sampling window are dependent on the relay algorithm.

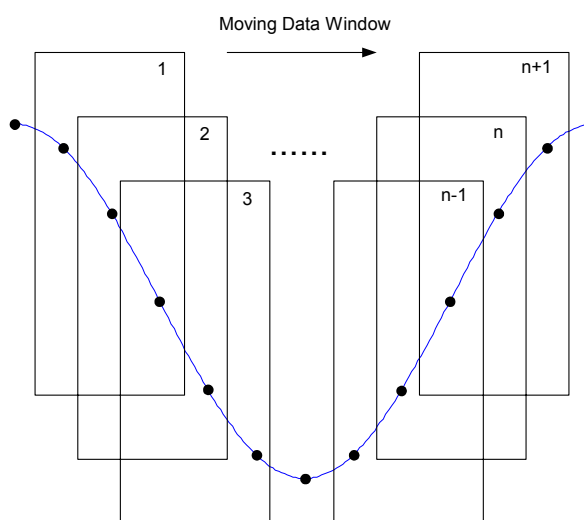


Figure 3.1.2 Data window for sampling

The relay algorithm stored in the processor is the core of the digital relay. It determines the way to reconstruct the input signal based on the digital samples from the A/D converter. As the input signal may contain unwanted components such as harmonics, interharmonics and dc, the algorithm is designed to remove them as much as possible. The algorithm functions as a digital filter to extract the fundamental component of the input signal. The relay operation is carried out based on the fundamental component. With different algorithm principles, the shape of the data window varies. The rectangular window, as shown in Fig. 3.1.2, is only one option. The length of the data window is dependent on the required decision speed of the algorithm and on the required tolerance against disturbances. The number of sampling points in the data window is determined by the sampling frequency.

In digital output system, a detection function is calculated based on the reconstructed signal. Such calculated function is then compared with the pre-set threshold. The decision on whether the relay should operate is made

according to this comparison. Sometimes an additional time delay is needed before the trip signal is sent out.

3.2 Digital algorithms for single-input relays

A “single-input relay” is a relay that operates on only one input signal. Many relays, which have either voltage or current as their inputs, are single-input relays. The philosophy of digital algorithms for such relays is to remove the unwanted components as much as possible so as to extract the fundamental component from the input signals. The fundamental component is then (possibly after further processing) compared with a threshold.

Several algorithms are available for this purpose. The most common ones are Discrete Fourier Transform (DFT), Least Squares (LS), Root Mean Square (RMS), Walsh, and Kalman algorithms.

3.2.1 Discrete Fourier algorithm (DFT)

The main concept of the Fourier algorithm is that any signal can be regarded as a combination of periodic components, provided that it meets the Dirichlet conditions, i.e. finite discontinuous points, limited extremes and limited integration value within any period [48].

The deduction of the Fourier algorithm is based on the following two assumptions:

1. measurement errors have constant covariance and are independent from sample to sample.
2. any dc offset term is eliminated (e.g. by an analog filter or by means of software)

The second requirement is in particular needed for the short-window Fourier algorithms.

The input signal to be sampled can be written as

$$y(t) = \sum_{n=1}^N Y_n s_n(t) + \varepsilon(t) \quad (3.2.1.1)$$

where the coefficients Y_n are unknown while the signals $s_n(t)$ are pre-selected as follows [49]:

$$\left. \begin{aligned} s_1(t) &= \cos(\omega_0 t) \\ s_2(t) &= \sin(\omega_0 t) \end{aligned} \right\} \text{fundamental component}$$

$$\left. \begin{aligned} s_3(t) &= \cos(2\omega_0 t) \\ s_4(t) &= \sin(2\omega_0 t) \end{aligned} \right\} \text{second harmonics}$$

...

$$\left. \begin{aligned} s_{N-1}(t) &= \cos\left(\frac{N}{2}\omega_0 t\right) \\ s_N(t) &= \sin\left(\frac{N}{2}\omega_0 t\right) \end{aligned} \right\} \frac{N}{2} \text{th harmonics}$$

$N/2$ is the highest harmonic order contained in the signal, assuming N is an even number; $\varepsilon(t)$ stands for the noise in the measurement.

The choice of $s_n(t)$ above is in accordance with the form of the Discrete Fourier Transform. The component at a certain harmonic order n is split into two orthogonal terms, $\sin(n\omega_0 t)$ and $\cos(n\omega_0 t)$. Equation (3.2.1.1) can be expressed in matrix form as follows:

$$\begin{bmatrix} y_1 \\ y_2 \\ \vdots \\ y_K \end{bmatrix} = \begin{bmatrix} s_1(\Delta t) & s_2(\Delta t) & \cdots & s_N(\Delta t) \\ s_1(2\Delta t) & s_2(2\Delta t) & \cdots & s_N(2\Delta t) \\ \vdots & \vdots & & \vdots \\ s_1(K\Delta t) & s_2(K\Delta t) & \cdots & s_N(K\Delta t) \end{bmatrix} \begin{bmatrix} Y_1 \\ Y_2 \\ \vdots \\ Y_N \end{bmatrix} + \begin{bmatrix} \varepsilon_1 \\ \varepsilon_2 \\ \vdots \\ \varepsilon_K \end{bmatrix}$$

or

$$y = S Y + \varepsilon \quad (3.2.1.2)$$

where K is the number of samples in one sampling window, and Δt represents the time interval between two neighboring sample points. To estimate all N parameters, $K \geq N$ is required. If the error vector ε is assumed to have zero mean, and a covariance matrix

$$E\{\varepsilon \varepsilon^T\} = W \quad (3.2.1.3)$$

then the solution to (3.2.1.2) using least square technique yields

$$\hat{Y} = (S^T W^{-1} S)^{-1} S^T W^{-1} y \quad (3.2.1.4)$$

With the assumption that the errors are uncorrelated and independent from sample to sample and have a constant covariance, W is a multiple of the unit matrix. Therefore the least square solution (when $\varepsilon^T W^{-1} \varepsilon$ is minimized) is

$$\hat{Y} = (S^T S)^{-1} S^T y \quad (3.2.1.5)$$

Substituting the orthogonal expressions of sine and cosine terms in (3.2.1.5), the ij^{th} entry of the matrix $S^T S$ is

$$\begin{aligned} (S^T S)_{ij} &= \sum_{k=1}^K s_i(k\Delta t) s_j(k\Delta t) \\ &= \begin{cases} K/2 & ; \quad i = j \\ 0 & ; \quad i \neq j \end{cases} \end{aligned} \quad (3.2.1.6)$$

The fundamental frequency components are given by

$$\hat{Y}_c = \frac{2}{K} \sum_{k=1}^K y_k \cos(k\theta) \quad (3.2.1.7)$$

$$\hat{Y}_s = \frac{2}{K} \sum_{k=1}^K y_k \sin(k\theta) \quad (3.2.1.8)$$

where $\theta = 2\pi/K$. The magnitude of the fundamental component can be calculated by

$$|Y| = \sqrt{\left(\hat{Y}_c\right)^2 + \left(\hat{Y}_s\right)^2} \quad (3.2.1.9)$$

Note that the results for fundamental frequency, in (3.2.1.7) and (3.2.1.8), are independent of the number of parameters N . The fundamental component obtained from the Fourier algorithm, is the optimal solution in the least square sense, under the assumption that the noise samples are uncorrelated.

3.2.2 Least Squares algorithm (LS)

The principles of Least Squares algorithm are quite similar to the one for Fourier algorithm, except that there is no requirement of dc offset removal from the input signal before signal processing.

The input signal in such a case can be written as:

$$y(t) = Y_0 e^{-t/\tau} + \sum_{n=1}^N Y_n s_n(t) + \varepsilon(t) \quad (3.2.2.1)$$

where Y_0 the magnitude of the decaying dc component at $t=0$
 τ the time constant of the decaying dc component

The other parameters are the same as in (3.2.1.1).

Because of the presence of the dc component in the signal, the matrix S also contains the dc component. The equation in frequency domain is then like:

$$\begin{bmatrix} y_1 \\ y_2 \\ \vdots \\ y_K \end{bmatrix} = \begin{bmatrix} s_0(\Delta t) & s_1(\Delta t) & s_2(\Delta t) & \cdots & s_N(\Delta t) \\ s_0(2\Delta t) & s_1(2\Delta t) & s_2(2\Delta t) & \cdots & s_N(2\Delta t) \\ \vdots & \vdots & \vdots & \vdots & \vdots \\ s_0(K\Delta t) & s_1(K\Delta t) & s_2(K\Delta t) & \cdots & s_N(K\Delta t) \end{bmatrix} \begin{bmatrix} Y_0 \\ Y_1 \\ Y_2 \\ \vdots \\ Y_N \end{bmatrix} + \begin{bmatrix} \varepsilon_1 \\ \varepsilon_2 \\ \vdots \\ \varepsilon_K \end{bmatrix} \quad (3.2.2.2)$$

where $s_0(k\Delta t) = e^{-k\Delta t/\tau}$, $k = 1, 2, \dots, K$

Similarly as in the case of Discrete Fourier algorithm, the following equation holds:

$$\hat{Y} = (S^T S)^{-1} S^T y \quad (3.2.2.3)$$

However, due to the presence of the dc component, the matrix $S^T S$ will no longer be a diagonal matrix as in the case of Discrete Fourier algorithm. The matrix $(S^T S)^{-1}$ will be a full matrix under any condition. Let

$$A = (S^T S)^{-1} S^T \quad (3.2.2.4)$$

The fundamental frequency components are estimated by

$$\hat{Y}_c = \sum_{k=1}^K y_k A(2, k) \quad (3.2.2.5)$$

$$\hat{Y}_s = \sum_{k=1}^K y_k A(3, k) \quad (3.2.2.6)$$

The magnitude of the fundamental component of the signal can be calculated by

$$|Y| = \sqrt{\left(\hat{Y}_c\right)^2 + \left(\hat{Y}_s\right)^2} \quad (3.2.2.7)$$

3.2.3 Root Mean Square algorithm (RMS)

Root Mean Square (RMS) algorithm is widely used in electrical parameter measurement. It is a method of calculating the total energy content of a waveform. Unlike the other relay algorithms which in one way or the other function as a filter, RMS algorithm does not differentiate to the frequencies being measured and thus will not reject the harmonics and dc components. The commonly used expression in calculating RMS value in power quality monitoring is the following form:

$$Y_{\text{RMS}} = \left(\frac{1}{K} \sum_{k=0}^{K-1} y^2(k\Delta t) \right)^{\frac{1}{2}} \quad (3.2.3.1)$$

where K is the number of samples in one sampling window
 Δt is the sampling interval

The RMS algorithm is useful for applications where measuring energy content to approximate heating characteristics is desirable, e.g. overexcitation relays [47]. Detailed principles and characteristics of the RMS algorithm will be discussed in Chapter 7.

3.2.4 Walsh algorithm

The Walsh algorithm is based on Walsh functions: a set of orthogonal signals on the interval $[0, 1]$ which only take on the values ± 1 . Compared with Fourier functions which deal with complex numbers, Walsh functions deal only with two integer numbers. This makes Walsh function more efficient to be implemented in a digital processor.

The Walsh function is defined in the following way [49]:

$$W_k(t) = \prod_{r=0}^{p-1} \text{sgn}(\cos(k-1)_r 2^r \pi t) \quad (0 \leq t < 1) \quad (3.2.4.1)$$

where k Walsh function number, positive integer

In binary system $(k)_2 = \sum_{r=0}^{p-1} k_r 2^r$ (i.e. the binary representation of the integer k)

p total digits of $(k-1)$ in binary expression

sgn sign function (only the sign of the result is taken)

For example, $W_6(t)$ can be deduced as follows:

$$6 - 1 = 5 = 1 \times 2^2 + 0 \times 2^1 + 1 \times 2^0$$

so $(k-1)_2=1$ $(k-1)_1=0$ $(k-1)_0=1$ (i.e. 101 in binary representation)

Since there is 3 digits in binary expression, $p=3$

Therefore

$$\begin{aligned} W_6(t) &= \prod_{r=0}^2 \text{sgn}(\cos(k-1)_r 2^r \pi t) \\ &= \text{sgn}(\cos(k-1)_2 2^2 \pi t) \cdot \text{sgn}(\cos(k-1)_1 2^1 \pi t) \cdot \text{sgn}(\cos(k-1)_0 2^0 \pi t) \\ &= \text{sgn}(\cos 4\pi t) \cdot \text{sgn}(\cos \pi t) \end{aligned} \quad (3.2.4.2)$$

Fig. 3.2.4.1 shows the waveforms of the first 8 Walsh functions.

For the convenience of comparing the Walsh function with trigonometrical functions, Walsh function can be further classified as

$$W_k(t) = \begin{cases} \text{sal}_m(t) & \text{when } k = 2m - 1, \quad m = 1, 2, 3, \dots \\ \text{cal}_m(t) & \text{when } k = 2m, \quad m = 1, 2, 3, \dots \end{cases} \quad (3.2.4.3)$$

Similarly as in (3.2.1.1), for the Fourier series, any periodic signal function can be expanded as a series of Walsh functions plus a noise term:

$$y(t) = \sum_{n=1}^N Y_n W_n(t) + \varepsilon(t) \quad (3.2.4.4)$$

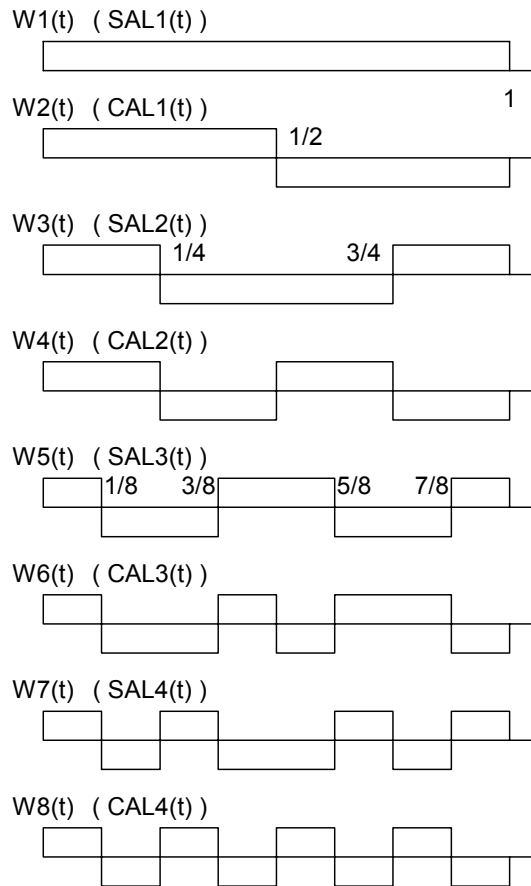


Figure 3.2.4.1 The first 8 Walsh functions

The functions $sal_m(t)$ and $cal_m(t)$ in (3.2.4.3) correspond to $\sin(m\omega t)$ and $\cos(m\omega t)$ in the Fourier algorithm.

In the same way as for (3.2.1.6), we obtain

$$\left(\mathbf{S}^T \mathbf{S}\right)^{-1} = \frac{1}{K} \cdot \mathbf{I} \quad (3.2.4.5)$$

with \mathbf{I} the unit matrix and K the number of samples per sampling window. The coefficients for fundamental component in Walsh series can be deduced as:

$$\hat{Y}_{\text{cal}} = \frac{1}{K} \sum_{k=1}^K y_k \text{cal}_1(k\theta) \quad (3.2.4.6)$$

$$\hat{Y}_{\text{sal}} = \frac{1}{K} \sum_{k=1}^K y_k \text{sal}_1(k\theta) \quad (3.2.4.7)$$

where $\theta = 1/K$.

The magnitude of the fundamental component of the signal can be calculated by

$$|Y| = \sqrt{\left(\hat{Y}_{\text{cal}}\right)^2 + \left(\hat{Y}_{\text{sal}}\right)^2} \quad (3.2.4.8)$$

The expression for the Walsh algorithm is quite similar to that of the Fourier algorithm, but the amount of computational effort is much less. However, for any smooth continuous waveform, the Walsh algorithm requires the calculation of more coefficient terms to obtain the same accuracy in estimation. Its simplicity in programming is counterbalanced by the need for a large number of terms. Its frequency response is indistinguishable from the full-cycle Fourier algorithm if a sufficient number of Walsh coefficients are used [49].

3.2.5 Kalman algorithm

The Kalman algorithm is designed for dynamic system estimation. Its application is justified when

- a. An initial status estimation is available
- b. The covariance of white noise cannot be assumed constant

As shown in section 3.2.1, the deduction of the Fourier algorithm does not hold if the noise covariance is not constant, and neither does the Walsh algorithm. In such a situation, the Kalman algorithm is a possible solution.

For any signal

$$y(t) = \sum_{n=1}^N (Y_{n,r} \cos(n\omega_0 t) + Y_{n,i} \sin(n\omega_0 t)) \quad (3.2.5.1)$$

The task is to find the value of $Y_{n,r}$ and $Y_{n,i}$ for given signal $z(t)$.

In Kalman filtering, a studied system is described by the following equation [49]:

$$Y_{k+1} = \varphi_k Y_k + \Gamma_k w_k \quad (3.2.5.2)$$

where

Y_k, Y_{k+1}	state vector for sample k, sample k+1
k	evolution number (sampling time moment k)
φ_k	state transition at time k
Γ_k	state noise transition matrix at time k
w_k	state noise at time k

$$Y_k = [Y_{1,r}(k) \quad Y_{1,i}(k) \quad \dots \quad Y_{N,r}(k) \quad Y_{N,i}(k)]^T$$

To have an estimation of the status Y , it is necessary to introduce as a feedback the difference between the actual sampled measurement value y_k and the predicted value of the measurement as

$$\hat{Y}_{k+1} = B_{k+1} \hat{Y}_k + K_{k+1} y_{k+1} \quad (3.2.5.3)$$

where

$$y_{k+1} = H_{k+1} Y_{k+1} + \varepsilon_{k+1}$$

y_{k+1}	measurement result at time k+1
H_{k+1}	measurement matrix at time k+1
ε_{k+1}	measurement noise at time k+1
B_k, K_{k+1}	parameters to be determined by optimization

In the above equations it can be observed that the estimation of status at $k+1$ is based on the y information up to $k+1$. In practice it is often required, particularly in controls and protections, to predict ahead, i.e. obtain status

estimation of \hat{Y}_{k+1} based on the information up to $\hat{Y}_k, \hat{Y}_{k-1} \dots$ which means

$$\hat{Y}_{k+1|k} = B_k \hat{Y}_{k|k-1} + K_k y_k \quad (3.2.5.4)$$

The terms w_k and ε_k are discrete time random processes representing state noise, i.e. random inputs in the evolution of the parameters, and measurement errors, respectively. The following assumptions about state noise, measurement noise and state are made to be able to estimate the state vector:

- w_k and ε_k are assumed to be independent of each other and uncorrelated from sample to sample

- w_k and ε_k are assumed to have zero means, which implies that their variances

$$\text{Var}(w_k) = E\{w_k(w_k)^T\} = Q_k = \sigma_q^2 \mathbf{I} \quad \text{and} \quad \text{Var}(\varepsilon_k) = E\{\varepsilon_k(\varepsilon_k)^T\} = R_k = \sigma_r^2 \mathbf{I}$$

are both positive definite

- The initial state y_0 is assumed to be independent of w_k and ε_k and with a known mean and covariance matrix $P_{0|0}$

The matrices Q_k and R_k are the covariance matrices of the random processes and are independent of the studied signal.

To have the best linear estimate of $\hat{Y}_{k+1|k}$, the way is to minimize the mean-square error [50]:

$$P_{k+1|k} = E\{Y_{k+1|k+1} - \hat{Y}_{k+1|k}\}^2 \quad (3.2.5.5)$$

Substituting (3.2.5.5) into (3.2.5.4) and taking derivative for φ_k and H_k yield

$$E\{(Y_{k+1} - \hat{Y}_{k+1|k})\hat{Y}_{k|k-1}\} = 0 \quad (3.2.5.6)$$

$$E\{(Y_{k+1} - \hat{Y}_{k+1|k})y_k\} = 0 \quad (3.2.5.7)$$

From the above equations it can be deduced that

$$B_k = \varphi_k - H_k K_k \quad (3.2.5.8)$$

So (3.2.5.4) can be rewritten as

$$\hat{Y}_{k+1|k} = \varphi_k \hat{Y}_{k|k-1} + K_k [y_k - H_k \hat{Y}_{k|k-1}] \quad (3.2.5.9)$$

where the Kalman gain matrix K_k can be determined together with the mean-square error $P_{k+1|k}$

$$K_k = \varphi_k H_k^T P_{k|k-1} [H_k P_{k|k-1} H_k^T + R_k]^{-1} \quad (3.2.5.10)$$

where

$$P_{k|k-1} = \varphi_{k-1} P_{k-1|k-1} \varphi_{k-1}^T + \Gamma_{k-1} Q_{k-1} \Gamma_{k-1}^T \quad (3.2.5.11)$$

$$P_{k|k} = [I - K_k H_k \varphi_k^{-1}] P_{k|k-1} \quad (3.2.5.12)$$

There are two models used to represent the input signal. One of the models is to define

$$\varphi_k = \text{diag}[M_1 \ M_2 \ \dots \ M_N] \quad H_k = [1 \ 0 \ \dots \ 1 \ 0]^T$$

with

$$M_n = \begin{pmatrix} \cos(2n\pi/K) & -\sin(2n\pi/K) \\ \sin(2n\pi/K) & \cos(2n\pi/K) \end{pmatrix}$$

where K sampling points in one cycle

Bear in mind that in this case, K does not imply something like a “sampling window” of K points. Unlike other algorithms such as DFT or RMS that are based on the information in a sampling window, Kalman algorithm is based on the state information in the last 2 or 3 sampling moments. In another words, it is an evolution prediction.

Based on the equations developed above, it is clear that the state estimation (prediction) can be made, starting from the known sampled results $z(t)$ and the mean and covariance matrix $P_{0|0}$.

The Kalman filtering process can be depicted by the following flow diagram [51]:

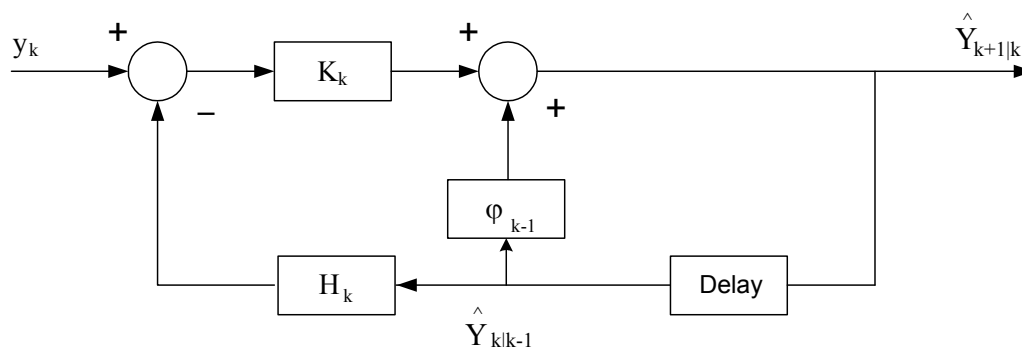


Figure 3.2.5.1 Kalman filtering process

If there is no initial information and the measurement error has a constant covariance, the Kalman algorithm estimate becomes a combination of discrete Fourier transform terms. This means that the Kalman algorithm will yield a result with an accuracy comparable to the case of Fourier algorithm, but involving considerably more computation. In this case, Kalman algorithm actually is much less efficient than the Fourier algorithm.

Because of the above reasons, Kalman algorithm is applied in the cases where the measurement error covariance decays significantly during the first cycle after the fault, e.g. transformer inrush due to fault [52] or fast decay current due to fault on transmission line [53].

3.2.6 Advantages and disadvantages of the above algorithms

In the above algorithms, Walsh algorithms can be regarded as a mathematical variation of Fourier algorithms. RMS algorithms have special application in particular type of protective relays. Comparison of advantages and disadvantages is mainly focused on the other three types of algorithms, which in principle are applicable to any single-input relay protection.

Based on the existing research [54][55][56], a summary of the algorithms discussed above is listed in the following table.

Table 3.2.6.1 Characteristics of the discussed algorithms

	Speed	Removal of Decay DC offset	System information required?	Accuracy during the 1 st cycle	Accuracy after the 1 st cycle
DFT*	--	--	no	--	++
LS*	~	++	no	~	+
Kalman	+	~	yes	+	-

++ excellent + good ~ average - poor -- bad

* Assume the sampling window be one fundamental cycle

From the characteristics listed in the above table, it is clear that Fourier algorithms are a good choice in practice if ultra high speed response (less than 1/4 fundamental cycle) is not crucial. This is actually the case at distribution level, where overcurrent relays are widely adopted. Among the three kinds of digital algorithm mentioned above, the Fourier algorithm has in general a much wider application in practice than the other two algorithms. In this project, the Fourier algorithm for single-input relay is studied.

3.3 Digital algorithms for dual-input relays

A dual-input relay here refers to a relay that requires two input parameters. Relays such as impedance relays, power factor relays and directional relays are dual-input relays. In this project, only the impedance relay that requires both voltage and current inputs is studied.

There are two main algorithms for dual-input impedance relays: Fourier algorithm and differential equation algorithm. Also some traveling wave based algorithms have been proposed for this purpose [57][58].

3.3.1 Discrete Fourier algorithm (DFT)

The principles of the Discrete Fourier algorithm for impedance relays are similar to those for the Discrete Fourier algorithm for single-input relays as discussed in section 3.2.1. The input signals, both voltage and current, are split into two orthogonal fundamental components by using the Fourier algorithm. Starting from these components, the real part and imaginary part of the apparent impedance are calculated as follows:

$$Z = \frac{U}{I} = \frac{U_c + jU_s}{I_c + jI_s} \quad (3.3.1.1)$$

so that, with $Z = R + j X$, we obtain

$$R = \frac{U_c I_c + U_s I_s}{I_c^2 + I_s^2} \quad (3.3.1.2)$$

$$X = \frac{U_s I_c - U_c I_s}{I_c^2 + I_s^2} \quad (3.3.1.3)$$

where U_c , U_s , I_c , I_s are the orthogonal components of voltage and current respectively.

Normally the Fourier algorithm is used to obtain the fundamental complex voltage and current, U and I respectively. But they can equally well be obtained by any other method, like Walsh algorithms or Kalman algorithms.

The U and I in the above DFT algorithm do not necessarily mean phase voltage and current in practical application. The meanings of U and I in case of phase-to-phase impedance relays are different from those of ground fault impedance relays. Details are given in Chapters 4 and 6.

3.3.2 Differential Equation algorithm (DEA)

Unlike Fourier algorithm that is based on the description of the waveform, differential equation algorithm is based on a system model. The line being protected is modeled as an R-L series connection by using the following differential equation:

$$RI(t) + L \frac{dI(t)}{dt} = U(t) \quad (3.3.2.1)$$

Supposing voltage and current signals are sampled at the equal-distant instants $k\Delta t$, $(k+1)\Delta t$, $(k+2)\Delta t$, the integration of (3.3.2.1) can be expressed as:

$$\int_{k\Delta t}^{(k+1)\Delta t} U(t)dt = R \int_{k\Delta t}^{(k+1)\Delta t} I(t)dt + L[I_{k+1} - I_k] \quad (3.3.2.2)$$

$$\int_{(k+1)\Delta t}^{(k+2)\Delta t} U(t)dt = R \int_{(k+1)\Delta t}^{(k+2)\Delta t} I(t)dt + L[I_{k+2} - I_{k+1}] \quad (3.3.2.3)$$

where $I_k = I(k\Delta t)$, etc.

The above two equations can be approximated using trapezoidal rule as follows:

$$\int_{k\Delta t}^{(k+1)\Delta t} U(t)dt = \frac{\Delta t}{2} [U_{k+1} + U_k] \quad (3.3.2.4)$$

where $U_k = U(k\Delta t)$, etc.

(3.3.2.2) and (3.3.2.3) can be written as a matrix equation:

$$\begin{bmatrix} \frac{\Delta t}{2}(I_{k+1} + I_k) & (I_{k+1} - I_k) \\ \frac{\Delta t}{2}(I_{k+2} + I_{k+1}) & (I_{k+2} - I_{k+1}) \end{bmatrix} \begin{bmatrix} R \\ L \end{bmatrix} = \begin{bmatrix} \frac{\Delta t}{2}(U_{k+1} + U_k) \\ \frac{\Delta t}{2}(U_{k+2} + U_{k+1}) \end{bmatrix} \quad (3.3.2.5)$$

from which the estimates of R and L are calculated as follows:

$$R = \left[\frac{(U_{k+1} + U_k)(I_{k+2} - I_{k+1}) - (U_{k+2} + U_{k+1})(I_{k+1} - I_k)}{(I_{k+1} + I_k)(I_{k+2} - I_{k+1}) - (I_{k+2} + I_{k+1})(I_{k+1} - I_k)} \right] \quad (3.3.2.6)$$

$$L = \frac{\Delta t}{2} \left[\frac{(I_{k+1} + I_k)(V_{k+2} + V_{k+1}) - (I_{k+2} + I_{k+1})(U_{k+1} + U_k)}{(I_{k+1} + I_k)(I_{k+2} - I_{k+1}) - (I_{k+2} + I_{k+1})(I_{k+1} - I_k)} \right] \quad (3.3.2.7)$$

The differential-equation-based algorithm can be further extended by adding the shunt capacitance of the line to the model [59]. Expression (3.3.2.1) would become more complicated but the solution remains possible. Alternatively, information from more samples could be used, extending the number of equations in (3.3.2.1). Resistance and inductance could be estimated by using a least square method[49].

3.3.3 Traveling wave based algorithm

Traveling wave based algorithms make use of the characteristics of traveling waves along the transmission lines for calculating impedance. There are several types of algorithms in this category, such as correlation technique by Vitins et al.[60][61], Kohlas' algorithm [62], Christopoulos' algorithm [63]

etc. Also traveling wave based algorithms are used in differential [64] and directional [65] protections. In this section, Kohlas' algorithm is introduced.

The assumptions for Kohlas' algorithm are:

- The line is considered to have frequency independent R, L and C
- When there is no fault on the line the voltage variation along the line is zero.

The algorithm uses the traveling wave equations of the line as a model relating voltages and currents.

$$-\frac{\partial U}{\partial z} = RI + L \frac{\partial I}{\partial t}$$

$$-\frac{\partial I}{\partial z} = C \frac{\partial U}{\partial t}$$

By using these equations an expression is obtained for the voltages at any point along the line as a function of time. Input to this expression are the voltages and currents measured at the line terminal over a certain measurement window T. The fault location is detected as the place where the estimated voltage is closest to zero.

The fault detection function by Kohlas' algorithm is as follows:

$$G(z) = \frac{d^2}{dz^2} \left[\frac{1}{T - 2z/c} \int_{z/c}^{T-z/c} U^2(z, t) dt \right] \quad (3.3.3.1)$$

where	c	propagation velocity of traveling wave
	T	measurement window length
	U(z,t)	voltage, is a function of distance and time
	z	distance away from the measurement terminal of the line

When a fault occurs at point z , its voltage remains zero during the traveling wave propagation period, i.e. after the fault until the traveling wave is reflected back to that point. Because of this, the duration of zero voltage level is longer at this point than the other points. So (3.3.3.1) will show up a very sharp maximum in $G(z)$.

Kohlas' algorithm develops complicated expressions for voltages and currents along the line. However, according to later research [66], the resistance R of a line has little effect on the accuracy of final results. By assigning $R=0$, the expressions become much simpler. It is also found that the following detection function can yield results with satisfying accuracy:

$$F(z) = \frac{1}{T - 2z/c} \int_{z/c}^{T-z/c} U^2(z, t) dt \quad (3.3.3.2)$$

The fault is located at the point z , which shows up as a minimum of $F(z)$.

However, such a technique has the following weak points:

- Faults close to one of the line terminals are not detected
- The calculation needs a lot of computation time

3.3.4 Advantages and disadvantages of the above algorithms

A summary of the characteristics of the discussed dual-input algorithms is listed in the following table.

Table 3.3.4.1 Characteristics of the discussed algorithms

	Speed	Simplification of system structure?	Accuracy during the 1 st cycle	Accuracy after the 1 st cycle
DFT	--	no	--	++
DEA	+	yes	~	+
Traveling Wave	++	yes	-	--

++ excellent + good ~ average - poor -- bad

For all the three algorithms, the accuracy during the 1st cycle is not so reliable: DFT cannot yield correct output theoretically due to lack of enough signal information; DEA cannot take into account the impact from the distributed shunt capacitance, which is ignored in its model; the accuracy of the afore mentioned traveling wave algorithm is much dependent on the voltage function along the line, which is much more complicated in case of transients.

The accuracy after the first cycle for traveling wave algorithm is affected by the reflected traveling wave.

Compared with the Fourier algorithm, the differential equation algorithm is faster and more suitable for transient conditions. However, the approximation of the line as an ideal R-L loop somewhat affects the accuracy of this algorithm. Both of them have application in line relaying.

Compared with the Fourier and differential equation algorithms, traveling wave algorithms demonstrate a completely new approach in dealing with distance protection. Experiments have shown that these algorithms make a fairly good discrimination between internal faults and external faults [67]. However, as traveling wave algorithms have problem with the accuracy as

discussed above, this technique remains to be improved before it can be adopted in practice.

Therefore in this project, the study is focused on DFT and DEA algorithms.

3.4 Existing relay algorithms and future fast relay algorithms

From the analysis of previous sections, it is clear that the digital algorithms based on Fourier principles are quite popular in practical application. The Fourier algorithm uses a moving sampling window to scan the input signal. The decision-making time of the relay is dependent on the length of the sampling window. In normal case, a 1-cycle (also called full-cycle) sampling window is adopted, which means that the decision-making time will be at least 20 ms.

Although ultra-high-speed relay algorithms (quarter fundamental cycle or less), most of which are based on traveling wave principles, have been proposed for many years, the product catalog of the main relay manufacturers show that most of their protective relays are based on the traditional Fourier algorithm. This is probably due to two main factors:

1. At distribution level, the customers have no strong motive to introduce relays of fast algorithm. On one side, these relays are expensive; on the other side, the customers are satisfied with the present response speed of the relays.
2. At transmission level, the customers don't have enough confidence in the dependability and security of the fast algorithms. On one side, the fast algorithms based on traveling wave can be interfered by many uncertain factors, such as the noise mixed in the traveling wave, the absorption of the traveling wave components by the shunt

capacitance, the penetrated traveling wave from the neighboring protected line etc; on the other side, while fast fault detection performance is demonstrated, few of the proposed algorithms have been tested under non-fault disturbances.

Therefore, the developed new quantification approach in this thesis can be applied in setting up a disturbance database in the viewpoint of the relay algorithms that are presently used in practice. Also the principle of such a method can be used in comparison between the existing algorithm and any new fast algorithm, so as to check if the new algorithm is proposed at the cost of relay security.

Chapter 4 Classification of Component Switching Transients

Power system transients can be due to steady-state load currents, dynamic operations as well as faults. Their presence in power systems has detrimental impacts on the operation of protective relays. For the purpose of testing the possible performance of relays under transient conditions, it is necessary to evaluate the potential influence of the transients, based on which the classification of transients can be made. In this chapter, the effect of component switching on relays in transmission systems is evaluated, based on which a database can be set up for testing relays' immunity against mal-trips. A methodology is developed for overcurrent relays and impedance relays, and applied to component switching events observed by the relay on the line being switched.

4.1 Way to quantify component switching impact

For any event, the interaction between a system and equipment can be described by a typical chain of source — phenomenon — impact. In this study the source is the switching action, the phenomenon is the transient in voltage and current waveforms, the impact is mal-trip of a relay.

The study of the impact of voltage and current transients shows clear similarities with power quality. The research on power quality concerns among others the potential impact of transients on end-user equipment. In this chapter a similar kind of approach is taken for the potential impact on protective relays.

With a given transient phenomenon, locating the source is an observation of the transient by the system operator, while the impact of the transient is an observation of the transient by the relay. From the viewpoint of relay manufacturers and users, transient impact evaluation is their practical need. Such an evaluation can be helpful in testing the possible mal-function of relays during transients, not only for the existing relays, but also future generations of relays and relay algorithms.

The impact of transients on protective relays should be assessed by their consequence, i.e. whether the mal-function of protective relays due to transients leads to severe damages or losses to the system. This becomes particularly important when the studied system is a transmission power network. The sources of the mal-function can be internal, external, or both. Internal source means the failure of the relay component itself, while external source refers to the wrong decision-making of a relay, which is strongly dependent on the algorithm used and on the relay setting.

As the first step in evaluating the transient impact, the focus of this chapter is on type V in table 2.1 in Chapter 2, i.e. mal-trip of protective relays due to non-fault events. In power systems the main non-fault events are switching of power system components. In this thesis, the term “power system components” include not only the electric equipment for generation, transmission, distribution or regulation, but also the electric loads.

A systematic way is needed to assess the possible detrimental impact of component switching on relay performance. Although electromechanical and solid-state relays are still in service in power systems, the application of digital relays has become more and more common. The study in this chapter is therefore based on the existing digital relays, whose kernel part is the filter,

or algorithm in a more formal way. Also the future generation of relays and relay algorithms are assumed to be digital.

This chapter seeks to explore a way to quantify the impact of switching transients on protective relays. The concept “switching severity” is introduced to quantify the impact of component switching events by protective relays. Starting from such concept, a relay characteristic diagram can be worked out to depict the impact of component switching events on a particular type of relay. The “immunity curve” in the relay characteristic diagram can be adopted for mal-trip checking in relay tests.

4.2 How to test relays under component switchings

Fig. 4.2.1 demonstrates the procedure for testing relays against mal-trip due to component switching events.

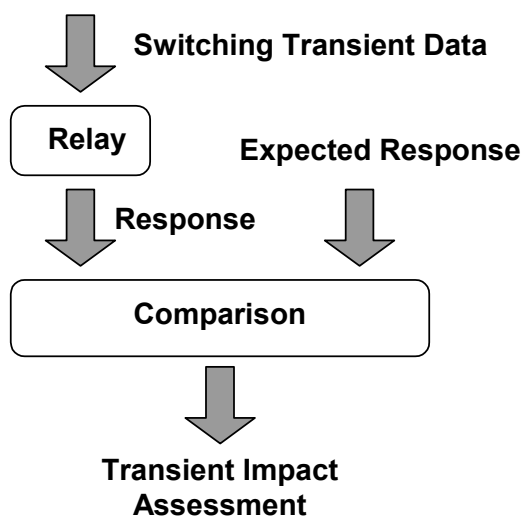


Figure 4.2.1 Procedures for testing relays under component switching

Relay testing is based on three key parts. First there should be testing signals. Second, there should be a relay under test. Third, the desired relay response under the testing signals need to be known.

In this study, the testing signals are the switching transient data. This includes both voltage and current data obtained during practical component switching events. The voltage and current data can also come from simulation of practical systems.

The relay under test can be either a relay device, or a relay model. In case of a digital relay the main test concerns the software so that a model will in many cases give acceptable results. In practice, complete protection systems are more common than a single stand-alone protective relay, which means that the complete system behavior has to be verified in a test with all the real devices involved. However as this study is focused on relay mal-trip test, mal-trip of any single protective relay in the complete protection system is undesirable. So each type of relay has to be considered in relay testing. As digital relays are the concern in this study, the tested relay is represented by a relay model, whose essential part is a digital filter, with sampled voltages and currents as input, and as output a detection function that is compared with a threshold. The output of this filter is the “response” in Fig. 1.

When testing actual relays, there are in many cases only two possible responses: “trip” and “non-trip”. For testing under component switchings the desired response is in those cases always “non-trip”. But the status “non-trip” of relay response can be either “far from trip” or “close to trip”. To draw more useful conclusions from the tests, relay response signal should be analyzed in detail. This is another reason for using a model of the relay.

In this study, the testing signals are imposed on a relay model. Its response is compared with the desired response. Based on the comparison, the transient impact on a relay can be assessed.

A protection relay will potentially be exposed to a large number of component switching transients. Some of these transients could endanger the correct operation of the relay, i.e. lead to a mal-trip because:

- It is difficult for a relay algorithm to be adaptive to all transients, i.e. the relay algorithm can yield unreliable output for certain transients.
- Different algorithms have different responses to different characteristics of voltage and current waveforms (e.g. 5th harmonic, zero-sequence etc.).
- A trade-off between speed and security requires insight in the risk of mal-trip.

To check the immunity of a relay to switching transients, it is desired that a set of the most significant known switching transient data be collected, based on which a database for relay testing is set up.

To set up such a database, enough data from switching operations should be obtained. Intuitively it is preferred to use actual measurement data, as they reflect the real situation. However, there are some factors that prevent measurements from providing enough information:

- Most of the transients measured stand for minor events, while only a small part of the data contains valuable information on switching transients. Severe transients are rare, which makes the data collecting time-consuming
- Most measurement campaigns do not result in a sufficient number of events to get an accurate distribution of the transient parameters.
- The digital fault recorders, which are adopted to provide the practical measurements, can discard some components of the measured

parameters when recording. These measured data are therefore different from the real ones, which are detected by relays.

Therefore it is important to include simulated switching data in the database. Compared with measured data, by simulated data are not affected by the three factors mentioned above, but by other factors such as model itself, estimates for power system parameters etc. Therefore it is important that accurate models are introduced and that the power system parameters are estimated based on actual operating power systems.

The application of simulation tools allows the generation of component switching transients over a wide range of systems, components and switching instants. This range is only limited by the practical constraints on system design, component limits etc. A relay should not trip whenever there is a component switching that is located inside the practical range.

— Selection of practical values in simulation studies

Although the combination of the system parameters for component switching can be set freely in simulation program, the restraints on equipment specifications in practice impose limits on the possible switching situations. Examples of such limits that set the maximum value for the devices in power systems are:

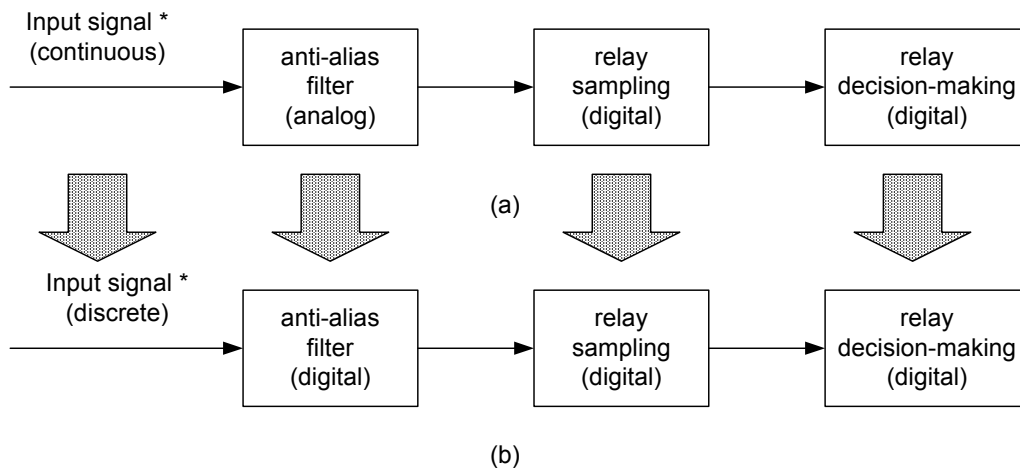
1. The transport capacity of a transmission line is dependent on its voltage level and limited by stability requirements.
2. The capacity of a transformer is normally chosen according to the estimated transport capacity of the line/cable and limited by manufacturing technology.

3. The length of a transmission line is limited by, among others, the distribution of voltage along the long line.
4. The capacity of a capacitor is limited by insulation requirements.
5. The breaking capacity of a circuit breaker limits the possible current that flows through the line in steady state.

The above restraints set the range of system operational states, within which switching events can occur. Applying all the above restraints when generating switching data can yield a reasonable border among the simulated data. Based on this, the expected response should be that a relay does not trip when the imposed switching disturbance is located inside this reasonable border.

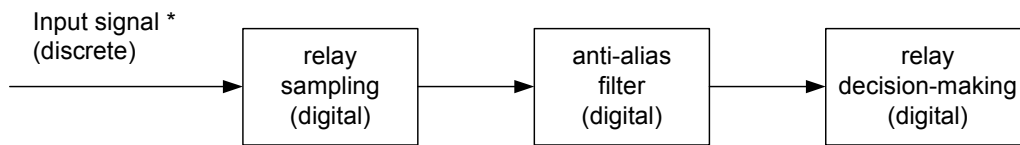
— Anti-alias filter in simulation

An important difference between actual relay testing and testing of a (digital) model is in the representation of the anti-aliasing filter. The actual input signal is continuous and anti-alias filter is analog, while in a simulation the input signal is discrete and the anti-alias filter is digital, as shown in Fig. 4.2.2. The frequency response of the digital anti-alias filter is dependent on the sampling rate, which does not reflect the unchanged frequency response characteristics of an analog anti-alias filter. To deal with it, the sequences of relay and anti-alias filter are exchanged to keep the unchanged performance of the anti-alias filter, as shown in Fig. 4.2.3.



* Input signals are after input-transformers of the relay-box

Figure 4.2.2 Anti-alias in practice and in simulation



* Input signals are after input-transformers of the relay-box

Figure 4.2.3 Simulation of anti-alias filter after sequence adjustment

4.3 Component switching analysis

To test the reliability of relays under switching transients, a sufficient amount of transient data is needed. To obtain such transient data, detailed information on component switchings should be analyzed.

In transmission systems, the following cases of component switching can be distinguished:

1. Generator-transformer group switching
2. Transmission line/cable switching (including the case in which there is a series capacitor)

3. Transformer switching (with/without load)
4. Shunt capacitor/inductor switching
5. Tap-changer operation

Further analysis on each of the cases is discussed below.

4.3.1 Generator-transformer group switching

The transients in current due to generator-transformer switching consist of a DC component plus harmonic distortion due to the transformer. There is a minor transient in the voltage when the generator-transformer unit is connected to a transmission system.

Normally it takes about 20 cycles for generator-transformer switching currents to reach steady state. The magnitude of the peak inrush current is dependent on the moment when switching is carried out. The maximum peak current is less than twice its steady state value. However the generator output at the moment of switching is set to be much lower in practice. The output of the generator is gradually increased up to the rated value after the switching is completed. This makes the instantaneous inrush current even smaller.

4.3.2 Unloaded transmission line/cable switching

Unloaded transmission line/cable switching can occur during fast automatic reclosure after a fault. When the circuit breaker at the sending terminal of the line/cable is closed, an electromagnetic wave propagates along the line/cable. This wave will then be reflected back at the receiving terminal of line/cable. When it reaches the sending terminal, part of it will be refracted to the source side and the remaining part will be reflected back to the receiving terminal. This process continues until a steady state is reached.

The switching inrush current of an unloaded transmission line is dependent on the line voltage and the wave impedance. The inrush current is of the same order of magnitude as the maximum rated current of the line/cable. The waveform of the inrush current contains many high frequency harmonics that last for several cycles.

4.3.3 Transformer switching (with/without load)

High inrush current is expected when transformers are involved. The inrush current generates large flux linkage, which pushes the transformer magnetizing core into saturation. This results in an extremely large current in the primary side winding, abundant in harmonics. The initial energizing inrush current can reach values as high as 25 times full-load current and will decay with time until the normal magnetizing current value is reached. The decay of the inrush current may vary from as short as 20 cycles to as long as minutes for highly inductive circuits [71].

Loaded transformer energizing can generate similar transients as mentioned above. However, the presence of load resistance leads to shorter attenuation periods and reduced harmonic distortion in the total current.

4.3.4 Shunt capacitor/inductor switching

For shunt capacitor switching two cases can be distinguished: isolated shunt capacitor switching and back-to-back shunt capacitor switching. The peak current in isolated shunt capacitor switching is normally less than the system short circuit current at the capacitor busbar, due to the limitation on capacitance size. In case of back-to-back shunt capacitor switching, the

inrush current is of higher magnitude and higher oscillation frequency. Back-to-back shunt capacitor switching current can be greater than the system short circuit current, as the current is only limited by the impedance between the capacitors. In both cases, transients in current attenuate in several cycles.

A shunt inductor is normally applied for transmission cables or very long lines at transmission level to compensate the shunt capacitance of the cables/lines. Compared with shunt capacitor switching, shunt inductor switching causes less severe current transients as the current through inductors cannot experience a sudden step. The impact on the voltage at the busbar is also small if the system is strong enough. Therefore shunt inductor switching is not discussed in this study.

4.3.5 Tap-changer operation

Tap-changer operation is also a switching event in a transmission system. In practice tap changer starts to operate some time after voltage drop happens. It makes a discrete step and then stays at that level for another time interval before the next change is allowed. As the voltage adjustment for each step is small, the tap-changer operation will normally not lead to any obvious transient in voltage or current waveforms. Therefore it is not taken into account in this study.

Besides the above-mentioned component switchings, the structure of some circuit breakers can also contribute to the transients. Both pre-strike [72] and re-strike [73] of circuit breaker can generate transient current.

Pre-strike may occur when a transmission line is energized at transmission level. A flashover between the moving contacts leads to an arc. If the arc is

maintained until the contacts are closed, the transient will be very similar to a normal switching transient. However with switching of capacitor banks or non-loaded transmission lines, the current may be too small to maintain the arc. The resulting transient may be rather severe in such a case.

Re-strike happens after the circuit breaker has switched off capacitive load at the moment of current zero-crossing. The high dielectric voltage stress that is established half cycle after switching-off can break down circuit breaker contact gap and lead to re-strike. The main consequence of re-strike is high-frequency re-strike current and, in some cases, overvoltage build-up leading to damage to the breaker [38].

In this study, these two phenomena are not separately considered. Instead, the transients due to these phenomena are incorporated into the categories of transients due to unloaded line switching and capacitor switching respectively. Table 4.3.1 summarizes the above information concerning switching currents.

Table 4.3.1 Characteristics of switching current for various events

Sources	Inrush Magnitude*	Inrush Decay Time	Harmonics
Generator-transformer switching	low	long	negligible
Unloaded line/cable energizing	low	short	high-freq
Unloaded transformer energizing	great	long	multi-freq
Loaded transformer energizing	great	short	multi-freq
Capacitor switching	great	short	low-freq

* referred to the steady state operation value

4.4 Detection of switching sources

Different sources generate different voltage and current waveforms. By applying power quality techniques, it is possible to locate the source of a component switching, based on voltage and current data measured locally. As can be seen in the later sections and chapters, knowing the source of component switching will facilitate the quantification of such switching events.

The impact of component switching on protective relays can be in two ways. It might be due to the switching of the component that is protected by the relay (local transients), or due to the switching of the component that is beyond the protection range of the relay (propagated transients). In this thesis, the study is focused on local transients. The discrimination of local transients from propagated ones can be made by checking the operation mode of the circuit breaker (“on” or “off”) for such local component.

In general, the required data for locating the source of component switching are: three phase voltages, three phase currents, three phase circuit breaker operation record. These data are not difficult to obtain from a digital fault recorder or a digital relay itself.

The common characteristics of component switching are:

- there is no current before the transient occurs
- the switching-on of the local circuit breaker can be detected the moment the transient occurs

Apart from these common points, the characteristics of some particular sources are listed in Table 4.4.1.

Table 4.4.1 Application of power quality technique in locating transient sources

	RMS	LS	DFT	Wavelet
	Voltage sag	Decaying DC In current	Considerable 2 nd Harmonics in current	Switching on voltage wave
Generator-transformer unit	—	yes	—	once
Transformer feeder	asymmetrical	—	yes	once
Transmission line	—	—	—	once
Capacitor	—	—	—	2 or 3 times
Induction motor	symmetrical	—	—	once

Voltage sags that arise during transformer and induction motor switchings are shown in Figs. 4.4.1 and 4.4.2.

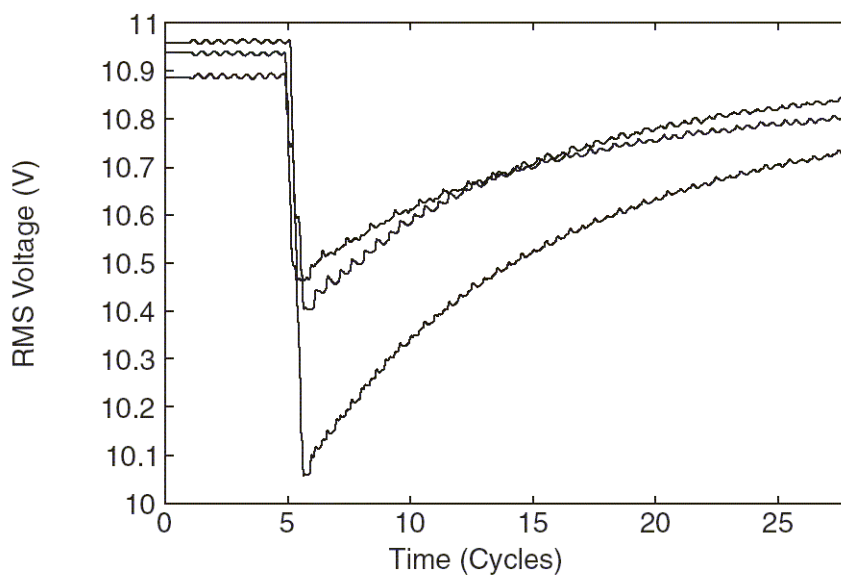


Figure 4.4.1 Voltage sag due to transformer energizing [75]

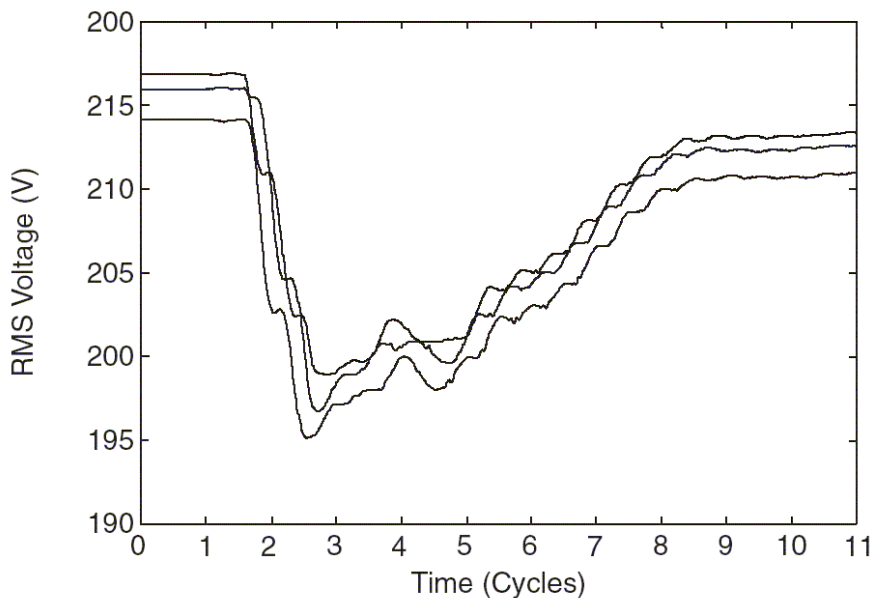


Figure 4.4.2 Voltage sag due to motor starting [75]

In case of transformer feeder switching, the voltage sag is due to transformer magnetic core saturation. As the saturation extent is different for different phase, the resulting voltage sags are asymmetrical. Switching of induction motor can also cause voltage sags on three phases. Unlike in the case of transformer feeder switching, the resulting voltage sags due to induction motor switching are balanced, as shown in Fig. 4.4.2.

In the case of generator-transformer switching, the only transient in voltages and currents is dc component, which decays with time, as shown in Fig. 4.4.3. The waveforms are obtained by simulating generator-transformer switching in a 230 kV system, with a generator of 120MW, 13.8kV connected with a Δ/Y transformer of 150 MVA, 13.8/230 kV.

The saturation current during transformer energizing contains a significant amount of harmonics, among which the 2nd harmonic is dominant. Figs. 4.4.4 and 4.4.5 show an example of the harmonics during transformer switching measured at 11 kV, in voltage and inrush current respectively.

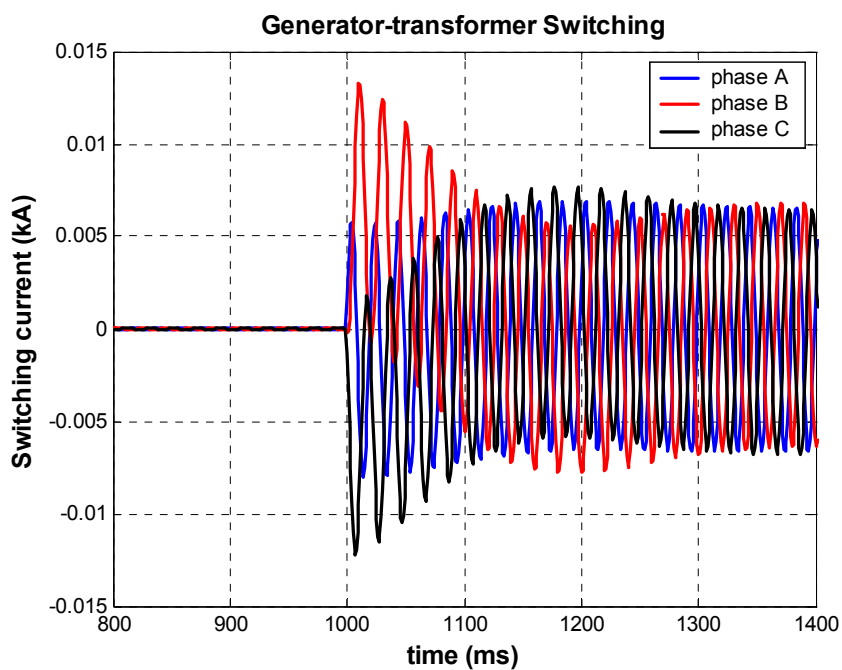


Figure 4.4.3 Current waveforms of generator-transformer switching (Simulation)

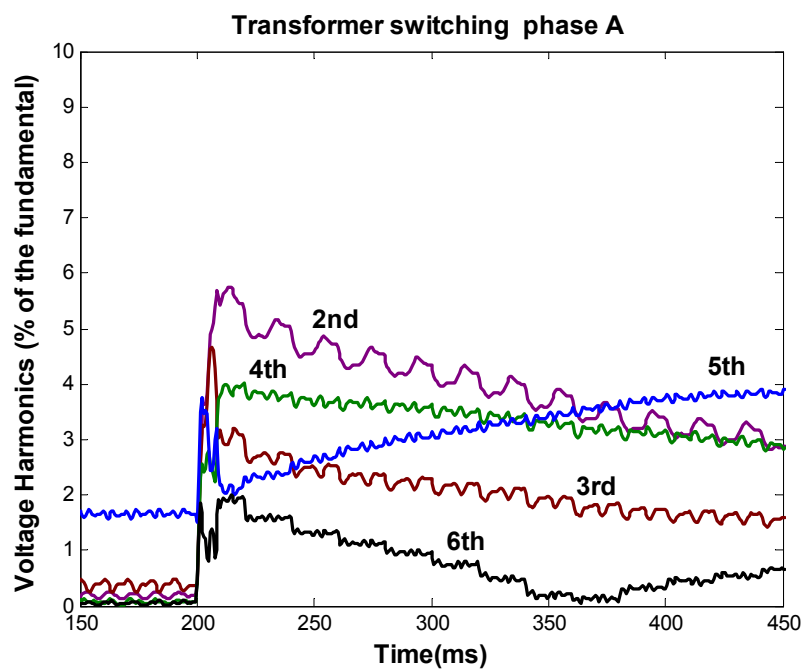


Figure 4.4.4 Harmonics in voltage during transformer energizing (Measurement)

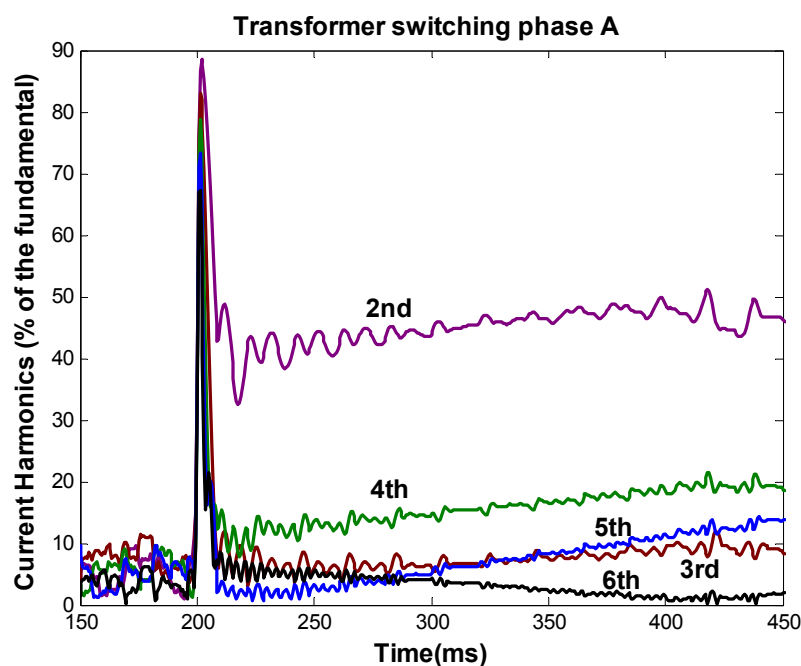


Figure 4.4.5 Harmonics in current during transformer energizing
(Measurement)

In transmission line switching, transient frequencies are generated by traveling waves. The dominant frequency is dependent on line length as well as the source impedance ratio (SIR). In case of unloaded line switching, which is carried out at transmission level, the steady state voltage will lag current by almost 90 degrees, as will be shown later in Chapter 6. In case of loaded line/cable switching, which is carried out at distribution level, there will initially be a sharp drop of voltage waveform toward value zero [5]. The steady state current will be more in phase with the voltage, depending on the power factor of the load.

In capacitor switching, the three phases are often switched on at different moments in order to reduce inrush current and voltage transient. There are two ways of synchronized capacitor switching: 1. switching on three phases one by one following their voltage zero-crossing moments; 2. switching on two phases when they have identical instantaneous voltage values, followed by switching on the third phase at the next voltage zero-crossing. The former

is mainly adopted in grounded capacitor banks while the latter in non-grounded star-connected capacitor banks. By applying discrete wavelet transform technique, it is possible to detect the capacitor switching on three phases. An example of wavelet detection (Low Wavelet Level) of capacitor switching in the second case mentioned above is shown in Fig. 4.4.6 [76].

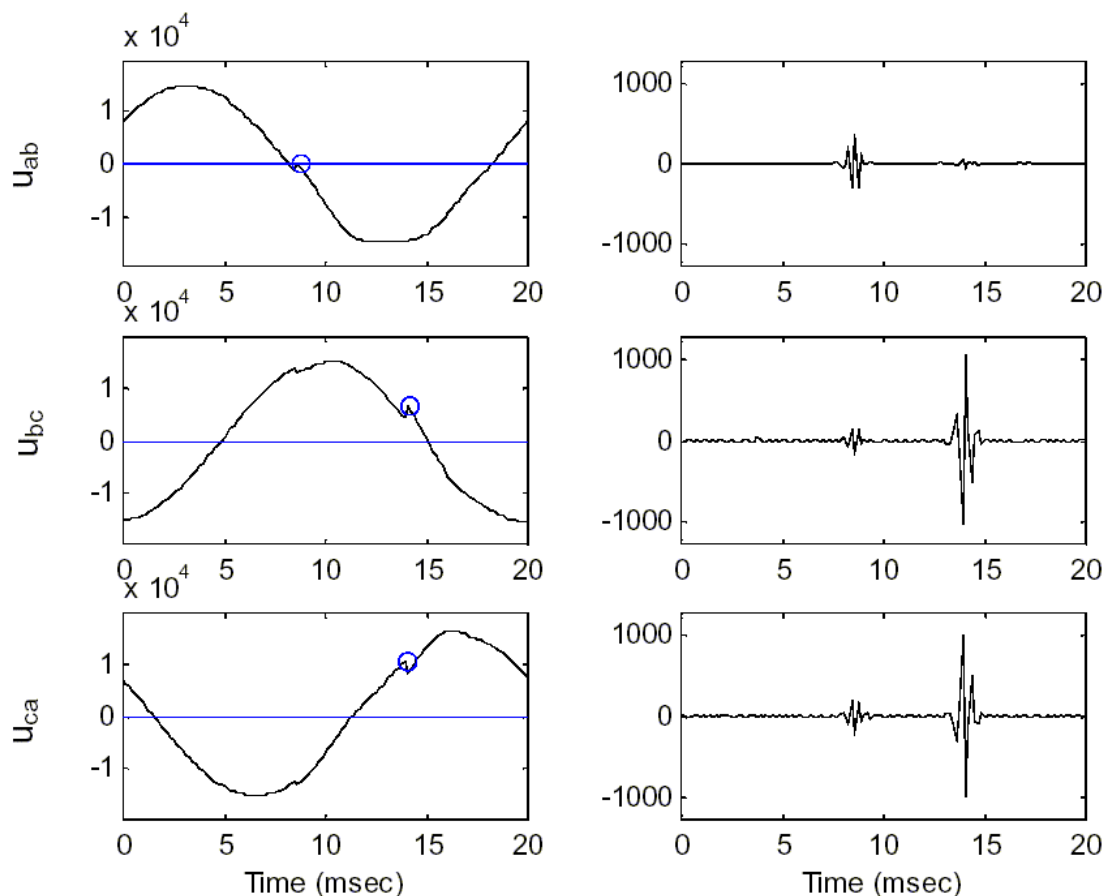


Figure 4.4.6 Wavelet detection of capacitor switching [76] (Measurement)

4.5 Quantification of component switchings

To test different relays under the conditions of component switching, databases that contain all typical component switching events will be helpful. The selection and categorization of the elements in such databases should be based on quantification of component switching events. For each type of relay, a unique database is needed. For the relays that are of the same type

but of different relay algorithms, the database for such relay type can be used to test the relative performance of the relay algorithms.

As mentioned in Chapter 2, this study is focused on the impact of component switching on overcurrent relays and impedance relays. When we consider the protection of the switched component, overcurrent protection may be present with any component whereas impedance protection is only present with lines or cables. These relays protect the components where the majority of faults occur. Since both of these two types of relay are based on a “range setting”: either overcurrent or underimpedance, this makes them more sensitive to events originating outside of the “zone-to-be-protected”. The way to quantify switching transients detected by these two types of relay is discussed below.

4.5.1 Overcurrent relays

Starting from the magnitude and decay time of the switching current, a matrix that contains all the typical switching current data can be set up as follows:

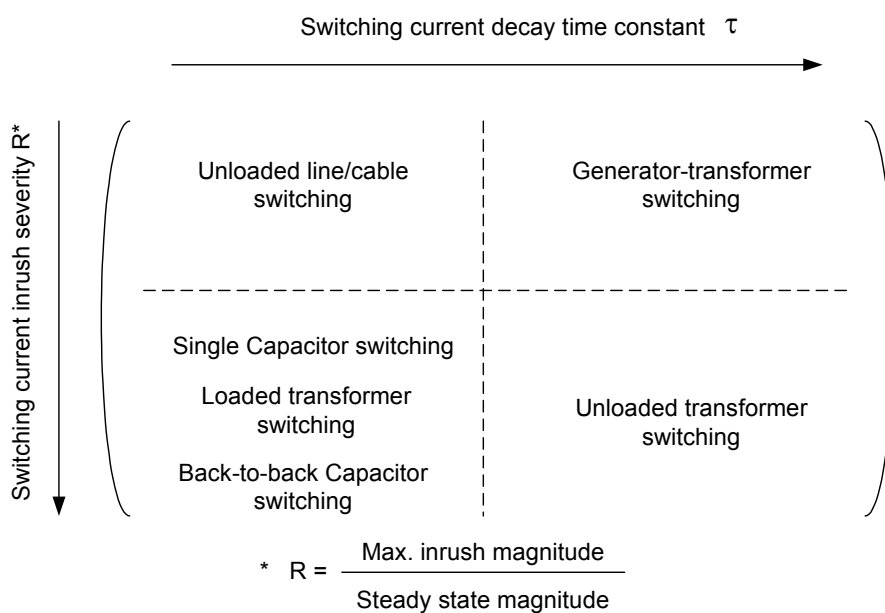


Figure 4.5.1.1 Component switching test matrix

This matrix can be interpreted as a database for testing relays under component switching events, if there is enough data for each particular case in the matrix. It is set up intuitively in the viewpoint of current waveforms. Bear in mind that the current waveforms here refer to the output of relay filters, i.e. the waveform output after being processed by relay filters.

In the above diagram, two concepts are proposed: inrush severity R and inrush decay time τ . The former is defined as the ratio of the maximum value of the relay filter output and the rated current. The rated current is used as a reference because relay thresholds are normally set according to the rated current. The inrush decay time τ is defined as the time constant of the switching transient, assuming that the transient will decay exponentially. The combination of these two factors disclose the potential risk of relay mal-trip in case of component switching transients.

Through simulation, a large number of component switching transient data can be generated at different combinations of component parameters, i.e. at various switching severity and decay time. The decay time can be defined in many ways. It can be defined as the elapsed duration between the inrush starting moment and the moment when the current waveform reaches its new steady state. It can also be defined as the decay time constant of the filter output.

All component switching events can then be plotted as points in a two-dimensional severity-time plane. Different sets of transient data are distributed over different regions. The union of all these sets forms the zone for relay mal-trip, as shown in Fig. 4.5.1.2. Such a union stands for all the switching transients that should not trip a relay.

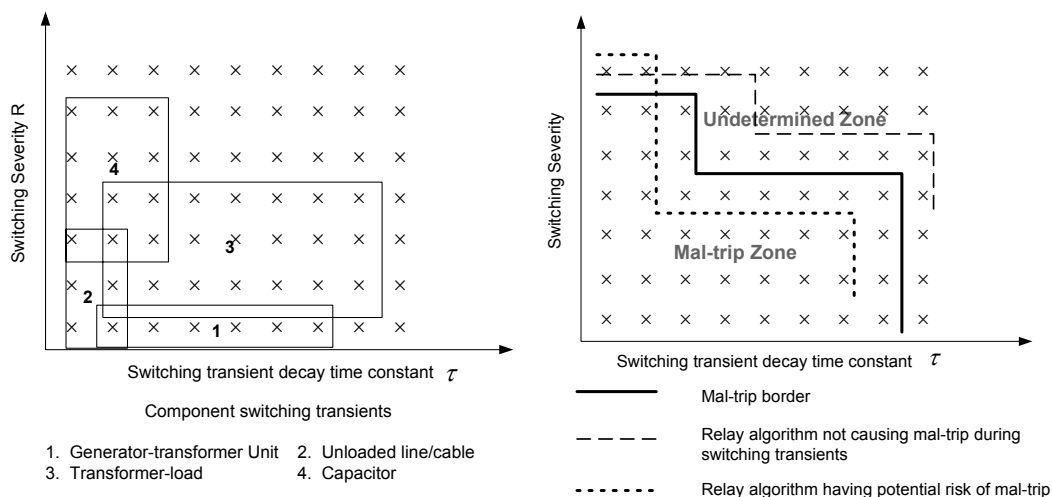


Figure 4.5.1.2 Union of component switching events

However, such an intuitive quantification method has the following shortcomings:

- a) A relay does not necessarily have to be imposed to all the component switching transients. The switching transients it might face are much dependent on its location. Instead of mixing all the switching transients in one database as shown in Fig. 4.5.1.2, separate database are needed for switching transients of different sources.
- b) The inrush severity R and decay time constant τ stand for partial and approximate description of the switching transient. This is actually an observation of switching transients in the viewpoint of *relay filter algorithm*, but not in the viewpoint of *relay setting*. As the output of a relay is dependent on the measured signal and relay setting, only the observation in the viewpoint of relay setting can really demonstrate the possible reaction of a relay in case of such switching transients.

The problem in item a) can be fixed by introducing detection of switching sources (as described in the previous section). Separate databases for different switching source should be set up.

The problem in item b) raises a question on how to generate a switching transient database that is suitable to practical application. The database proposed in Fig. 4.5.1.2 just tells that a relay should have immunity from some switching transients. However, it does not tell how dangerous these switching transients are. The severity of such switching transients can only be evaluated by taking into consideration the relay setting.

Therefore a new approach based on relay setting is essential in quantifying switching transients. This will be done in Chapter 5.

4.5.2 Impedance relays

Impedance protection takes positive sequence component into account when measuring impedance.

The decision-making of a impedance relay is based on the impedance value the relay detects. In steady state any relay filter can measure the correct impedance observed from the relay terminal. But during a transient, the impedance measurement is unpredictable and may show irregular variation. This will affect the decision-making of a relay and potentially lead to a mal-trip, if the transient causes much reduced filter output (impedance estimates) during this period and the decision-making cycle is short.

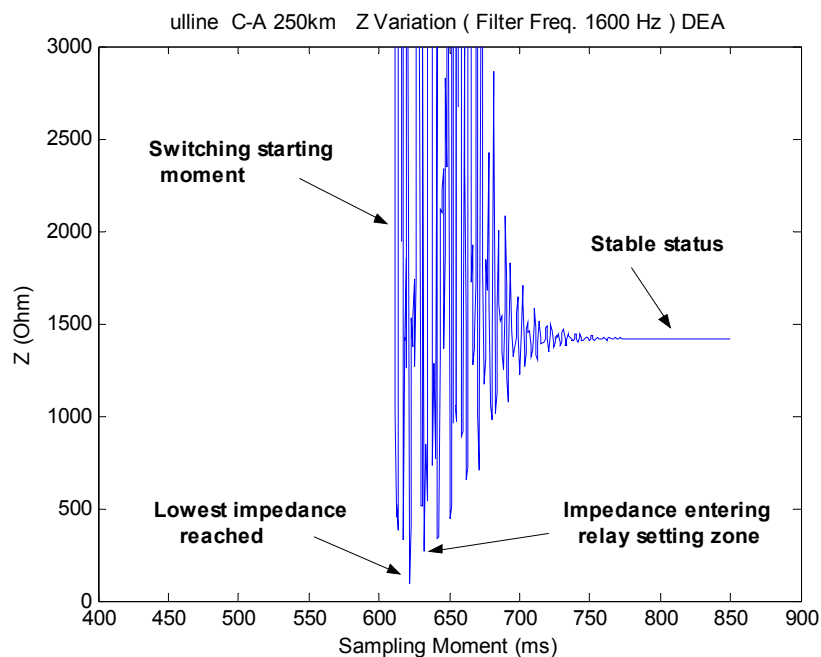
The following case study shows as an example the impedance estimation obtained by the relay filter during the switching of an unloaded 130 kV line. It can be observed that the estimated impedance shows much smaller value during the switching. In the example the lowest estimated impedance during the transient is as low as 62 Ohm, while its steady-state value (after several cycles) is around 1400 Ohm. This simulation is done on a transmission line

of 250 km (in parallel with another transmission line of the same length) in a 130 kV system. The per unit length reactance along the transmission lines is 0.4632 Ohm/km. The shunt conductance is 10^{-7} Mho/km. A series compensated capacitor is installed in the middle of transmission line at 70% compensation. The impedance trace detected by relay filter (DEA) as well as the impedance points near the origin are shown in Fig. 4.5.2.1.

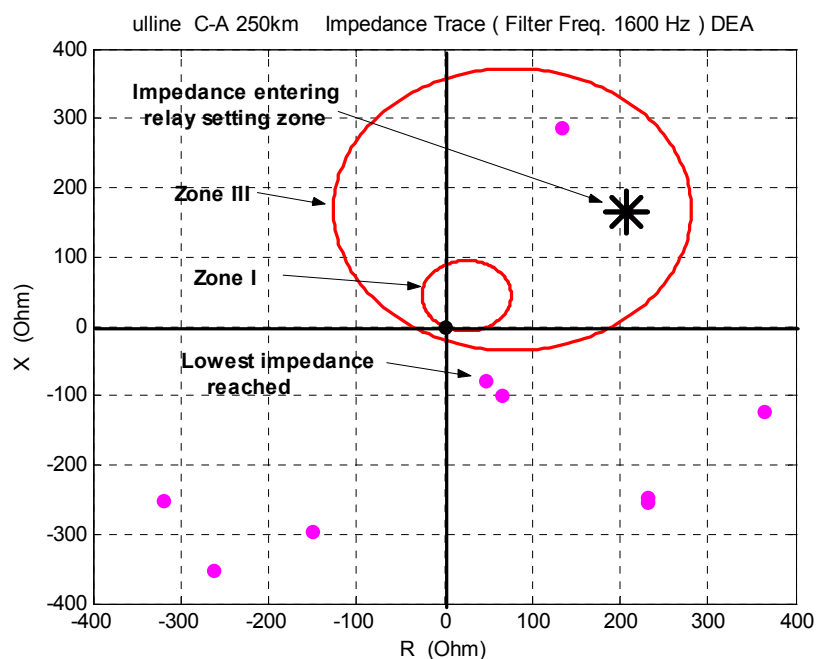
However, unlike the case for overcurrent relays, the trip criterion for impedance relays is two-dimensional: it uses not only the absolute value of the apparent impedance, but also its phase angle.

In such a case, the impact of switching transient on impedance relays should be evaluated by taking into consideration the impedance relay setting. As the setting zones of most impedance relays are not symmetrical to the origin, the detected impedance points whose absolute impedance values are identical may have different impact severity on impedance relays: the ones closer to the setting zone are of higher potential risk to cause relay mal-trip. As shown in Fig. 4.5.2.1, the impedance point closest to origin does not necessarily need to be the one that is closest to the relay setting zone, i.e. the most dangerous one to cause relay mal-trip.

The approach based on relay setting is introduced in Chapter 6 to quantify the switching transient severity and assess the risk of mal-trip.



(a) Impedance trace



(b) Zoomed region for the lowest impedance

Figure 4.5.2.1 Impedance trace during unloaded line switching

Chapter 5 Impact of Component Switching on Overcurrent Relays

This chapter seeks to study the transient currents in the viewpoint of overcurrent relays. As proposed in Chapter 4, quantification is to be made based on the detrimental effect of the transients on relays, i.e. the potential risk of relay mal-trip caused by these transients. This requires consideration of relay setting. A characteristic curve is to be developed for each transient current to assess its impact on parameter selection of each type of relay characteristic. Collection of these curves leads to formation of a transient current database for overcurrent relays.

In normal case, definite-time-delayed overcurrent relays, inverse time overcurrent relays and thermal overcurrent relays are the main forces of single-element type relay protection.

When a transient current is detected by an overcurrent relay, the only information that the relay can get is the signal waveform of the current. To classify the transient currents in term of relay mal-trip impact, the analysis should start from relay operation and detection principles.

In the later sections, the term “overcurrent relays” refer to definite-time-delayed, inverse-time-delayed and thermal overcurrent relays.

5.1 Operation principles of overcurrent relays

5.1.1 Definite-time-delayed overcurrent relays

The operation rule for definite-time-delayed overcurrent relays can be expressed in the following way:

$$T = \frac{2T_s}{1 + \text{sgn}(I - I_s)} \quad (5.1.1.1)$$

where

- T relay operation time
- I_s current setting threshold
- I current detected by relay (after relay filtering)
- T_s relay delay setting
- sgn sign function (sign taken from the result, value being 1)

Equation (5.1.1.1) means that:

$$T = \begin{cases} \infty & I < I_s \\ T_s & I > I_s \end{cases}$$

If we define a function $f(t)$ for the denominator in the above equation:

$$f(t) = \frac{1 + \text{sgn}(I(t) - I_s)}{2} \quad (5.1.1.2)$$

and assign t_1 as the moment when $I(t)$ exceeds I_s (Note: t_1 can be more than one moment), then it is clear that to trip the definite-time-delayed overcurrent relay, the following requirement must be met:

$$\int_{t_1}^{t_1+T} f(t)dt \geq T_s, \text{ for } I(t) > I_s, t \in [t_1, t_1 + T] \quad (5.1.1.3)$$

The simplified expression of above equation is actually $T \geq T_s$, for $I(t) > I_s, t \in [t_1, t_1 + T]$. In order to facilitate the explanation of transient quantification approach later in general sense, we keep the form as shown in (5.1.1.3).

5.1.2 Inverse-time-delayed overcurrent relays

According to IEC and IEEE standards [77][78], the characteristic of inverse-time overcurrent relays (excluding induction type) can be depicted by the following expression:

$$T = \frac{C}{\left(\frac{I}{I_S}\right)^\alpha - 1} \quad (5.1.2.1)$$

- where
- T relay operation time
 - C constant for relay characteristic, proportional to the time multiplier setting
 - I_S current setting threshold
 - I current detected by relay (after relay filtering), $I > I_S$
 - α constant representing inverse-time type, $\alpha > 0$

When $I < I_S$, T becomes infinite long.

If we define a function $f(t)$ for the denominator in the above equation:

$$f(t) = \left(\frac{I(t)}{I_S}\right)^\alpha - 1 \quad (5.1.2.2)$$

and assign t_1 as the moment when $I(t)$ exceeds I_S , then it is clear that to trip the inverse-time overcurrent relay the following requirement must be met

$$\int_{t_1}^{t_1+T} f(t)dt \geq C, \text{ for } I(t) > I_S, t \in [t_1, t_1 + T] \quad (5.1.2.3)$$

where T is the time during which $I > I_S$

Mathematically speaking, (5.1.2.3) can have no solution, one solution or multiple solutions, depending on the coordination between the function in (5.1.2.2) and the relay preset values of C and I_S . If C and I_S are set too high,

there is no solution for (5.1.2.3), which means the overcurrent relay will not operate in this case. If $f(t)$ shows fluctuation in its waveform, it is possible to adjust C and I_s to find more than one time interval during which (5.1.2.3) holds. In this case there are multiple solutions, i.e. the relay might trip more than once.

By assigning different values to α and C , there are different types of inverse characteristics. Table 5.1.2.1 shows the definitions of various types by IEC and IEEE respectively.

Table 5.1.2.1 Parameters for various types of inverse characteristics

	α		C^*	
	IEC	IEEE	IEC	IEEE
Standard Inverse (SI)	0.02	0.02	0.14	0.0515
Very Inverse (VI)	1	2	13.5	19.61
Extreme Inverse (EI)	2	2	80	28.2
Long Inverse (LI)	1	—	120	—

* at 1.0 time multiplier setting, in practical relay, value C can be adjusted to be multiple of the value listed in this table

Fig. 5.1.1 shows a typical overcurrent relay (MCGG type of GEC-Alstom) used in practical engineering. The inverse type and time multiplier are adjustable on the surface of the relay.



Figure 5.1.1 MCGG type overcurrent relay

Different types of inverse characteristics are applied based on the type of protected equipment as well as system structure. In the later sections their application in the cases of the aforementioned component switchings will be discussed.

5.1.3. Thermal overcurrent relays

According to the IEC standard for thermal electrical relays [79], the relay characteristic is defined as follows:

$$T = \tau \ln \frac{I^2}{I^2 - (K * I_s)^2} \quad (5.1.3.1)$$

- where
- T relay operation time
 - τ heating time constant
 - I_s current setting threshold
 - I current detected by relay (after relay filtering), $I > I_s$
 - K constant representing the type of thermal relay

The above expression is called “cold” relay characteristics, which means that the motor is not running before relay detection happens. This is the case for motor starting.

Similarly as in the case of time-delayed overcurrent relay, let

$$f(t) = \left(\ln \frac{1}{1 - \left(K * \frac{I_s}{I(t)} \right)^2} \right)^{-1} \quad (5.1.3.2)$$

Then to trip a thermal relay the following expression must hold:

$$\int_{t_1}^{t_1+T} f(t)dt \geq \tau, \text{ for } I(t) > I_s, t \in [t_1, t_1 + T] \quad (5.1.3.3)$$

where T is the time during which $I > I_s$

The above expression is similar to (5.1.2.3). In (5.1.3.3), both τ and K are adjustable. K is determined by the type and construction of the motor.

5.2 Determination of the constants for different types of overcurrent relay

As demonstrated in the previous section, inverse-time-delayed and thermal overcurrent relays can have different characteristics at different type constant α or τ . To study the response to current by a relay, its operation characteristics need to be fixed first.

Table 5.2.1 lists the type of overcurrent relay for different power system components, which are the sources of non-fault switching [47][85][86][87][88].

Table 5.2.1 Overcurrent relay type for power system components

	Overcurrent relay type
Generator-transformer unit	Long Inverse
Transformer feeder	Extremely Inverse
Transmission line (short)	Definite Time
Transmission line (long)	Standard Inverse
Capacitor	Extremely Inverse
Induction motor	Thermal

The overcurrent relay for generator-transformer unit is actually a voltage controlled time delayed inverse relay. It works as back-up protection for the neighboring transmission lines. The characteristics of such overcurrent relay can be either standard inverse or long inverse, depending on the voltage detected at terminal busbars. During a fault the terminal voltage becomes low, the overcurrent relay is of standard type. But if the terminal voltage is around the nominal value, such as the case of normal switching of the unit, long inverse characteristic is adopted. Therefore long inverse characteristic is considered in this project.

Extremely inverse characteristics are adopted for transformer feeders. It is desirable to set the overcurrent relays as sensitive as possible in the case of a transformer feeder. Also it is required that the overcurrent relay should protect a transformer against thermal damage due to fault current passing through the transformer. In case that transformer capacity is very small, fuses are used to protect the transformer feeder.

Standard inverse characteristics are adopted for long transmission lines. Long transmission lines here refer to the lines whose system impedance ratio SIR is

less than 2. This is in accordance with the requirement of fast fault clearing at transmission level.

Definite-time-delayed characteristics are adopted for short transmission lines. Short transmission lines here refer to those lines whose system impedance ratio SIR is greater than 2. The reason of applying definite-time-delayed characteristics is that for short lines, there is no substantial reduction of relay operating time as the fault is moved from remote end to near end if inverse-time-delayed characteristics are applied. Compared with inverse-time-delayed overcurrent relays, definite-time-delayed overcurrent relays are also more economic.

Capacitor is normally equipped with internal fuse for its protection. But there are also cases that it is protected by overcurrent relay. If it is protected by a relay, an extremely inverse characteristic is needed for fast trip when the current is high.

Choosing a thermal relay in the case of induction motor is in accordance with the motor starting characteristic curve. In such a case the relay should function as an overload protection. The overload is detected in the form of overheating, which is treated by thermal relays.

Therefore if the source of a non-fault switching is known, the overcurrent relay characteristics can be fixed by assigning the α or τ parameter that corresponds to the type of the non-fault switching source. In the case of transmission lines, two different characteristics are adopted for lines of different lengths. This is implemented in practice by combining the two characteristics in a relay of IDMTL type (inverse definite minimum time lag). This relay shows definite-time-delayed characteristic for large overcurrent

(near end) and standard inverse-time-delayed characteristic for small overcurrent (remote end).

5.3 Impact severity curve

To compare the effect of transients on overcurrent relays at different input currents, it is necessary to quantify the impact severity. To quantify the impact severity, it is necessary to know the current after relay filtering and how the relay interprets such a current signal.

5.3.1 Current after relay filtering

In power systems, the current after relay filtering in time domain can be one of the following typical waveforms:

1. Straight line
2. Fluctuating curve
3. Attenuating curve

The first case represents normal sinusoidal signals that consist of stationary fundamental and harmonic components, at steady state of power systems. The effective value in such a case is the square root of the sum of the square of each component. Since $f(t)$ is constant, relay operation time can be calculated directly from (5.1.2.1) and (5.1.2.3). There is only one solution in this case.

The second case refers to the situation when there is intermittent load. The current waveform changes irregularly, leading to fluctuations of the effective value. Theoretically if T_s , C or τ are small enough, (5.1.1.3), (5.1.2.3) and (5.1.3.3) can yield multiple solutions, causing repeated trip of relay

(assuming automatic resetting by overcurrent relay itself in case of low input current).

The third case corresponds to the situation when there is transient inrush current, as discussed in the previous section. The current magnitude increases at the switching instant and then decays with time. During the process the effective value might not only decay, but also show fluctuation in some cases, such as during transformer autoreclosing. This is due to the changing harmonics in the current. Since the effective value in time domain keeps on changing, integration calculation in (5.1.1.3), (5.1.2.3) and (5.1.3.3) is needed for getting the relay operation time. Theoretically, if the fluctuation magnitude is high enough, more than one solution is possible for (5.1.1.3), (5.1.2.3) and (5.1.3.3).

The current after filtering is observed by the overcurrent relay detection circuit or algorithm. The following section studies the detection principle of overcurrent relays and propose a new approach to interpret the processed current.

5.3.2 Impact severity curve — way to interpret the processed current

In practical engineering, the rated current on the secondary side of the current transformer is either 1 Ampere or 5 Amperes, regardless of the rated current on the primary side. In normal operation of power systems, the current on the secondary side is around such rated value. Because of this, the relay threshold value I_S is set starting from the rated value.

As discussed before, an input current signal might cause one or more relay trips, depending on particular cases. If the input current is due to switching at

normal operation, a trip in such situation is a mal-trip. It is not the theoretical number of mal-trips, but the fact that mal-trip happens that matters. Therefore one solution in (5.1.1.3), (5.1.2.3) or (5.1.3.3) is enough.

From (5.1.1.3), (5.1.2.3) and (5.1.3.3) it is clear that for each T_s , C or τ , there is always one unique I_s that makes the equation just holds. In other words, there will be no solution if I_s is smaller. This can be illustrated by Fig. 5.3.2.1, where T is just equal to relay delay setting T_s , and Fig. 5.3.2.2, where the shadowed area formed by I_s and $f(t)$ is just equal to C or τ . It means that at such threshold setting, a relay is at its critical border of tripping.

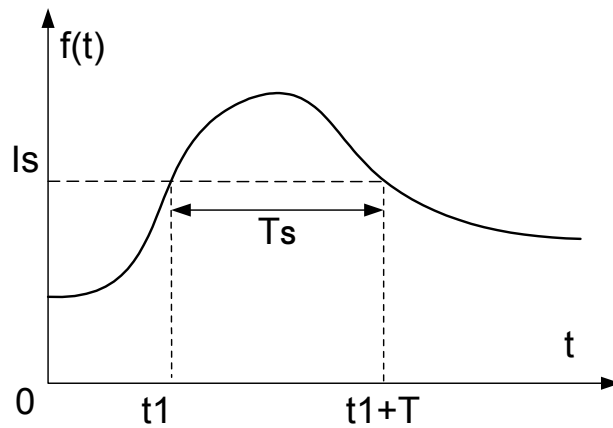


Figure 5.3.2.1 Current setting for critical border of relay trip (definite-time-delayed overcurrent relays)

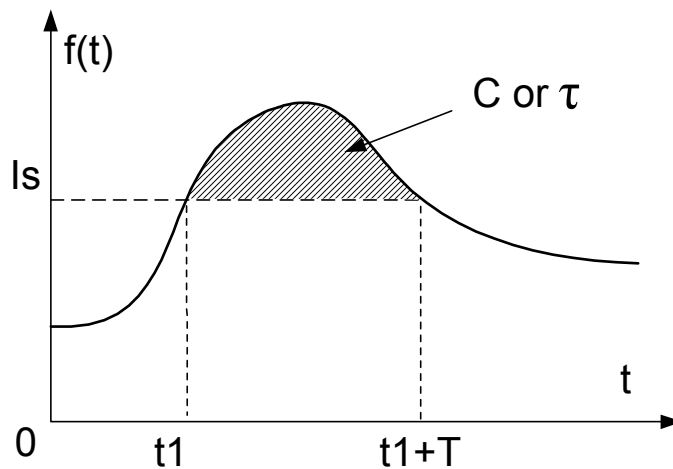


Fig. 5.3.2.2 Current setting for critical border of relay trip (inverse time and thermal overcurrent relays)

By varying T_s , C and τ from 0 to infinite, a setting value I_s as a function of T_s , C or τ results. Plotting the variation of threshold setting I_s versus constant T_s , C or τ yields the impact diagram as shown in Fig. 5.3.2.3. This diagram demonstrates the requirement on the coordination between threshold setting and characteristic constant. To avoid relay trip due to the studied input current, the setting point (for both current threshold and fault clearing time) should be above the curve in the diagram. Note that increasing T_s , C or τ corresponds to increasing fault clearing time.

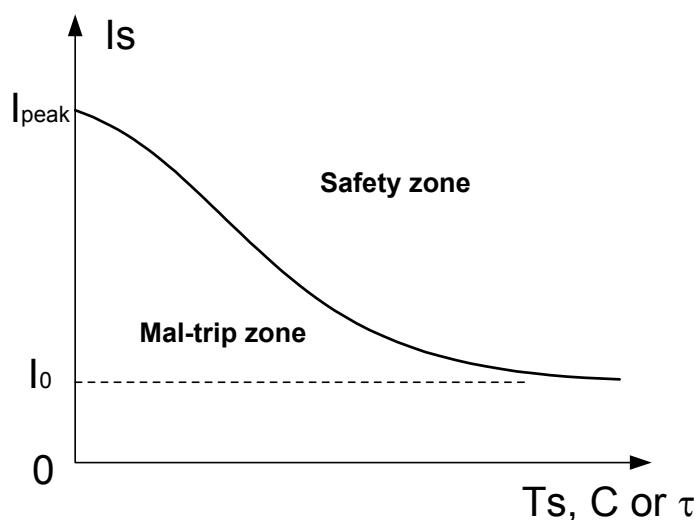


Fig. 5.3.2.3. Impact curve for overcurrent relay due to transient current

Fig. 5.3.2.3 also shows that at $T_s=0$, $C=0$ or $\tau=0$, the curve reaches its peak point. This actually corresponds to the highest value of the input current signal observed by the relay (after relay filtering). With the characteristic constant T_s , C or τ increases, the threshold setting I_s gradually moves to a stable value I_0 . Such stable value is the current magnitude observed by the relay at steady state after the transient.

Generally there are three typical conditions for the impact curve, as shown in Fig. 5.3.2.4. Curve a shows the case when the current magnitude observed by the relay is a straight line. This corresponds to the situation when the input

current signal is stationary. In such a case, the impact severity curve is a straight line. Curve b represents the case in which the current magnitude observed by the relay is fluctuating. This can be due to either the input current has intermittent characteristic, or the input current is stable but contains some components that do not have stable frequency response when passing through the digital filter. In such a case, the impact curve is at higher threshold setting I_S when T_S , C or τ is small, and quickly reaches stable value with increasing T_S , C or τ . Depending on the magnitude of fluctuation observed by the relay, such attenuation duration has different length. The greater the fluctuation magnitude, the longer the duration is. Curve c is for the transient input currents. In normal case it has obviously higher threshold setting at low characteristic constant T_S , C or τ . The threshold setting decays with increasing T_S , C or τ increases. The duration is determined by the transient duration of the input current.

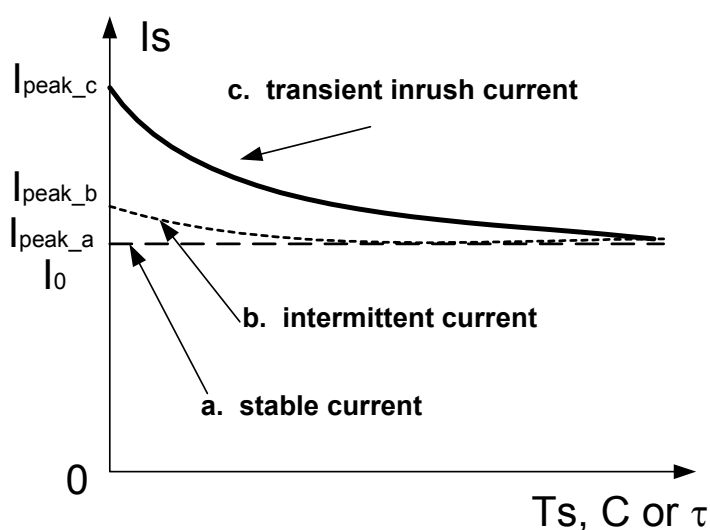


Fig. 5.3.2.4. Impact curves for different current waveforms

So the impact diagram can tell:

- the relay mal-trip zone due to the studied current
- the peak value of the studied current
- the current magnitude at steady state

Based on the impact curves, it is possible to compare among different input currents their impact on relay operation. If one impact severity curve is above another one, as shown in Fig. 5.3.2.5(a), it can be concluded that the current in the former case has more impact on overcurrent relays than that in the latter case. If there is intersection between the two curves, as shown in Fig. 5.3.2.5(b), it means that the impact on relays in one case can be better or worse than the other case, depending on different characteristic constant T_s , C or τ .

In the case of inverse-time-delayed overcurrent relays, this is in practice related to the structure of the distribution power system. Fig. 5.3.2.6 shows the meaning of C for relay characteristics at different location. For coordination purpose, a relay at downstream has a lower C for its characteristic. Therefore the impact on relays is different at different relay locations.

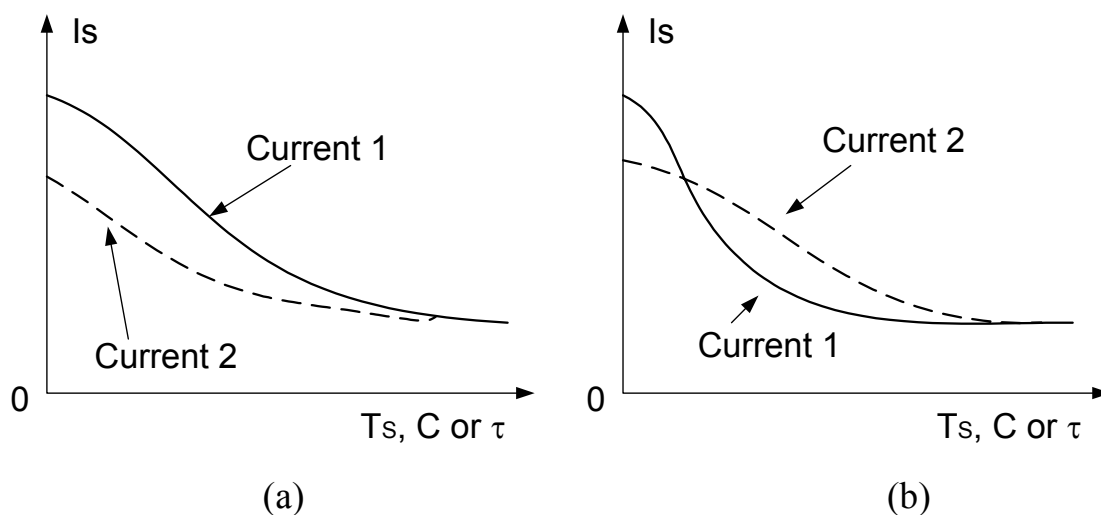


Fig. 5.3.2.5 Comparison between different impact curves

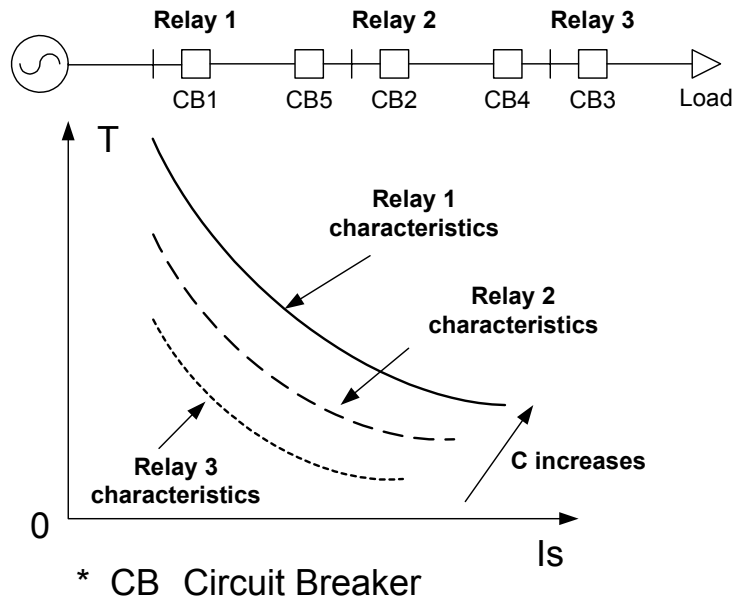


Fig. 5.3.2.6 Meaning of constant C in overcurrent relay coordination

In a more general sense, an impact curve can be transformed to an impact severity curve by having all the I_s value divided by I_0 , as shown in Fig. 5.3.2.7. The purpose of doing this is to create a unique platform for comparison between two different cases, whose steady state current values are not the same. In such way it is possible to check the relative impact severity of a transient current.

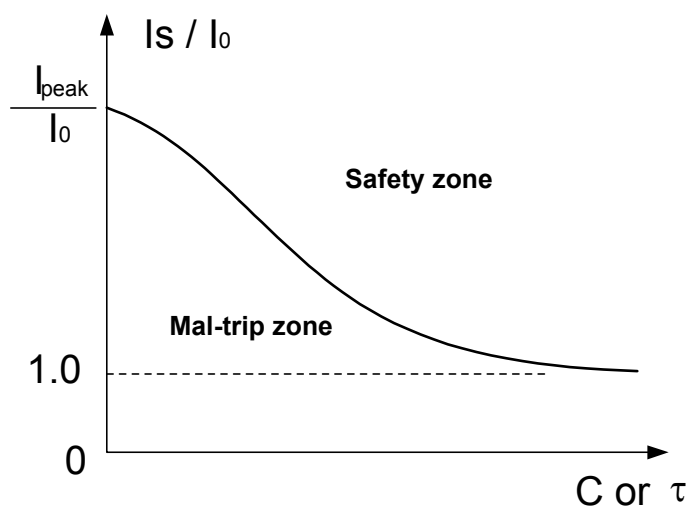


Figure 5.3.2.7 Impact severity curve

However, as mentioned in the introduction section, different power system components require different types of inverse-time-delayed or thermal overcurrent characteristics, i.e. they have different constant α or K and different limit on constant C or τ . In such a case, the impact severity curve should be made based on different combination of these parameters. To do that, it is first necessary to understand the source of the studied input current. Knowing the source of the switching induced current, the above overcurrent characteristic parameters can be determined and the impact severity curve can be worked out accordingly.

5.4 Case studies of impact severity curves

In all the following case studies, overcurrent relays are simulated as digital relays with DFT 1-cycle algorithm, at sampling frequency 1600 Hz. Before being processed by DFT algorithm, an anti-alias filter with a cut-off frequency of $1600/3 = 533$ Hz is simulated to remove the high frequency components.

Case 1 Transformer energizing (Measurement)

Figs.5.4.1 and 5.4.2 show the current waveforms (before and after relay filtering) during transformer energizing. The impact severity curve based on the afore mentioned approach is shown in Fig. 5.4.3.

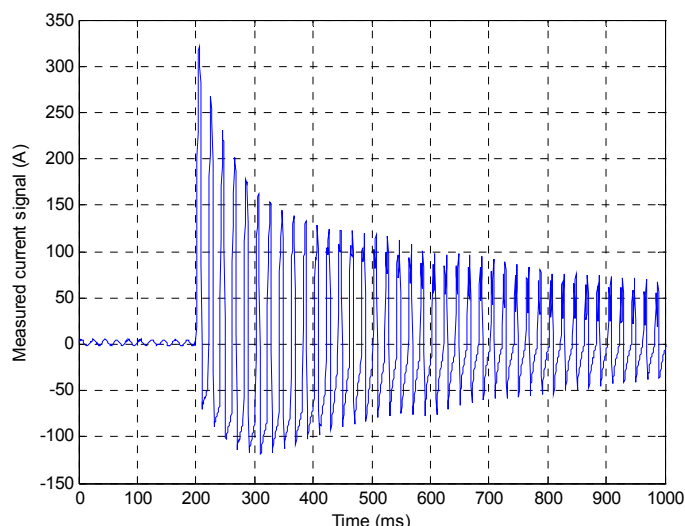
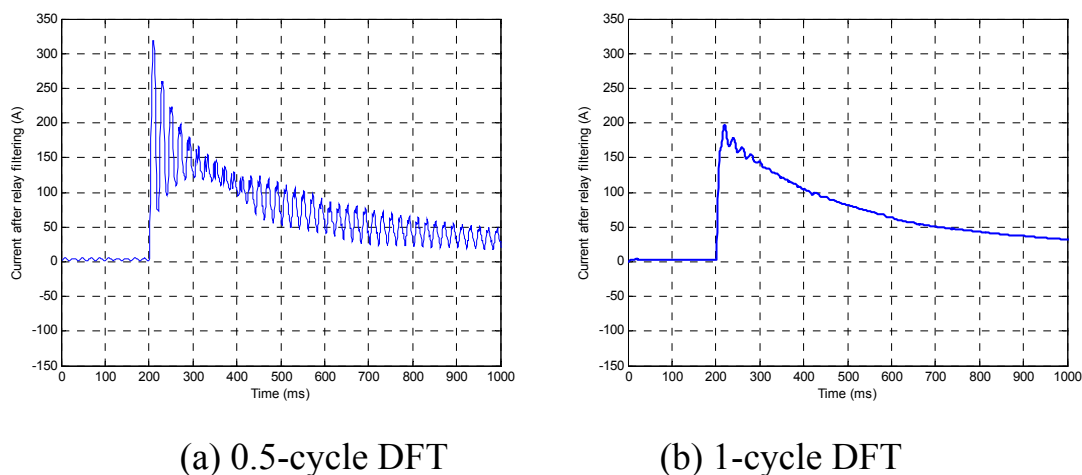


Figure 5.4.1 Current waveforms during transformer energizing

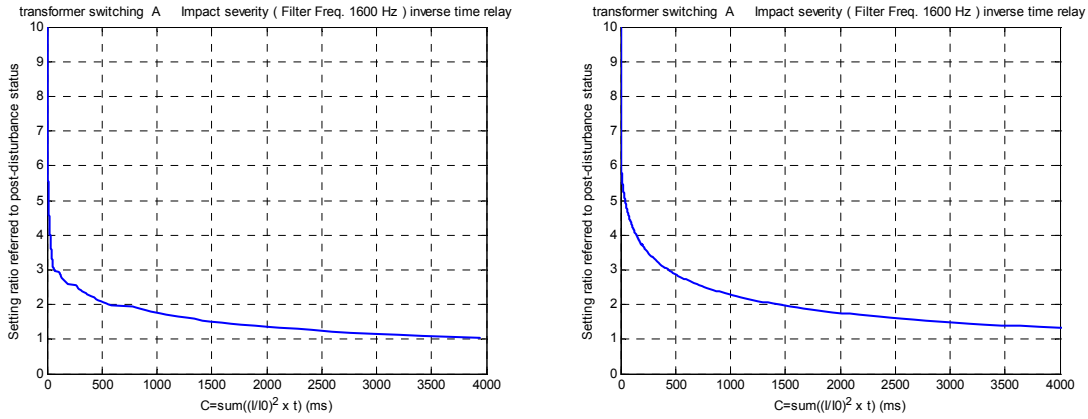


(a) 0.5-cycle DFT

(b) 1-cycle DFT

Figure 5.4.2 Current after relay filtering for transformer energizing

The interpretation of Fig. 5.4.3 (b) is shown in Fig. 5.4.4. According to IEC standard as shown in table 5.1.2.1, the value of C at 1.0 time multiplier setting is 80 for extremely inverse overcurrent relays. Taking a MCGG overcurrent relay as an example, the minimum value of the time multiplier is 0.025, which means that $C = 0.025 \times 80 = 2 \text{ s} = 2000 \text{ ms}$.



(a) 0.5-cycle DFT

(b) 1-cycle DFT

Figure 5.4.3 Impact severity curve during transformer energizing

From Fig. 5.4.4 it can be observed that to avoid mal-trip during transformer switching, the setting value of the overcurrent relay should be at least more than 1.75 times the post disturbance current value.

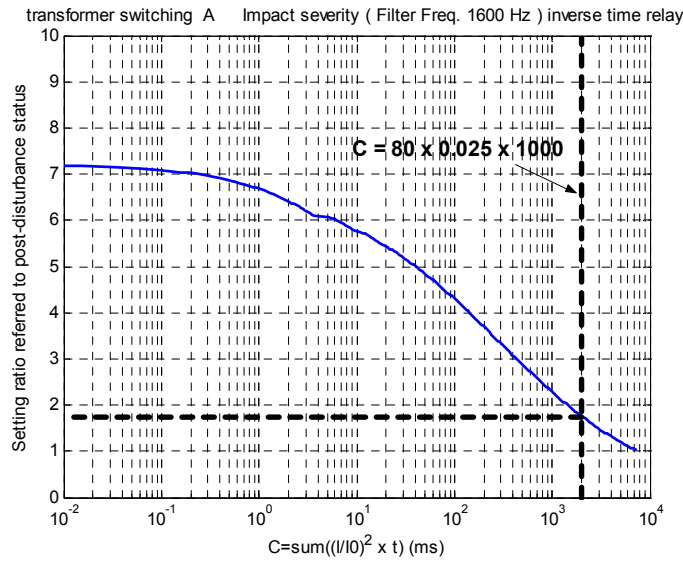


Figure 5.4.4 Selection of setting value based on impact severity curve

Also from Fig. 5.4.2 it can be observed that due to the presence of 2nd harmonics in current waveform, the current after relay filtering shows higher magnitude. Because of this, the impact severity curve in case of 0.5 cycle DFT is below the one in case of 1 cycle DFT. However if the recording window is long enough until the disappearance of the harmonics, the results will be different.

Case 2 Capacitor switching I (Measurement)

Capacitor switching transient waveforms before and after relay filtering are shown in Fig. 5.4.5 The measurement was made at a 10 kV distribution substation.

From the current waveform it is clear that this is not a transient due to the switching of the protected component, but a transient propagating from elsewhere. Although there is obvious rise in current magnitude, this effect is almost completely eliminated after relay filtering. The impact severity curve shows that this switching transient does not cause any potential risk of relay mal-trip.

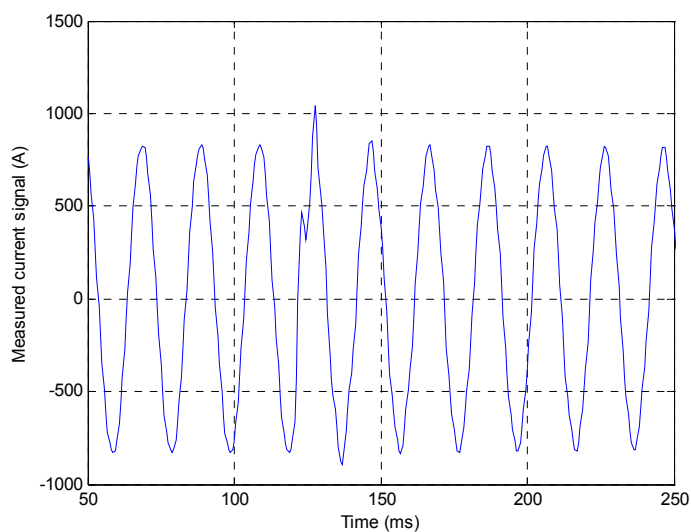
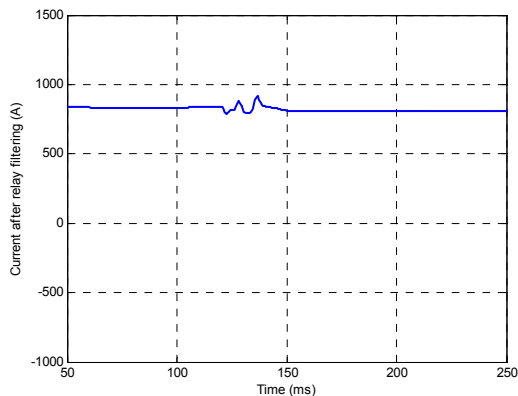
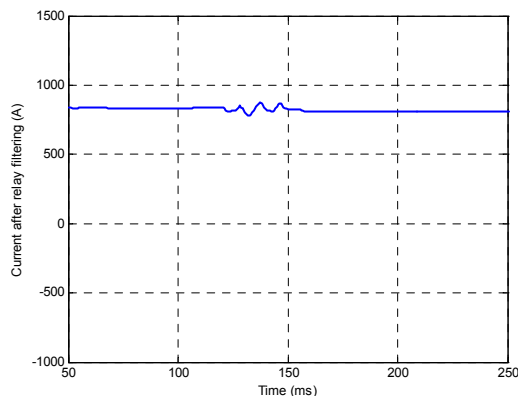


Figure 5.4.5 Current waveforms during capacitor switching

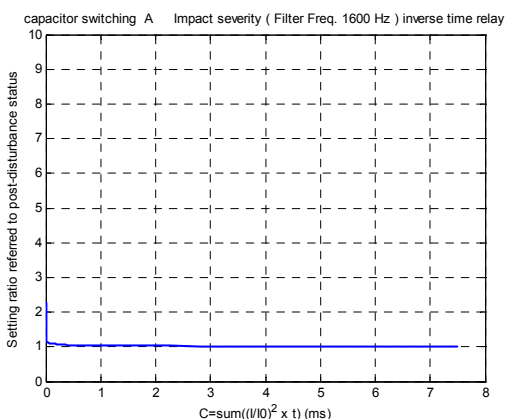


(a) 0.5-cycle DFT

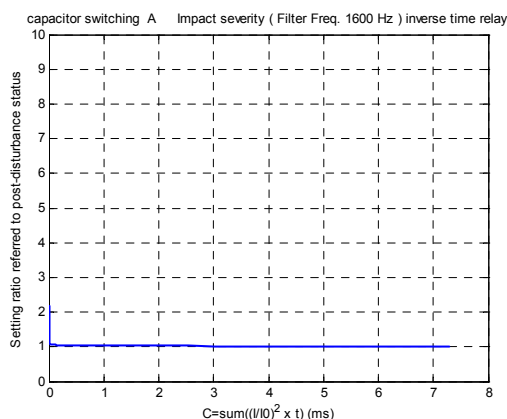


(b) 1-cycle DFT

Figure 5.4.6 Current after relay filtering for capacitor switching



(a) 0.5 cycle DFT



(b) 1-cycle DFT

Figure 5.4.7 Impact severity curve for capacitor switching

Case 3 Transmission line switching (Simulation)

Unloaded transmission line switching is simulated using EMTDC. The line length is 250 km at 130 kV voltage level, with 70% series capacitor compensation in the middle of the line. The transmission is modeled to be in parallel with another line of the same length.

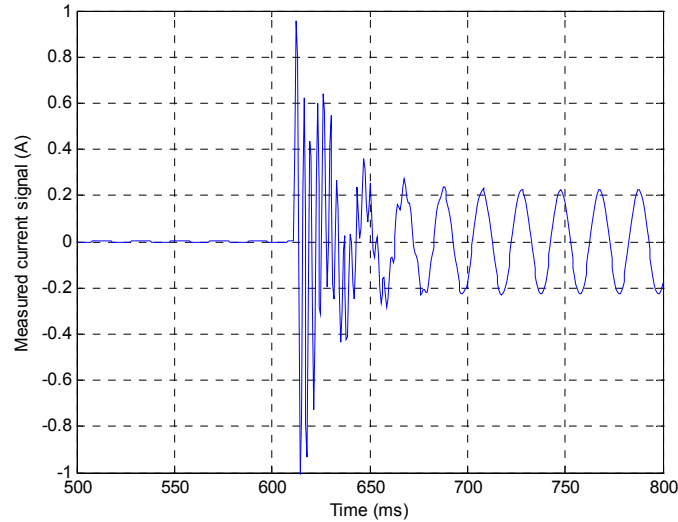


Figure 5.4.8 Current waveforms during transmission line switching

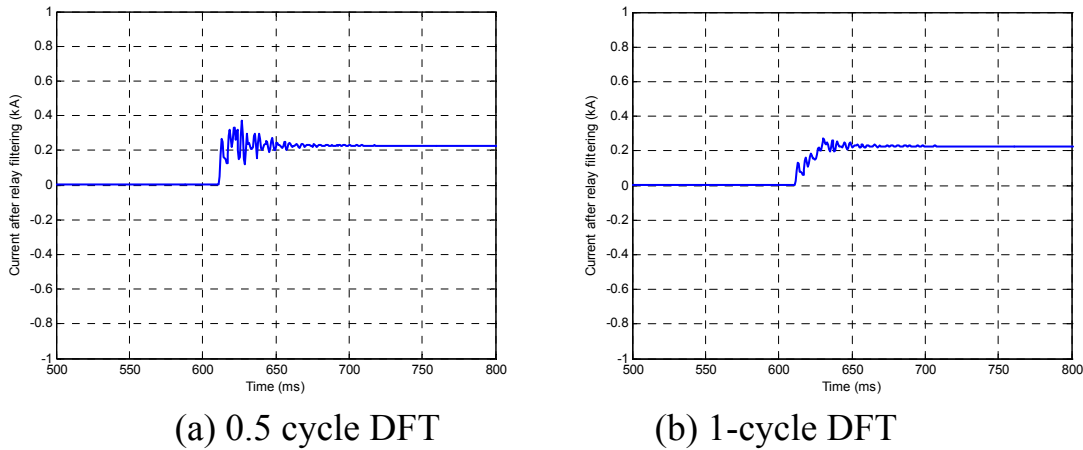


Figure 5.4.9 Current after relay filtering for transmission line switching

Fig. 5.4.8 shows the traveling wave arising during unloaded transmission line switching. The traveling wave mainly consists of the harmonic components whose dominant harmonic orders are dependent on the length of the line. The shorter the line, the higher the frequency of the harmonic components. As the higher harmonic components will be blocked by anti-alias filter before relay filtering, it is the components with lower harmonic orders that affect the detected current waveform. This means that longer transmission lines have more severe impact on relay operation than shorter lines.

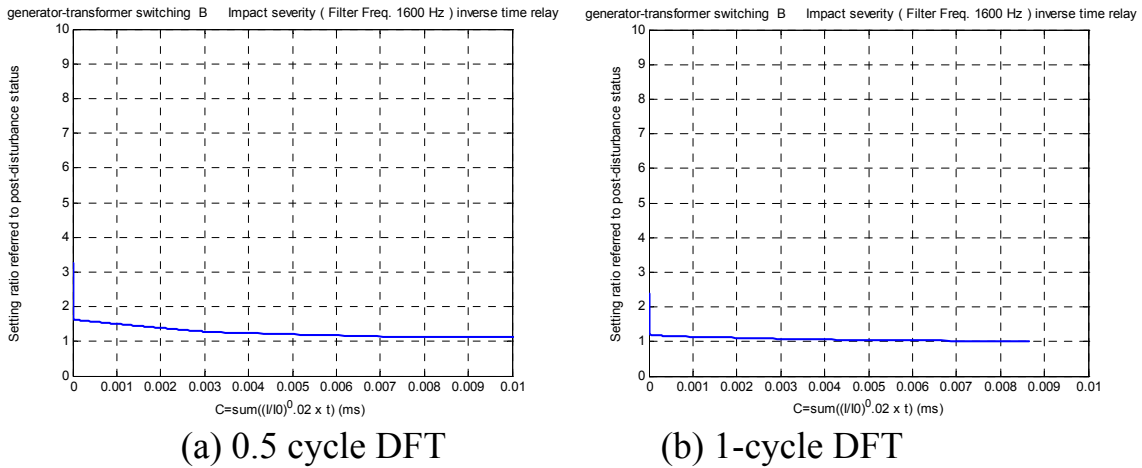


Figure 5.4.10 Impact severity curve for transmission line switching

Case 4 Motor starting (Measurement)

The following diagrams show the transients during induction motor starting at 0.4 kV level.

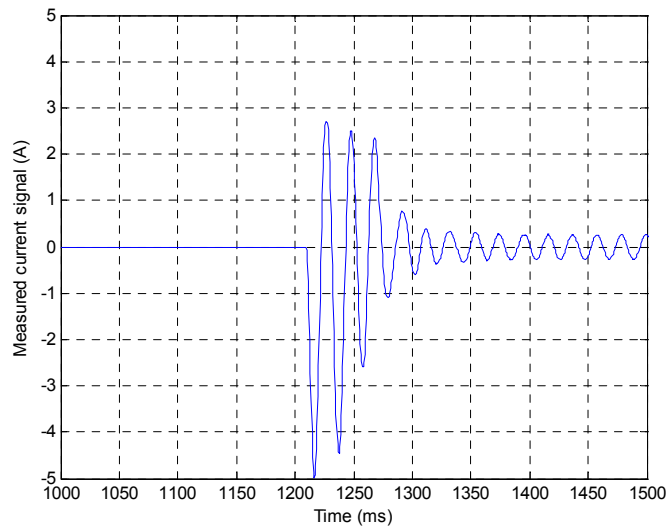


Figure 5.4.11 Current waveforms during induction motor switching

From the diagram it can be observed that the inrush current is much higher than the steady-state current. An overcurrent relay of 0.5 cycle DFT algorithm is more likely to cause mal-trip than a relay of 1 cycle DFT algorithm, as shown in Fig. 5.4.13. The difference is however not very big.

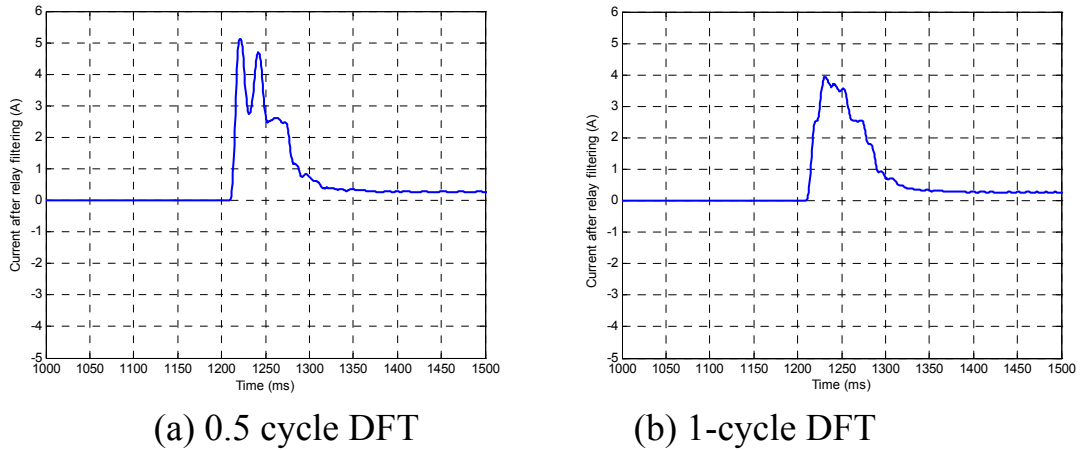


Figure 5.4.12 Current after relay filtering for induction motor switching

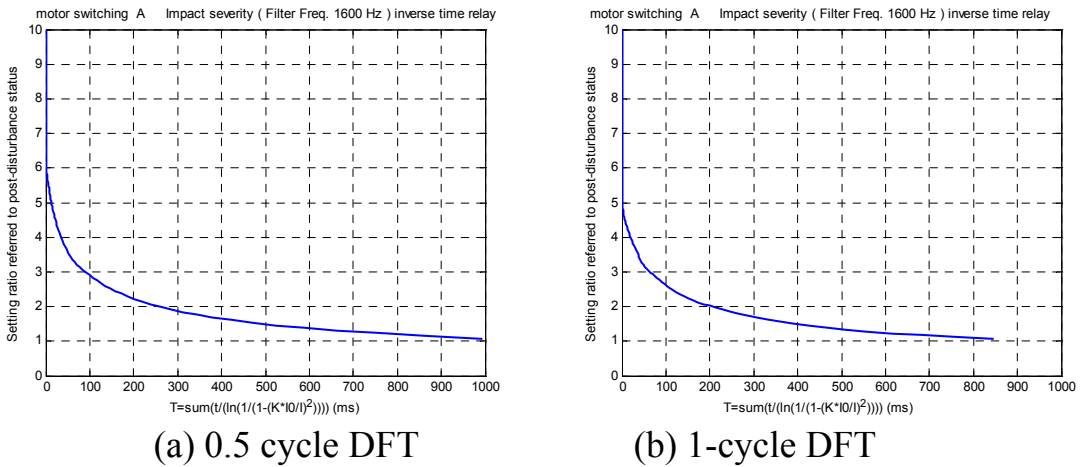


Figure 5.4.13 Impact severity curve for induction motor switching

Case 5 Generator-transformer switching (Simulation)

Simulation results for generator-transformer unit switching are shown in the following diagrams. A generator of 120 MW is connected to the 230 kV system through a 13.8/230 kV transformer.

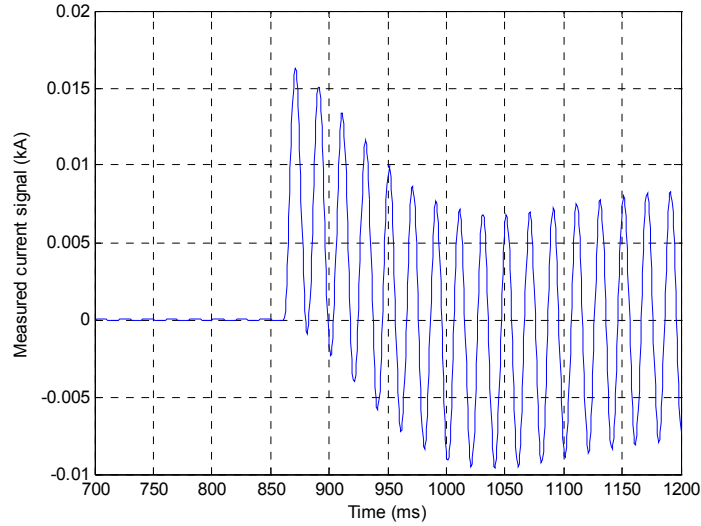
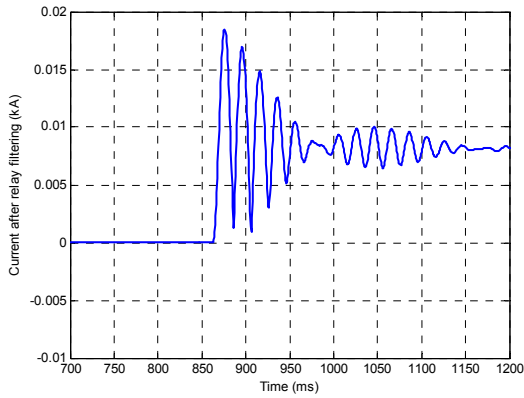
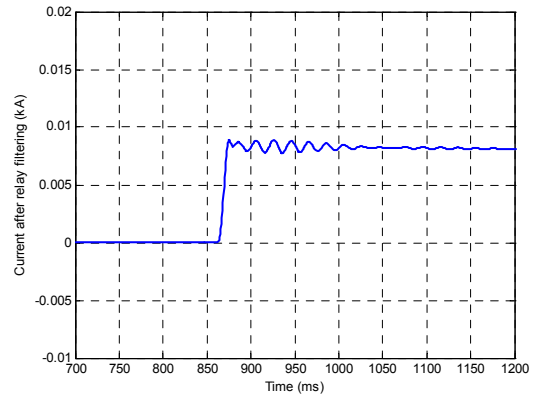


Figure 5.4.14 Current waveforms during generator-transformer switching

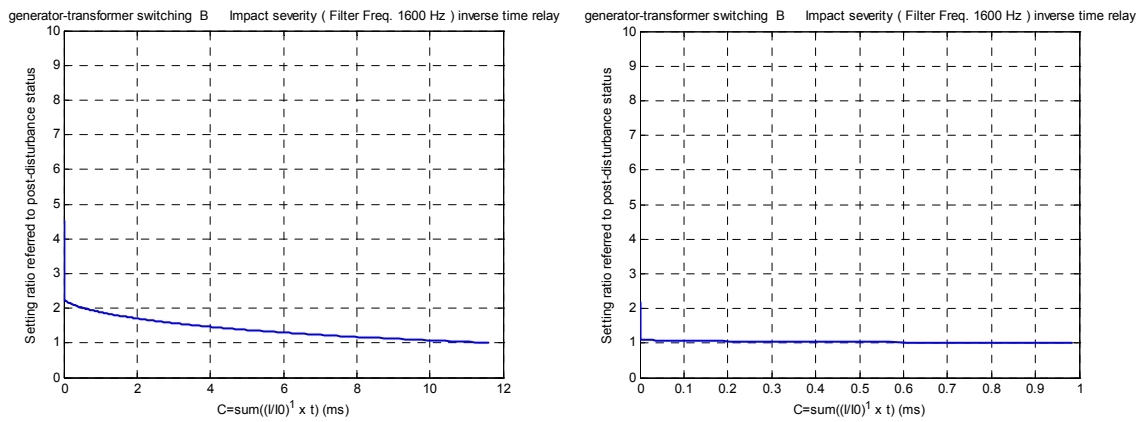


(a) 0.5 cycle DFT



(b) 1-cycle DFT

Figure 5.4.15 Current after relay filtering for generator-transformer switching



(a) 0.5 cycle DFT

(b) 1-cycle DFT

Figure 5.4.16 Impact severity curve for generator-transformer switching

In the above case of generator-transformer switching, an overcurrent relay of 0.5 cycle DFT can have potential risk of mal-trip during generator-transformer switching, while a relay of 1-cycle DFT is not affected by such switching transient.

Chapter 6 Impact of Component Switching on Impedance Relays

This chapter starts with the discussion on relay operation principles and the existing relay algorithms. Analysis is made of traveling waves and the potential mal-tripping risk for digital impedance relays, during unloaded transmission line energizing. Various case studies are carried out at different line lengths to show their impact on impedance relays. Fault evaluation principles are also discussed for quantifying the potential risk of mal-trip as well as the detection speed of different relay algorithms. Based on the performance of relay algorithms during both faults and non-fault events, a method of general assessment of relay algorithm performance is proposed that can be applied to any particular transmission line.

6.1 Component switching at transmission level

At transmission level, the main non-fault event is unloaded line switching. This occurs either during line energizing or during auto-reclosure. Unloaded line energizing involves the operation of the circuit breakers at one of the two terminals of the transmission line. During unloaded line switching, electromagnetic traveling waves are generated and propagate along the line. The propagation and reflection of such traveling waves leads to transients, both in voltage and current. Depending on the line length, point-on-wave and system topology, transients occur with differing oscillation frequencies and decay times. Especially during auto-reclosure it is important that a fault is detected fast. The system is already disturbed by the first fault so that a mal-operation during the reclosing transient would not be acceptable.

Whenever there are transients, there is detrimental impact on the operation of power system components. Among all the components, protective relay devices are the key items that determine the security of a system. The proper performance of protective relays and their immunity from the transients are essential to power systems. Impedance relays are the most commonly used type of transmission line protection. Compared with overcurrent relays, impedance relays have advantages in both the selectivity and the independence of the source impedance. Compared with differential relays, impedance relays are more economic, can operate without communication and can provide backup protection for neighbouring lines.

The apparent impedance observed by a relay during transients can be quite irregular and inaccurate. Although, during switching transients the final steady state impedance point is far from the relay characteristic, some of the apparent impedance points during the transient may be inside the relay characteristic. There is potential risk of mal-trip whenever the apparent impedance enters the relay characteristic.

In this chapter the relay operation principles and relay algorithm characteristics are analysed at first, followed by a study on the process of line switching transients. Simulation case studies are presented evaluating the impact of switching transients for different line lengths. A method of quantifying the detrimental impact of line switching is proposed.

6.2 Impedance relay operation principles

The operation of impedance relays is dependent on the following three factors:

1. Relay characteristic
2. Relay module (algorithm)
3. Fault evaluation

The *relay characteristic* determines the set of apparent impedance values for which the relay will generate a trip signal. The relay characteristic is dependent on the structure and operation mode of the system to be protected. The *relay module* is responsible for measuring and calculating the electrical parameters. In digital relays, the relay module is a computer algorithm for the evaluation of the apparent impedance. *Fault evaluation* refers to the criteria for confirming the presence of a fault by applying the results of the relay module to the characteristic, in many relays it functions like a cumulative counter.

Relay characteristic and relay algorithm are somewhat independent, while the fault evaluation part relies on both of them. The speed of fault evaluation is dependent on the convergence performance of a relay algorithm. Limitations on the speed of fault evaluation are set by system stability requirements as well as by the speed of the circuit breaker clearing the fault.

— Relay characteristics

The shape of the relay characteristic used depends on the nature of the protected system. Mho self-polarized and quadrilateral characteristics are the most commonly adopted types, though there are some other characteristics which are mainly modified schemes of the two types. Examples of the two main types of relay algorithms are shown in Fig. 6.2.1

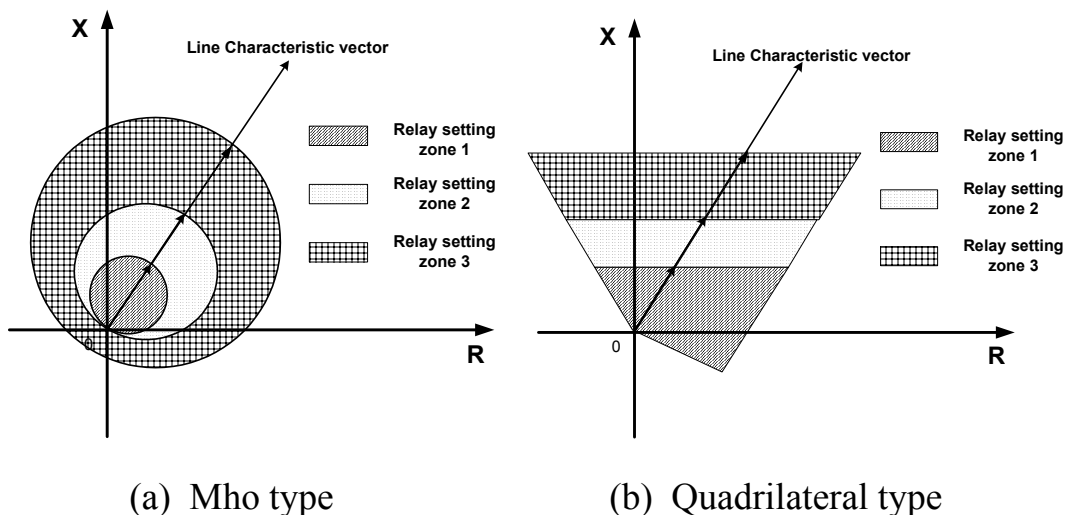


Figure 6.2.1 Examples of relay characteristics

In normal case, zones 2 and 3 of relay characteristic are for the back-up protection of the neighbouring lines. They cover a larger area than zone 1 and have a fixed time delay. As the stay of the switching transients inside zones 2 and 3 is shorter than such fixed time delay, the transients are therefore normally ignored for zone 2 and zone 3 settings.

However, in some protection schemes switching transients might cause false fault detection by zone 3. It is not uncommon that the zone 3 characteristic is used to provide a ‘switching-on-to-fault’ or ‘line-check’ protection to cover the conditions of manually closing on to a line fault [87]. This is actually the case of a close-up three-phase fault due to non-removal of safety earthing clamps from the line after maintenance. For this purpose the zone 3 time delay is bypassed for a short time following manual switching. Since zone 3 is much larger than zone 1, the presence of such ‘switching-on-to-fault’ scheme by zone 3 greatly increase the probability that the switching transients enter the relay characteristic and cause mal-trip.

Because of this, zone 3 is selected in the later case studies. However, the proposed study procedures in the later part of this chapter can be applied generally, including zone 1 and zone 2 settings.

— Relay module (algorithm)

As discussed in Chapter 3, the relay algorithms studied in this thesis are DEA and DFT [49] [89].

In digital relays, all the voltage and current signals are sampled with a fixed sampling frequency. These discrete data need to be processed before they can be used in calculating the apparent positive-sequence impedance.

For phase-to-phase and phase-to-ground faults, the calculation principles are different. For a phase-to-phase fault, the calculated positive sequence impedance is

$$Z_{\text{positive}} = \frac{U_a - U_b}{I_a - I_b}$$

While for single-phase-to-ground faults

$$Z_{\text{positive}} = \frac{U_a}{I_a + I_0(z_0 - z_1)/z_1}$$

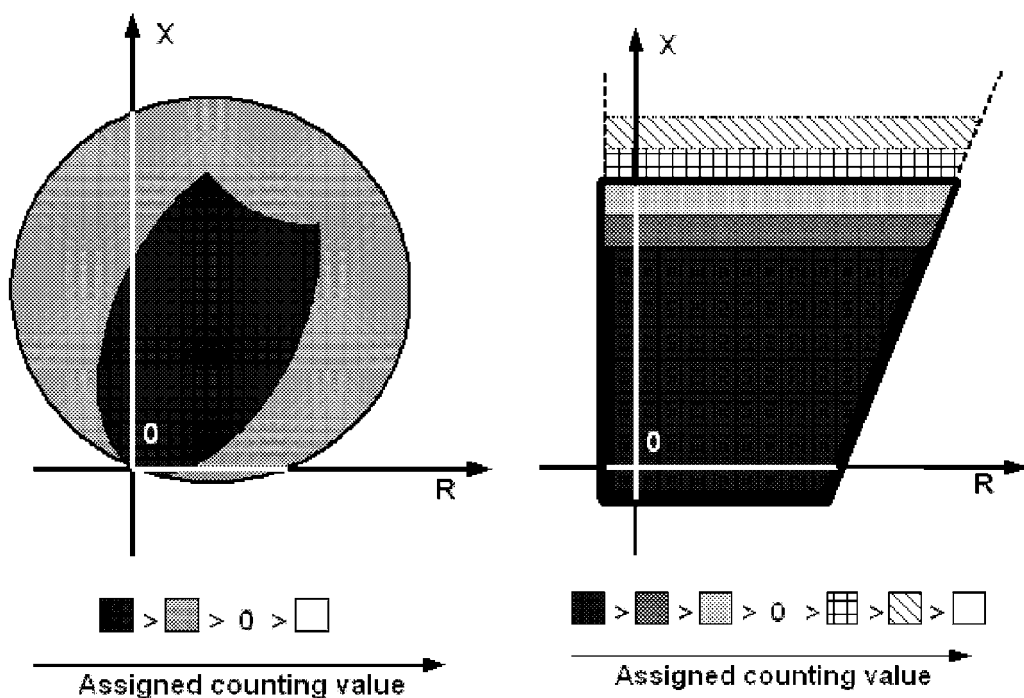
where a and b stand for 2 different phases, I_0 is the zero-sequence current, z_0 and z_1 stand for the zero-sequence and positive-sequence impedance per unit length for the transmission line to be protected.

— Fault evaluation

The main idea in fault evaluation is to assign different weighting values to each calculated apparent impedance point that enters the relay characteristic.

This makes the relay operate faster for some faults than for others, depending on factors such as electrical distance and the location of the apparent impedance compared to the relay characteristic.

To quantify the potential risk of mal-trip during the transients, it is helpful to study the fault evaluation principles for impedance relays. Examples of the principles are shown in Fig. 6.2.2. The basic idea is to assign a positive counting value for an apparent impedance value inside the relay characteristic, and a negative value for a value outside. The darker the color for the region, the higher the counting value assigned. The counter has a lower bound limit of zero. Trip decision is made based on cumulative counting.



(a) Mho relay [93]

(b) Quadrilateral relay [94][100]

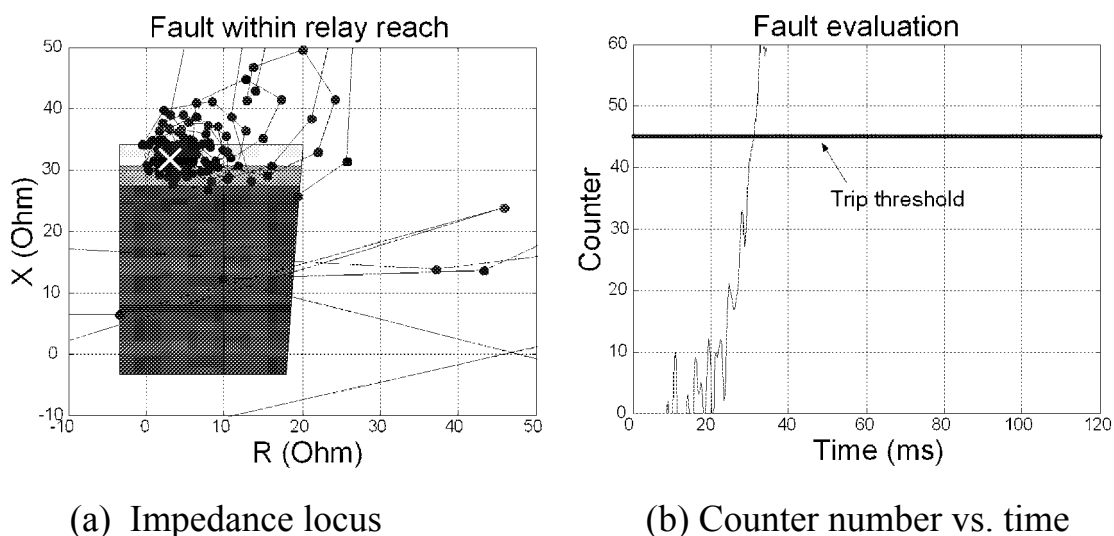
Figure 6.2.2 Fault evaluation principles for digital impedance relays

In Fig. 6.2.2(a), the speed of fault evaluation is dependent on the position of the calculated apparent impedance in the relay characteristic. The smaller the angle between the calculated impedance and the polarised vector, and the

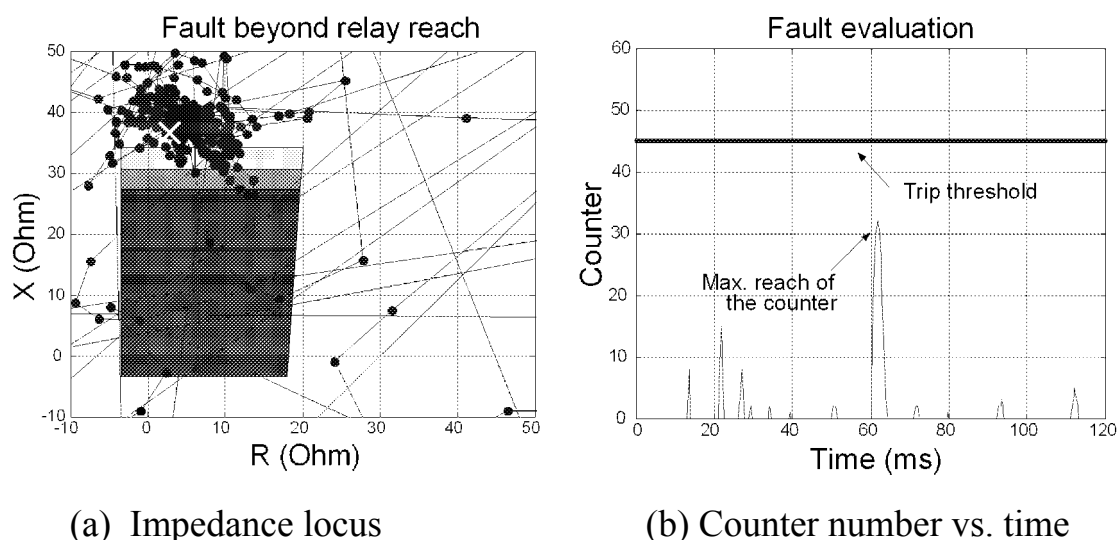
smaller the relative amplitude of the calculated impedance to the polarized vector, the faster the fault evaluation will be. Therefore a calculated impedance point is assigned a higher counting value if it is closer to the polarising axis and the zero impedance point. Higher counting value for the central area and lower one for the area close to the border are for the consideration of fast operation and system stability respectively.

The approach in Fig. 6.2.2(b) is based on the idea that reactance reach is the key criterion for fault evaluation, while resistance reach is quite case-dependent. Resistance reach depends on the fault resistance and the contribution of both line sides to the fault current. The counting value assignment is thus according to the calculated reactance value plus the characteristic borders. This approach even takes into consideration the possible oscillation situation near the border. Bear in mind that applying this characteristic is accompanied by a directional blocking element which is just above and in parallel with the R-axis. The trip counter can increase only if the threshold of such element is exceeded (i.e. the detected X is larger than a preset value) [94][100]. Because of this, such a characteristic will not trip at backward line faults. It is one of the approaches that are similar to the commercial application version.

Figs. 6.2.3 and 6.2.4 show two examples of the operation of fault evaluation counter. The relay tries to detect a single-phase-to-ground fault on a 250 km transmission line at 400 kV level. Fig. 6.2.3 is for a fault that is within the relay reach while Fig. 6.2.4 is for a fault beyond the relay reach. It can be observed that due to the oscillation of the impedance locus, the counter goes up and down during the process.



(a) Impedance locus (b) Counter number vs. time
Figure 6.2.3 Fault evaluation counter for a fault within relay reach



(a) Impedance locus (b) Counter number vs. time
Figure 6.2.4 Fault evaluation counter for a fault beyond relay reach

From this example, it can be deduced that for any locus that once enters the relay characteristic, there is corresponding recording on the fault evaluation counter. For a fault (within the relay zone) the counter will finally reach the threshold and a tripping command will be generated. For a non-fault event, its transient might or might not cause the counter reach the threshold. But at least there is a maximum reach by the counter during the transient process. Such a maximum reach quantitatively tells the potential risk of mal-trip. Note that the counter threshold in both cases is chosen at a rather high value. This

will slow down the tripping of the relay during faults, though it is a good mal-trip precaution measure.

The following section studies the process of switching of unloaded transmission lines and its impact on impedance protection.

6.3 Analysis of switching transients for unloaded transmission lines

For a long transmission line, traveling waves are generated during energizing. The propagation of traveling waves is a non-fault disturbance to relays and thus should not lead to the relay trip. To check the immunity of relays against such transient, it is necessary to study the locus of impedance (i.e. the path of the apparent impedance through the complex plane) as calculated by different relay algorithms.

Fig. 6.3.1 shows the impedance locus during the energisation of an unloaded line. At the instant of energisation, the apparent impedance is equal to the surge impedance, which is independent of line length and point-on-wave. This condition will persist for twice the wave transit time which, for a long line, can be several milliseconds. The impedance locus starts from this point and moves towards the final steady state point, which is located very close to the negative reactance-axis. When the line is fully charged and all transients have decayed, the steady-state impedance apparent to the relay is dominated by the shunt capacitance of the line.

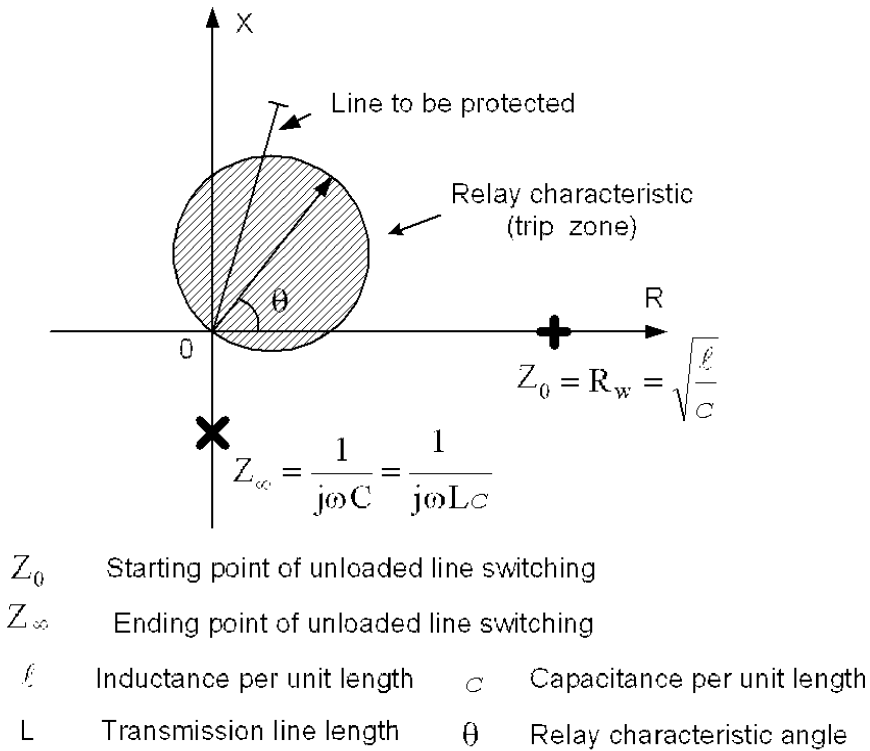


Figure 6.3.1 Starting and ending points of unloaded line switching

The setting of a relay is dependent on the line length. For a mho characteristic the diameter of the relay characteristic is proportional to the line length. So

$$Z_{\text{ref}} = jX = jLx$$

where x is the reactance per unit length

With increasing line length, the steady-state impedance will move towards the relay characteristic whereas the relay characteristic expands, increasing the possibility for the impedance locus to enter the relay characteristic. This can be quantified by calculating the relative impedance observed during unloaded line energizing as follows:

$$Z_{\text{relative}} = \begin{cases} \left| \frac{Z_0}{Z_{\text{ref}}} \right| = \frac{R_w}{LX} \propto \frac{1}{L} & t = 0 \\ \left| \frac{Z_\infty}{Z_{\text{ref}}} \right| = \frac{1}{\omega L^2 X C} \propto \frac{1}{L^2} & t = \infty \end{cases}$$

Lower relative impedance increases the potential risk of mal-trip. Thus intuitively switching of longer transmission lines is more likely to cause mal-trip compared with switching of shorter lines.

Fig. 6.3.2 shows the possible impedance locus during switching transients. If any point of the impedance locus falls inside the relay characteristic, it might contribute to a mal-operation.

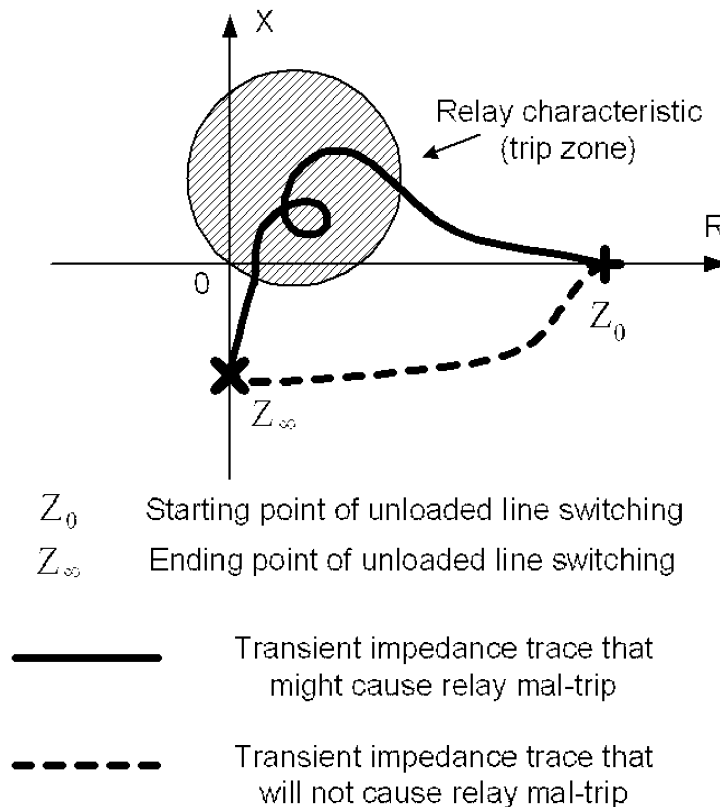


Figure 6.3.2 Impedance locus during unloaded line switching

6.4 Impact of switching transients on impedance relays

The impedance locus observed during switching transients is mainly determined by two factors: relay algorithm and relay characteristic zones.

For each relay algorithm, its frequency response clearly describes its ability to reject components other than the fundamental one. However, all frequency response considerations are related to steady-state effects and are therefore invalid when a transient process is concerned. In the case of long-distance transmission lines, the situation becomes worse than for short lines. The reason is that the longer the line length, the closer the dominant transient frequency is to the fundamental one, as well as the longer the time needed for the switching traveling wave transient to decay. In the viewpoint of signal processing, the traveling wave transient can be described as a non-stationary process.

Fig. 6.4.1 shows an example of the impedance locus observed under different relay algorithms, for a 400 kV line of 350 km length. The line is 70% compensated using series capacitor located at the middle of the line. For comparison, the relay characteristics (mho) of zones 1 and 3 are also shown. In each diagram, the impedance calculated by the relay algorithms during switching transients is shown as a dot.

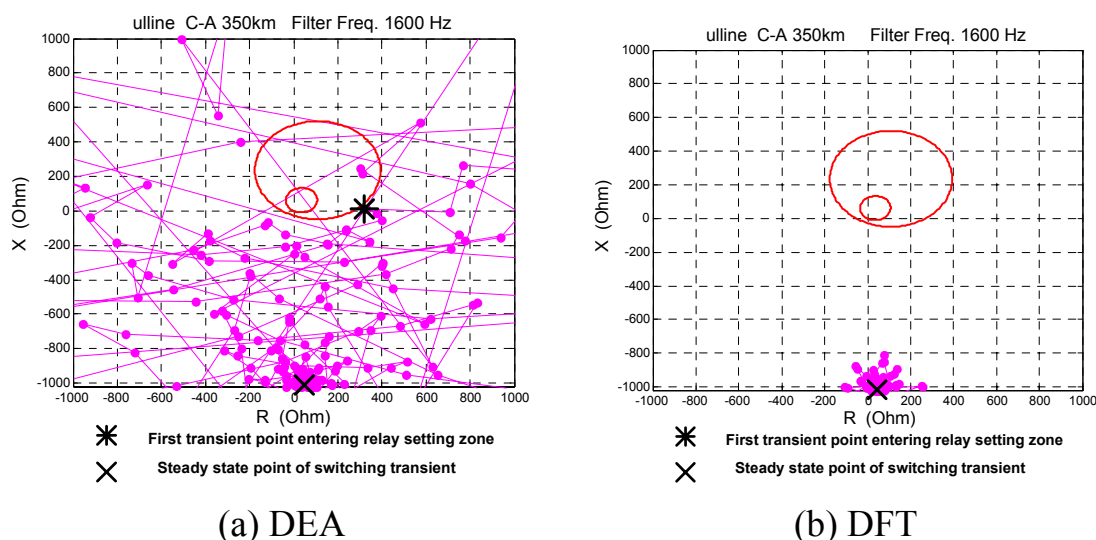


Figure 6.4.1 Transient impedance locus calculated by different relay algorithms

From the diagrams it is clear that the impedance locus calculated by the DEA shows significant oscillations and that the locus passes through the relay characteristic. The impedance loci calculated by DFT are far away from the relay setting border when moving towards the ending point.

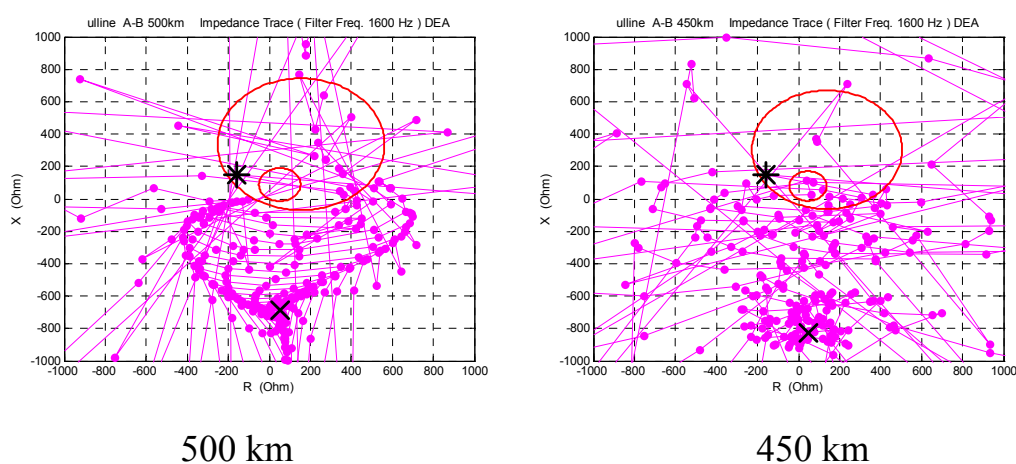
6.5 Simulation test of switching transients on impedance relays

Case studies are presented in this section on evaluating the impact of switching transients on impedance relays using the DEA.

The case studies are for a 400 kV transmission system. The length of the transmission line is set at 500 km, 450 km, 400 km, 350 km, 300 km, 250 km, 200 km, 150 km and 100 km. The impedance relay type is digital Mho, with a characteristic angle of 60 degrees. The relay filter sampling frequency is set at 1600 Hz, with fundamental frequency being 50 Hz. The simulated voltage and current signals are digital signals at a frequency of 6400 Hz. The anti-alias filter, which is normally analog, is simulated digitally in this study.

For each case, a series capacitor compensation of 70% is simulated with the capacitor placed in the middle of the line. Simulation is made using EMTDC software.

Fig. 6.5.1 shows the impedance locus near the relay setting at different line length, calculated by phase-to-phase-fault protective relays. For each line, there are three such phase-to-phase-fault protective relays. Due to different point-on-wave, the impacts of switching transients on these three relays are of different severity. Only the relay that suffers the most severe impact is shown in the figure. In each case, zones 1 and 3 of the relay characteristic are indicated in the diagrams. Zone 3 is set with a forward length of 3 times the line length, and a backward length of 20% the line length. Similar to the case in Fig. 6.4.1, the stable status point is marked with a cross and the first point that enters relay characteristic is marked with an asterisk. The steady-state point in the diagram moves away from the origin with the line length increases. In order to indicate the steady-state point in the diagram, the vertical scales of some diagrams have to be adjusted.



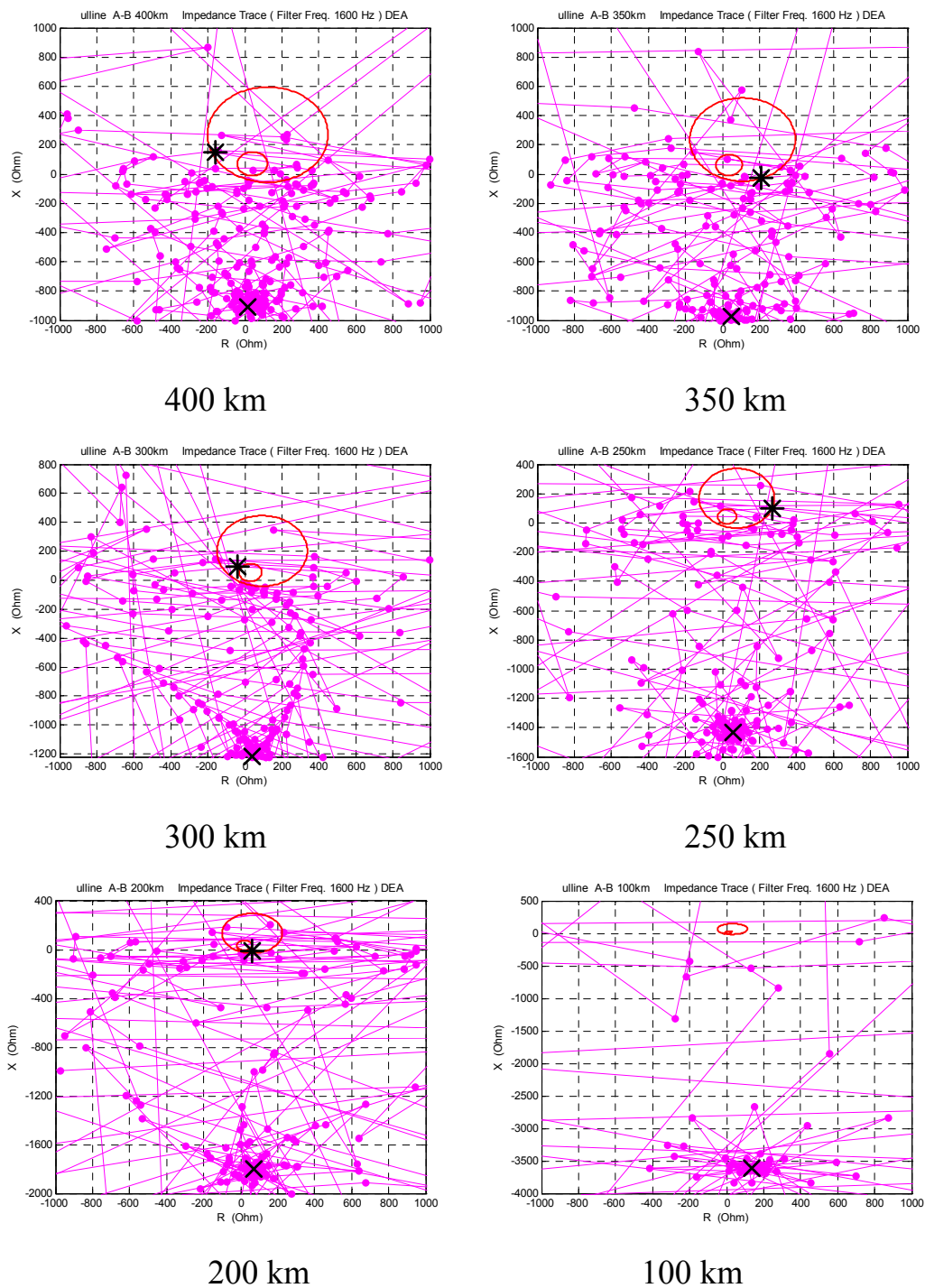
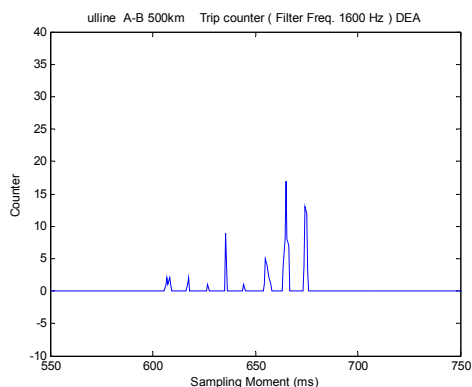


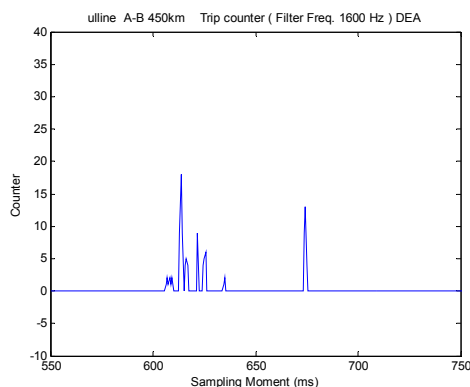
Figure 6.5.1 Impedance loci by phase-to-phase-fault relay at different line length (the circles indicate the relay characteristic)

Similar results were obtained for the phase-to-ground-fault relays.

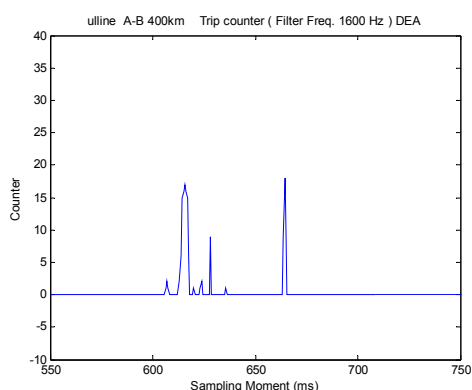
Corresponding to the cases in Fig. 6.5.1, Fig. 6.5.2 shows the trip counter condition for each case. A trip counter for a particular relay is dependent on relay characteristic as well as some practical consideration, which will be discussed in the later section. The greater the value of a trip counter, the higher the potential risk for relay mal-trip.



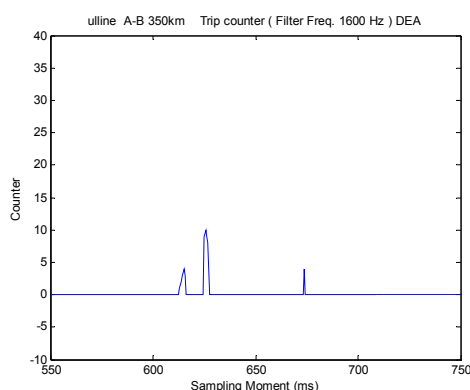
500 km



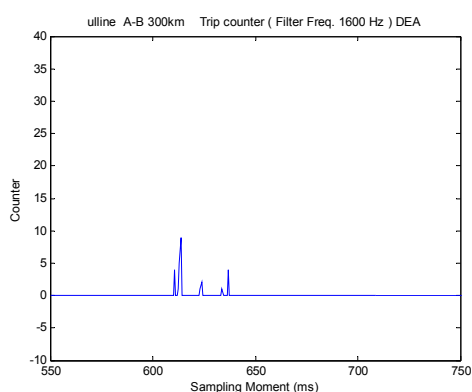
450 km



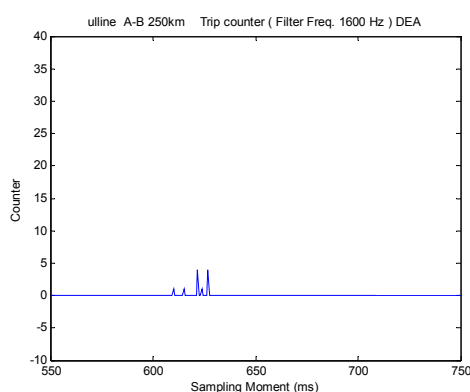
400 km



350 km



300 km



250 km

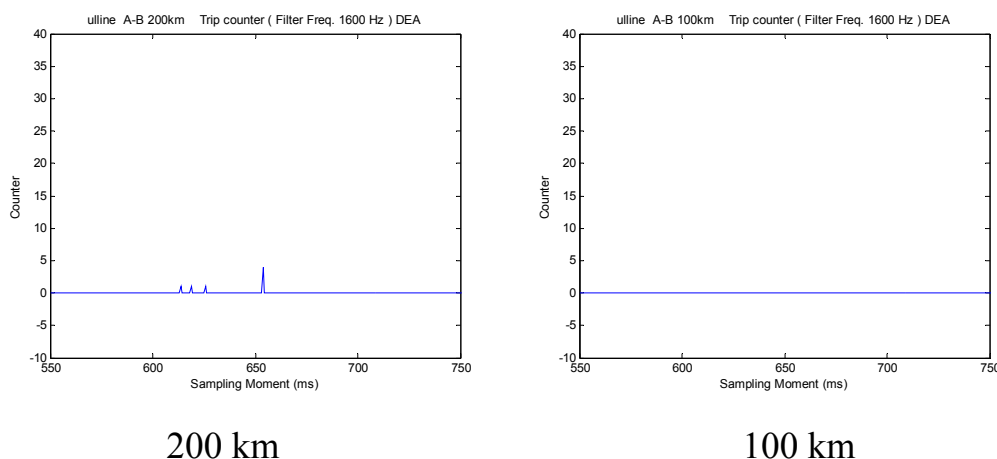


Figure 6.5.2 Trip counter by phase-to-phase-fault relay at different line length

From the simulation results above, it can be observed that unloaded line switching does cause a potential risk of mal-operation when the line is long. The longer the line, the more transient apparent impedance values occur inside the relay characteristic, thus making the potential mal-operation risk higher. The transient will affect either phase-to-phase-fault relays or phase-to-ground-fault relays, or both. This is in accordance with the analysis of the relationship between switching transients and line length. Additionally this can be explained by the fact that a longer line not only makes the transient decay time longer, but also generates lower-frequency oscillations that cannot be completely removed by the anti-alias filters. The presence of such lower-frequency components can contribute to apparent impedance values entering the relay characteristic.

6.6 Impact severity curve

Taking a Mho impedance relay as an example, the setting zone of the relay is a circle whose axis is along the line impedance vector, as shown in previous sections.

The trip of a relay is related to the duration of the measured impedance points staying inside the setting zone. Intuitively as shown in Fig. 6.6.1, the staying duration of a transient inside the impedance circle can be counted based on the impedance points inside and the sampling frequency of the digital relay. It is calculated as N/F_{sample} , where N is the number of the consecutive impedance points inside the impedance circle and F_{sample} is the signal sampling frequency ($1/F_{\text{sample}}$ stands for the time interval between two consecutive impedance points in the figure). For an impedance trace, there might be more than one staying duration, as shown in Fig. 6.6.1.

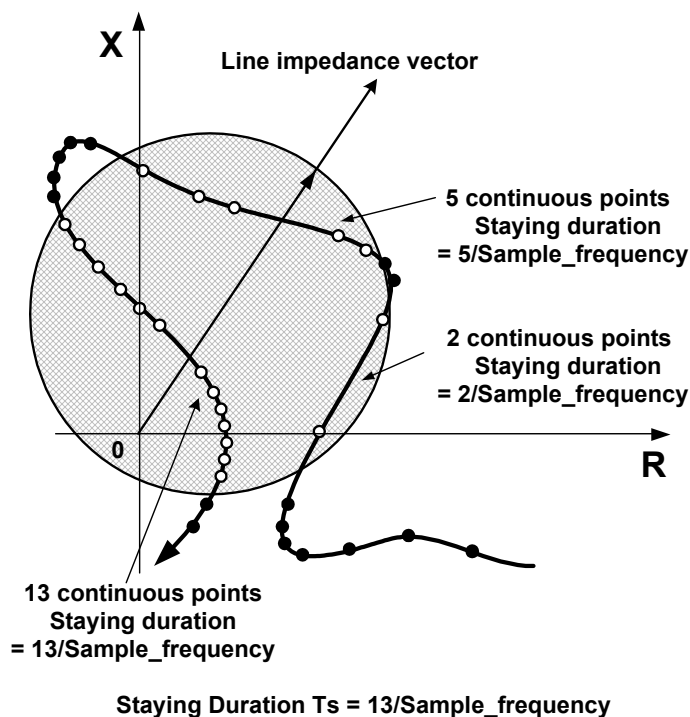


Figure 6.6.1 Staying duration of transients inside setting zone

However, staying duration cannot properly describe the process of relay decision-making. As mentioned in previous sections, the decision-making (or fault evaluation) is dependent on the trip counter of a relay, examples of whose principles are illustrated in Fig. 6.2.2. This means that at different locations inside the setting zone the assigned counting values are different.

Even in the case of the area outside setting zone, the one that is closer to setting zone border has different value than the one far away from the border. Therefore it is more reasonable to use the accumulated counter value (as shown in case studies in Figs. 6.2.3, 6.2.4 and 6.5.2) other than the staying duration to study the impact on relay trip due to transients.

When the trip counter value is equal to the largest accumulated counter value of the transient, it is a critical state for relay mal-trip. Such trip counter value is the minimum one that will not lead to mal-trip.

Fig. 6.6.2 shows a group of different impedance circles for an impedance protection relay with Mho characteristic. For a given impedance trace due to a switching transient, each circle's impedance value corresponds to a given trip counter value. The smaller zones have shorter trip counter values.

As shown in Fig. 6.6.2, for a particular trip counter value C_t , there is always an impedance circle (setting zone) that just leads to mal-trip. The diameter of this impedance circle is referred to as the “propagation depth of the transient”. Minimum trip counter value C_{t0} corresponds to the minimum propagation depth Z_{t0} . So the propagation depth is a function of the preset trip counter. The shorter the trip counter value (the faster the relay), the smaller the propagation depth is, thus the higher the risk of a mal-trip.

Based on the above analysis, the impact severity S for a particular trip counter value C_t can be defined as

$$S = \frac{Z_{line}}{Z_t} \quad (6.6.1)$$

Where Z_t is the propagation depth of the switching transient and Z_{line} is the impedance of the transmission line (in this project the positive length of the 3rd setting zone).

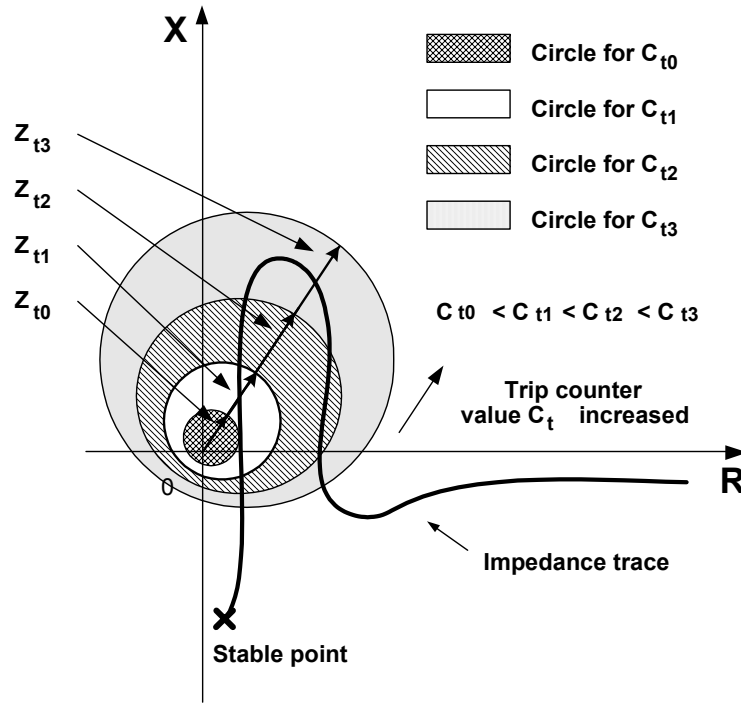


Figure 6.6.2 Series of impedance propagation depth at various trip counter values

If the axis of Mho circle is not at the vector direction of line impedance, a new value Z'_{line} should replace Z_{line} . Under such a situation, $Z'_{line} = Z_{line} / \cos\theta$, where θ is the angle between line impedance vector and Mho circle axis.

As explained above, the impedance propagation depth is different with different trip counter values. A switching transient with impact severity equal to one will be detected as a fault at the remote line terminal. A switching transient with severity equal to two will be seen as a fault in the middle of the line.

A plot of the severity of the transient versus the minimum trip counter value is referred to as the “impact severity curve” of the transient. An example of such a diagram is shown in Fig. 6.6.3. Note that a characteristic diagram holds for a specific protection algorithm: in this case the differential equation algorithm together with the Mho characteristic. As analyzed before and shown in case studies in Fig. 6.5.2, the curve does not necessarily need to be a smooth one, due to the discontinuity character in selecting the maximum accumulated trip counter value.

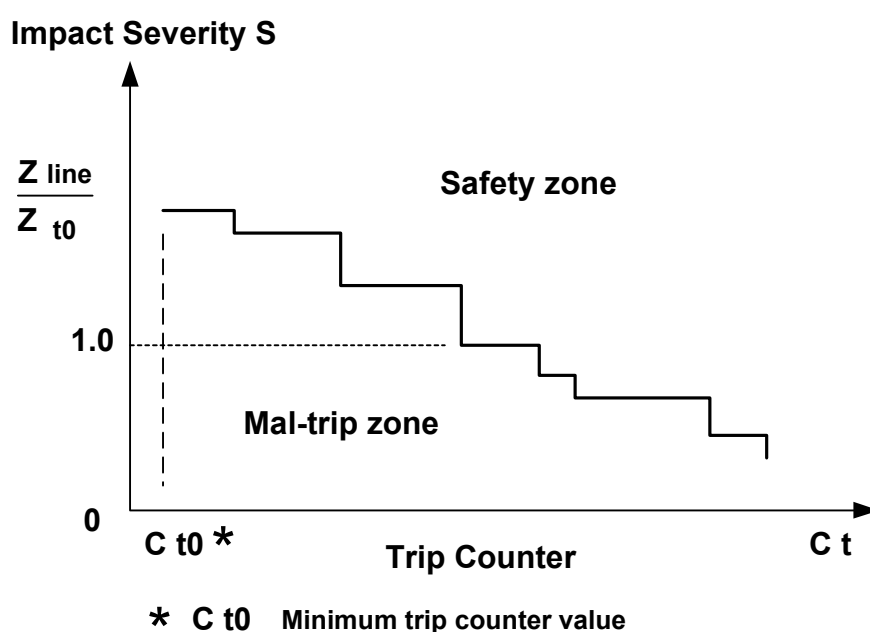


Figure 6.6.3 Impact severity curve

The different curves in Fig.6.6.4 represent line switching events of different line lengths. In general, the curves for long lines are above those for short lines. As the length of the transmission line increases, the setting zone of impedance relay for a transmission line increases with its length, making the impedance trace remain longer within the relay setting zone. The result is that the measured impedance becomes closer to the relay setting zone, and the severity of the switching transient increases with increasing line length.

The characteristic diagram shown in Fig. 6.6.4 can be used in impedance relay testing. Any new relay algorithm can be tested using the data in the characteristic diagram, with each curve standing for one switching transient. The test goes on, from the curves at the bottom to upwards, until mal-trip is encountered. If the final tested curve is below the mal-trip border, a relay under such a relay algorithm can lead to mal-trip. The relative comparison of two relay algorithms can be made by testing them with the same group of curves in the characteristic diagram. The one whose final tested curve is above the others has better mal-trip immunity during switching transients.

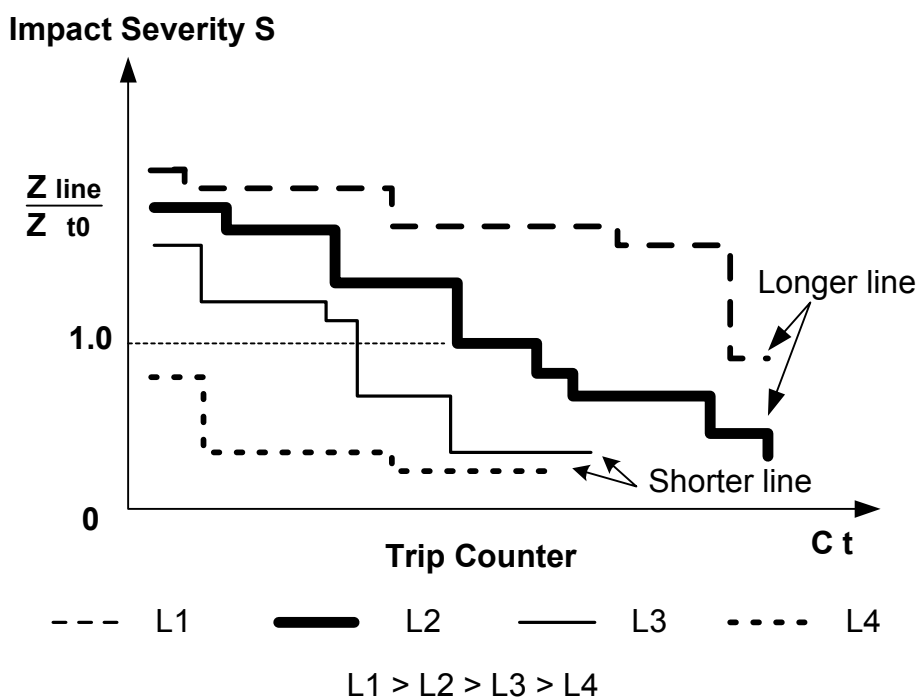


Figure 6.6.4 Impact severity curves at different line lengths

During the development of a relay, the longest practical line length may be taken. For the setting of a specific relay, the actual line length can be taken. The curves have to be determined for different operational states and for different switching instants.

6.7 Case studies of impact severity curve

Two case studies are made to check the feasibility of impact severity curve: in the first case, impact severity curves for unloaded transmission line switching on different phase-phase relays; in the second case, impact severity curves for unloaded transmission line switching at different line lengths.

— Impact severity on different phase-phase relays

Fig. 6.7.1 demonstrates the impact severity on different phase-phase relays when there is unloaded transmission line switching. The switching transient has been calculated for a 500 km transmission line at 400 kV, the same as for the case in Fig. 6.5.1.

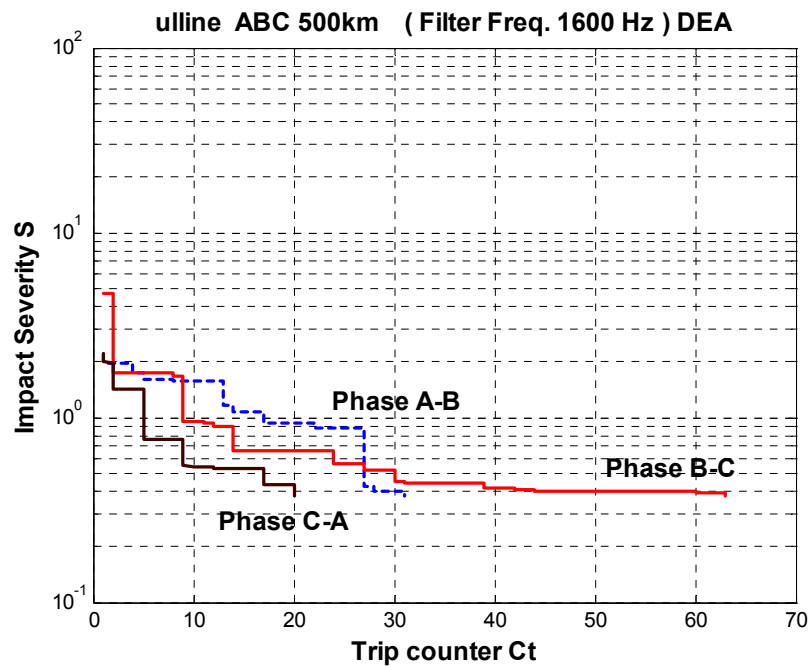


Figure 6.7.1 Impact severity on different phase-phase relays
(switching instant $t = 0.611$ s)

From the above diagram it can be observed that the impact severity is different for different phase-phase relay. In the case in Fig. 6.7.1, A-B and B-

C relays experience more severe impact than C-A relay during the switching transient. However, this is much dependent on the point-on-wave and different closing instants for the three phases. In Fig. 6.7.1, the results are shown for a different closing instant.

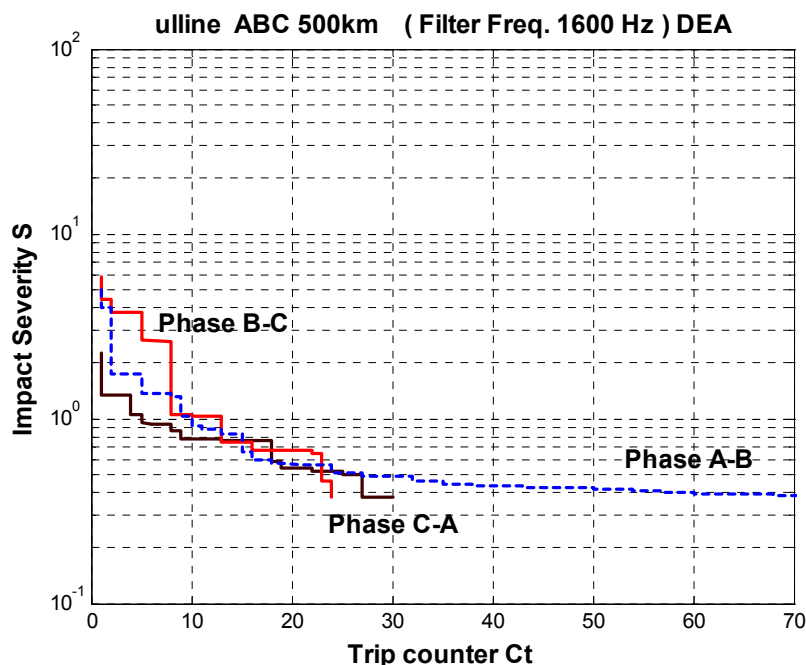


Figure 6.7.2 Impact severity on different phase-phase relays (switching instant $t = 0.605$ s)

— Impact severity at different line lengths

Fig. 6.7.3 shows the different impact severity curves at different transmission line lengths. The operation conditions are the same as in Fig. 6.7.1. The impact severity curves are for phase A - phase B relay.

Fig. 6.7.3 shows that the impact severity curves for 500 km, 400 km and 300 km are obviously above the curve for 200 km. This means that the relays for these longer transmission lines suffer much more detrimental impact than the shorter 200 km line during unloaded line switching, which is in accordance with the situations shown in Fig. 6.5.1.

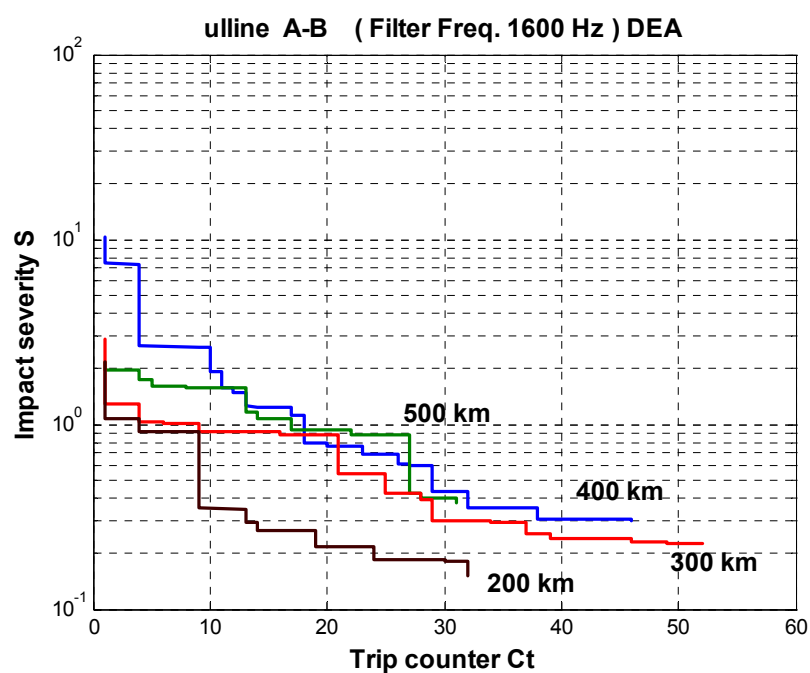


Figure 6.7.3 Impact severity at different line lengths

Also worth noticing is that the relay for 400 km line suffers more impact than that for 500 km in general. This is actually much dependent on the adopted relay algorithm and fault evaluation (trip counting) method.

Chapter 7 Impact of Frequency Deviation on RMS-based Relays

RMS calculation is a popular method adopted in power system parameter classification. Typical examples are its application in voltage sag classification and relay protection. Starting from the viewpoint of frequency response, this chapter seeks to study the characteristics of RMS method, for both the single frequency and mixed frequency signals. Analysis is made on its dependence on sampling rate, sampling window size as well as point-on-wave through strict mathematical deductions. Interesting discoveries include the locations of the “pitfall” frequencies (multiples of the Nyquist sampling rate), the minimum sampling points for correct RMS output as well as the fluctuation of RMS magnitude. Estimation is made on the maximum RMS output errors due to the presence of harmonics as well as due to frequency deviation. Reasonable approximation is adopted in such estimation. Such error estimations are useful in measurement of power system voltages, or any other parameters with relatively higher fundamental but lower harmonics levels.

7.1 RMS expression in general form

The RMS method is widely used in quantifying the effective magnitude of an ac signal. In power-quality monitoring, the RMS value of the voltage is used for the characterization of voltage sags as well as for voltage variations. In the power-quality measurement standard IEC 61000-4-30 a one-cycle (of the power-system frequency) window is prescribed for the characterization of voltage sags and a 10 or 12 cycle for voltage variations. A half-cycle window

was recommended in an early draft of IEEE 1159.2, and is mentioned as an alternative in [4]. Despite the emphasis of more advanced methods in the scientific literature [94][101][102] the RMS voltage is by far the most commonly used method for characterizing the magnitude of the voltage. In this chapter we will study some of the properties of the RMS calculation and its effect on the magnitude estimation, as well as the output error of RMS in case of frequency deviation. The situations in cases of both single frequency signal and mixed frequency signal are analyzed.

The well-known formula for calculating RMS for a continuous signal is as follows:

$$Y_{\text{RMS}} = \left(\frac{1}{T} \int_0^T x^2(t) dt \right)^{\frac{1}{2}} \quad (7.1.1)$$

In practical applications, the ac signal is treated as a discrete signal and (1) is transformed to

$$Y_{\text{RMS}} = \left(\frac{1}{K} \sum_{k=0}^{K-1} x^2(k\Delta t) \right)^{\frac{1}{2}} \quad (7.1.2)$$

where $k=0, 1, 2 \dots K$

Δt is the sampling interval

The RMS value represents the average magnitude of the signal during the sampling window: T in (7.1.1) or $K\Delta t$ in (7.1.2). From these expressions it can be concluded that the RMS value is the average signal energy during the sampling window.

The RMS method is one of the most widely applied techniques in monitoring and characterizing power system parameters. There are different ways developed to calculate RMS. While the classical way that will be studied in

this chapter is based on discrete integral, there are some novel proposals on applying wavelet transform [103][104].

Previously, one uses 1 cycle sampling window in calculating RMS value in normal case. Recently there are discussions on whether a shorter sampling window is acceptable in practical implementation.

To study the feasibility of applying RMS method, it is necessary to study the frequency response of such method. Frequency response tells the relationship between the RMS output and the input signal, assuming the input signal is stable and periodic. The following sections start from analyzing the frequency response of the fundamental and periodic harmonic signals. Studies and discussions will be made on the RMS output and its error estimation for

- Stationary single frequency signals
- Stationary mixed frequency signals
- Stationary single frequency signals with asynchronous fundamental frequency
- Stationary mixed frequency signals with asynchronous fundamental frequency

7.2 RMS output for an arbitrary signal

To study the response of the RMS method, (7.1.2), which is an expression in time domain, is transformed into its equivalent expression in frequency domain.

According to Parseval's theorem [105], for any input signal $x(t)$

$$\int_{-\infty}^{\infty} x^2(t)dt = \frac{1}{2\pi} \int_{-\infty}^{\infty} \overline{X(\omega)}X(\omega)d\omega = \frac{1}{2\pi} \int_{-\infty}^{\infty} |X(\omega)|^2 d\omega \quad (7.2.1)$$

If the input signal is treated as a discrete one, it can be expressed in the way like $x(k\Delta t)$, $k=0,1, 2, \dots$. The transformation is then

$$\sum_{k=0}^{K-1} x^2(k\Delta t) = K \sum_{m=0}^{K-1} |a_m|^2 \quad (7.2.2)$$

where K is the points to be sampled for RMS calculation, which actually reflects the sampling window size

$$a_m = \frac{1}{K} \sum_{k=0}^{K-1} x(k\Delta t)e^{-j2\pi km/K} \quad (7.2.2a)$$

In the above equation, Δt and N stand for the sampling rate and the sampling window size respectively. a_m is actually the Fourier series coefficient of $x(k\Delta t)$ for harmonic order m .

For any signal $y = x(k\Delta t)$, the RMS output shall be

$$Y_{\text{RMS}} = \left(\frac{1}{K} \sum_{k=0}^{K-1} x^2(k\Delta t) \right)^{\frac{1}{2}} = \left(\sum_{m=0}^{K-1} \left| \frac{1}{K} \sum_{k=0}^{K-1} x(k\Delta t)e^{-j2\pi km/K} \right|^2 \right)^{\frac{1}{2}} \quad (7.2.3)$$

The right side of (5) tells the process of calculating Y_{RMS} at a particular frequency f . There are many terms in it because we need so many sampled points to calculate the frequency response at this frequency. This expression is applicable to all the periodic signals, especially when the input signal expression is unknown.

7.3 Frequency response for single frequency signals

Here we consider the RMS calculation as a filter

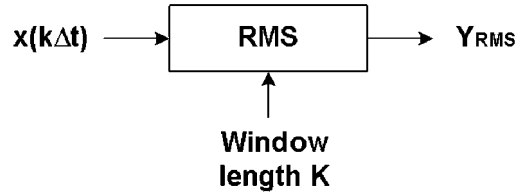


Figure 7.3.1 RMS calculation as a filter

Assume that the input to the RMS filter is a single-frequency sinusoidal signal with frequency f :

$$y(k\Delta t) = \sqrt{2} \cos(2\pi f k \Delta t + \alpha_t),$$

The RMS value over an infinite window is unity, so that we will consider any deviation from unity of any RMS calculation as an error. The time-dependence of the input signal is not explicitly indicated but included in the point-on-wave α_t , which stands for the phase angle of the studied signal at the start of the sampling window. The time dependence of the output signal will be considered in more detail later.

The RMS value over the sampling window $[0, K\Delta t]$ is obtained by substituting signal function into (2):

$$\begin{aligned} Y_{\text{RMS}}^2(\alpha_t) &= \left(\frac{1}{K} \sum_{k=0}^{K-1} (\sqrt{2} \cos(2\pi f k \Delta t + \alpha_t))^2 \right) \\ &= \left(\frac{1}{K} \sum_{k=0}^{K-1} (1 + \cos 2(2\pi f k \Delta t + \alpha_t)) \right) \\ &= 1 + \frac{1}{K} \sum_{k=0}^{K-1} \cos 2(2\pi f k \Delta t + \alpha_t) \end{aligned} \quad (7.3.1)$$

We can write this as:

$$Y_{\text{RMS}}^2(\alpha_t) = 1 + \varepsilon_{\text{MS}} \quad (7.3.1a)$$

with the error in the mean square value of input signal

$$\varepsilon_{\text{MS}} = \frac{1}{K} \sum_{k=0}^{K-1} \cos(2(2\pi f k \Delta t + \alpha_t)) \quad (7.3.1b)$$

If we define $f_s = 1/\Delta t$ sampling rate
 $T_w = K/f_s$ sampling window size

The error according to (7.3.1b) can be rewritten into:

$$\begin{aligned} \varepsilon_{\text{MS}} &= \frac{e^{-j4fT_w\pi} \left(e^{j4fT_w\pi} - 1 \right) \left(\left(e^{j4fT_w\pi} + e^{j\frac{4f}{f_s}\pi} \right) \cos 2\alpha_t + j \left(e^{j4fT_w\pi} - e^{j\frac{4f}{f_s}\pi} \right) \sin 2\alpha_t \right)}{2T_w f_s \left(e^{j\frac{4f}{f_s}\pi} - 1 \right)} \\ &= \frac{\cos \left(2 \left(\left(T_w - \frac{1}{f_s} \right) f \pi + \alpha_t \right) \right) \sin(2fT_w\pi)}{T_w f_s \sin \left(\frac{2f}{f_s} \pi \right)} \end{aligned} \quad (7.3.2)$$

The above equation stands for the MS error at frequency f .

Also bear in mind that it only stands for the RMS value over the sampling window $[0, K\Delta t]$ with point-on-wave α_t . Among the three parameters defined above, sampling rate and sampling window size are independent of time, while the point-on-wave α_t changes with time. It reflects the relative position of the sampling window versus the signal.

Note that in the above sinusoidal signal there is a coefficient $\sqrt{2}$. This is based on the fact that a sinusoidal signal with a peak value of 1 yields an efficient magnitude of $1/\sqrt{2}$.

As indicated in (7.3.1), the 2nd term is actually an error item. If such term is equal to zero, Y_{RMS} will become 1.0, which is desired in RMS output.

From (7.3.2) we can conclude that the error is zero when:

$$(\sin(2fT_w\pi) = 0) \cap (\sin(2f\pi/f_s) \neq 0) \quad (7.3.2a)$$

This is the case for those signal frequencies whose periods are an integer multiple of twice the length of the sampling window, i.e.

$$(fT_w = p/2) \cap (f/f_s \neq q/2), p, q \in \mathbb{N} \quad (7.3.2b)$$

The second condition states that the signal frequency should not be an integer multiple of half the sampling frequency. For those frequencies the resulting error is:

$$\varepsilon_{\text{MS}} = \cos 2\alpha_t \quad (7.3.2c)$$

Note that this value is dependent on the point-on-wave, thus time varying.

The second condition in (7.3.2b) is a reformulation of the sampling theorem. All those frequencies will give the same response as a dc signal. The frequencies according to (7.3.2b) are not the only frequencies for which expression (7.3.2) gives zero. But they are the only solutions that are independent of the point-on-wave, thus independent of time.

The performance of RMS output is dependent on three factors:

1. *Sampling rate*, which determines the time interval between two consecutive sampling points.
2. *Point-on-wave*, which stands for the initial location of the sampling window.
3. *Sampling window size*, which determines the duration for signal sampling before RMS calculation can be made.

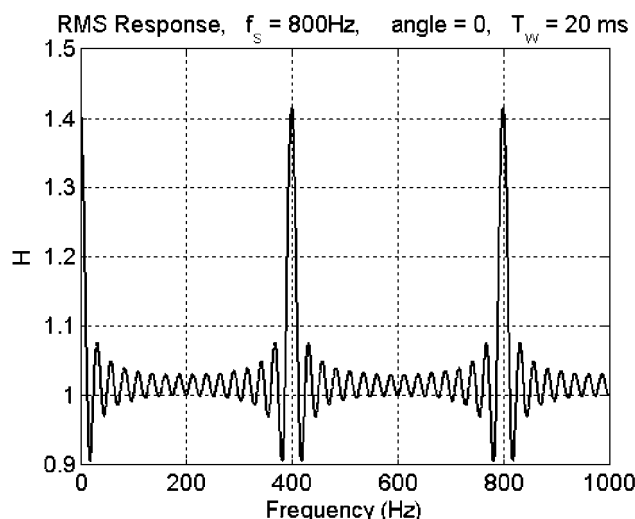
The impacts of these factors on the RMS value are studied in the following sections. In this study the fundamental frequency is assumed to be 50 Hz.

7.3.1 Impact of sampling rate on RMS output

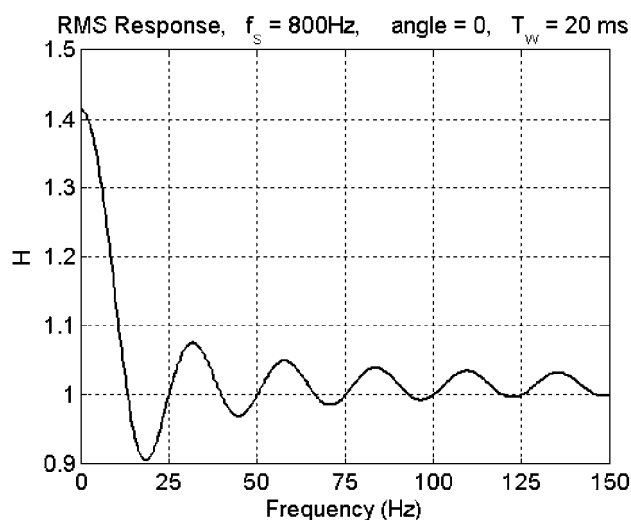
As an example, the RMS response for a single-frequency sinusoidal signal is presented in Fig. 7.3.2, by assuming that

- Sampling rate $f_s=800$ Hz
- Sampling window size $T_w=0.02s$
- Point-on-wave is at the positive peak point of the sinusoidal signal, i.e. $\alpha_t=0$

Fig. 7.3.2 can be interpreted as an RMS response diagram at constant window length, single but variable frequency input signal and constant phase angle of the input signal at the start of the window. As discussed before, the phase angle (point-on-wave) varies with time. So such a diagram is the RMS response at moment when $\alpha_t=0$.



(a) wide range



(b) zoomed

Figure 7.3.2 Example of RMS frequency response

From Fig. 7.3.2(a) it can be observed that in most cases the RMS values at integer multiples of half the fundamental frequency are equal to 1.0, i.e. the RMS value truly reflects the magnitude of the input signal at these frequencies. However at 400 Hz and 800 Hz, the RMS outputs show strange value amplifying the magnitude of the input signal by $\sqrt{2}$. From now on we call these frequencies “pitfall frequencies” because they yield incorrect RMS outputs.

Another interesting point is the slope around 50 Hz, as shown in Fig. 7.3.2(b). This shows the error in RMS when the window is not synchronized with the power system frequency. This will be discussed in later sections.

If the sampling rate in the above case is reduced from 800 Hz to 500 Hz, the RMS response is shown in Fig. 7.3.3.

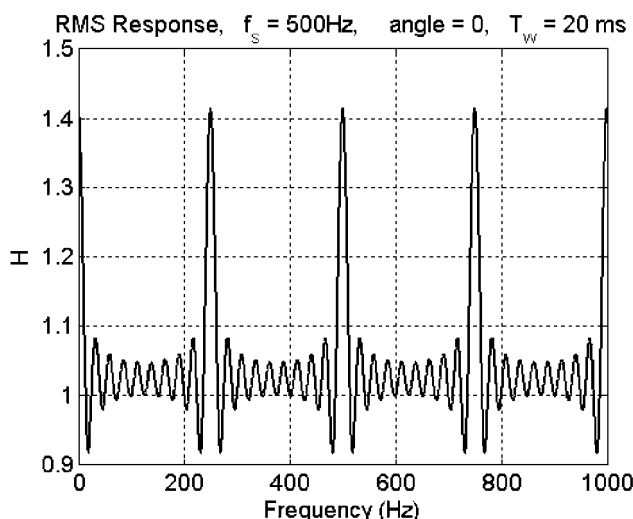


Fig.7.3.3 RMS frequency response at reduced sampling rate

Comparing Fig. 7.3.3 with Fig. 7.3.2, it can be found that the difference between two consecutive pitfall frequencies is reduced. In this case, 250 Hz, 500 Hz, 750 Hz etc. are the harmonics that can yield output error. As expected, tests by decreasing the sampling rate show that the interval between “pitfall frequencies” is narrowed.

The reason for such pitfall frequencies when calculating RMS can be explained by studying Eqns. (7b) and (7c).

From Eqns. (7b) and (7c) it can be observed that

- When $fT_w = p/2$, $f / f_s \neq q/2$, $p, q \in \mathbb{N}$,

This corresponds to the frequencies whose periods can exactly divide double the sampling window size. In such a case, the error item in Y_{RMS} expression becomes zero. The RMS output in such a case is identical to the magnitude of the input single-frequency sinusoidal signal. So

$$Y_{\text{RMS}}(\alpha_t) = 1.$$

- When $f/f_s = q/2$, $q \in \mathbb{N}$,

This corresponds to the frequencies that are integer multiple of half the sampling frequency. At these frequencies, the RMS output is not identical to the magnitude of the input single-frequency sinusoidal signal. According to (7c)

$$Y_{\text{RMS}}(\alpha_t) = (1 + \cos 2\alpha_t)^{\frac{1}{2}}$$

In the case of Fig. 7.3.2, $f_s = 800$ Hz. So the pitfall frequencies are at 400 Hz, 800 Hz, 1200 Hz etc. In the case of Fig.3, $f_s = 500$ Hz, which implies the pitfall frequencies are at 250 Hz, 500 Hz, 750 Hz etc.

Theoretically, the errors at such frequencies result from the fundamental or a harmonic aliasing to dc. Since the true RMS value of a periodic signal is a dc quantity, this aliasing means the RMS value cannot be distinguished from the aliased signal. As half sampling rate is the Nyquist sampling rate, these frequencies are actually multiples of the Nyquist sampling rate.

So it can be concluded that for any sampling rate f_s (frequency), the RMS value will yield a considerable error at frequencies $f = qf_s/2$, $q \in \mathbb{N}$. For any frequency f , $f_s / f = K_f$ stands for the quantity of the sampling points in one cycle of such a frequency signal. So the error occurs when

$$K_f = 2/q \quad K_f, q \in \mathbb{N}$$

Therefore to avoid the RMS error K_f cannot be equal to 1 or 2, i.e. *at least 3 sampling points* per cycle are needed for extracting the correct efficient magnitude of the signal.

7.3.2 Impact of point-on-wave on RMS output

The point-on-wave, or the initial location of RMS sampling window, is actually its relative angle to the input signal. This can be represented by the initial angle of the input signal. If the initial angle of the input signal is set at 1.0 radian (57.3 degrees) instead of 0, the RMS frequency response will be different as shown in Fig. 7.3.4.

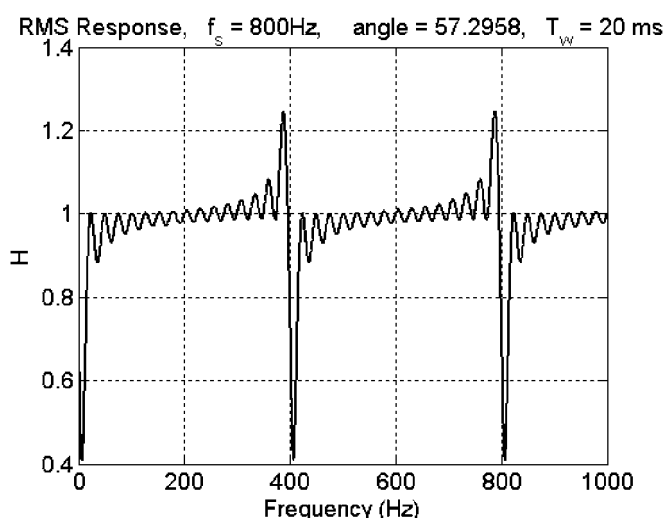


Fig. 7.3.4 RMS frequency response at $\alpha_t = 57.3^\circ$

The range in output values due to the uncertainty in point-on-wave is interesting. As the sliding window moves through the signal, the point-on-wave will change and the output will show an oscillation. This means that the

RMS outputs at some frequencies are not only amplified or attenuated, but also unstable with the sampling window sliding.

However, at the frequencies (except some multiples of the Nyquist sampling rate) whose periods can exactly divide double the sampling window size, the RMS output is identical to its input magnitude and stable, independent of the window sliding, as shown in Fig. 7.3.4. This is in accordance with the analysis in the previous section.

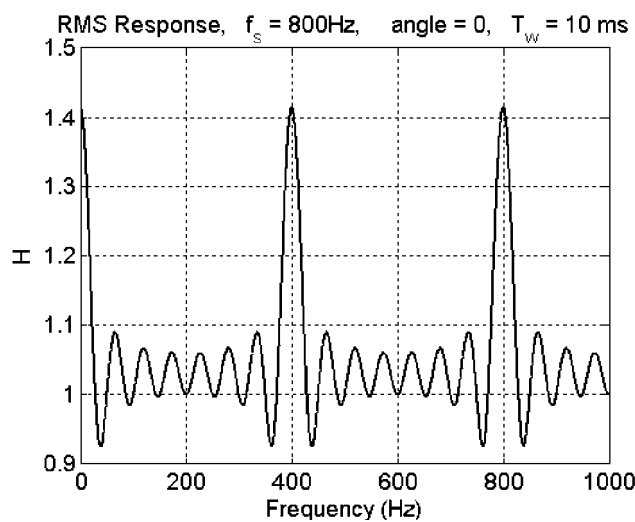
The change in point-on-wave determines the fluctuation of RMS output as a function of time. The fluctuation period is half the studied frequency cycle in this case, as suggested by (7.3.2), where α_t varies between $[0, \pi]$, *regardless of the sampling rate or sampling window size*. The fluctuation magnitude will be estimated in a latter section.

7.3.3 Impact of sampling window size on RMS output

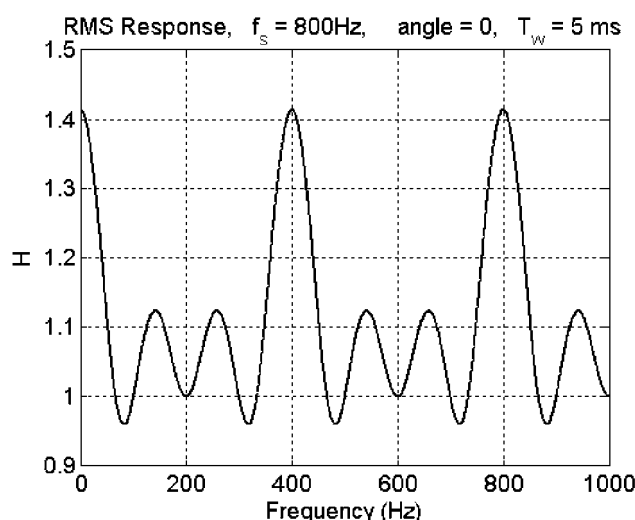
If the sampling window size is changed, say, from 20 ms to 10 ms without altering the sampling rate as the case in Fig. 7.3.2, the RMS response is like in Fig. 7.3.5(a).

The result shows that with the sampling window size reduced, the response curve in the diagram becomes less tight compared with the case of Fig. 7.3.2. There are obvious changes on the responses at different frequencies. However, as suggested by the analysis in section A, there is no change in the RMS responses at the frequencies whose periods can exactly divide double the sampling window size. In the case of Fig. 7.3.5(a), these frequencies are $f=50p$ Hz, $p \in \mathbb{N}$.

If the sampling window size is reduced further, say 5 ms, the RMS response is shown in Fig. 7.3.5(b). The frequencies that can still yield the desired fixed RMS output are in this case $f=100p$ Hz, $p \in \mathbb{N}$.



10 ms sampling window



5 ms sampling window

Fig.7.3.5 RMS frequency response with reduced sampling window size

From (7.3.2) it can also be noticed that if the sampling window size increases, there will be more frequencies that yield fixed RMS output equal to 1.0. By choosing proper window size, it is possible to get the correct effective value at any designated frequency.

In general the sampling window size determines at which frequencies the desired RMS output of 1.0 will be obtained.

7.4 RMS output error for single frequency signals

The RMS output error can be estimated by studying equations (7.3.1) and (7.3.2). As

$$-1 \leq \cos\left(2\left(\left(T_w - \frac{1}{f_s}\right)\pi + \alpha_t\right)\right) \leq 1$$

so that

$$\left(1 - \left|\frac{\sin(2fT_w\pi)}{T_w f_s \sin(2f\pi/f_s)}\right|\right)^{\frac{1}{2}} \leq Y_{\text{RMS}} \leq \left(1 + \left|\frac{\sin(2fT_w\pi)}{T_w f_s \sin(2f\pi/f_s)}\right|\right)^{\frac{1}{2}} \quad (7.4.1)$$

For any frequency f , the maximum amplitude of its RMS output fluctuation is approximated using Taylor formula as follows:

$$\Delta Y_{\text{RMS(max)}} \approx \left|\frac{\sin(2fT_w\pi)}{2T_w f_s \sin(2f\pi/f_s)}\right| \quad (7.4.2)$$

If $f_s \gg f$, the above expression can be further simplified as

$$\Delta Y_{\text{RMS(max)}} \approx \left|\frac{\sin(2fT_w\pi)}{2T_w f_s (2f\pi/f_s)}\right| = \left|\frac{\sin(2fT_w\pi)}{4fT_w\pi}\right| \leq \frac{1}{4fT_w\pi} \quad (7.4.2a)$$

In another word, the maximum error in RMS output is approximately inverse proportional to the signal frequency.

7.5 Frequency response for mixed frequency signals

The previous part of this study focus on sinusoidal signals at a particular frequency. In practice the input signal is a mixture of the fundamental and harmonic components. The frequency response of the RMS method for such a signal will be discussed in this section.

Any signal $y(t)$ that is periodic with the power system frequency can be written as a sum of harmonic components:

$$y(t) = \sqrt{2} \cos(2\pi f_0 t + \alpha_t) + \sum_{h=2}^H A_h \sqrt{2} \cos(2\pi h f_0 t + \alpha_{ht}) \quad (7.5.1)$$

where h harmonic order

A_h effective magnitude of h th harmonic component

α_{ht} initial angle of h th harmonic component at the start of the window

H the highest harmonic order

The amplitude of the fundamental component is set to be $\sqrt{2}$ as before. Its total RMS value is calculated as

$$Y_{\text{RMS}(\text{total})}^2 = \frac{1}{K} \sum_{k=0}^{K-1} (y(t))^2 = Y_1^2 + Y_2^2 + Y_3^2 + Y_4^2 \quad (7.5.2)$$

with:

$$Y_1^2 = \frac{2}{K} \sum_{k=0}^{K-1} (\cos(2\pi f_0 k \Delta t + \alpha_t))^2 \quad (7.5.2a)$$

$$Y_2^2 = \frac{2}{K} \sum_{k=0}^{K-1} \sum_{h=2}^H (A_h \cos(2\pi h f_0 k \Delta t + \alpha_{ht}))^2 \quad (7.5.2b)$$

$$Y_3^2 = \frac{4}{K} \sum_{k=0}^{K-1} \sum_{m=2}^H A_m \cos(2\pi f_0 k \Delta t + \alpha_t) \cos(2\pi m f_0 k \Delta t + \alpha_{mt}) \quad (7.5.2c)$$

$$Y_4^2 = \frac{2}{K} \sum_{k=0}^{K-1} \sum_{l=2}^H \sum_{\substack{m=2 \\ m \neq l}}^H A_l A_m \cos(2\pi l f_0 k \Delta t + \alpha_{lt}) \cos(2\pi m f_0 k \Delta t + \alpha_{mt}) \quad (7.5.2d)$$

The first term Y_1^2 in (7.5.2) is the same expression as (7.3.1) for the RMS value of a single-frequency signal. The error analysis as discussed in the previous part of this chapter, applies directly to this term.

The second term Y_2^2 gives the sum of the RMS values of the individual harmonic components, as obtained by (7.3.1). This term could be interpreted as an error term when the RMS value is used as an estimate of the magnitude of the fundamental component. However generally it is not considered as an error term. The exact value is again obtained under the conditions discussed before.

Terms Y_3^2 and Y_4^2 are the terms that cause an additional error in RMS output. They will be discussed in further details below.

Below, we study the four terms in (7.5.2) separately.

7.5.1 Impact of sampling rate on total RMS output

In the case when terms Y_3^2 and Y_4^2 in (7.5.2) are neglected (i.e. no additional error in RMS output) it is easy to calculate the RMS frequency response by knowing the frequency response for each single frequency component.

At the frequencies that are multiple of half the fundamental frequency, their RMS outputs exactly reflect their effective magnitude, except at multiples of the Nyquist sampling rate. As discussed in the previous section, the main

impact of the sampling rate is that it will shift the multiples of the Nyquist sampling rate. The lower the sampling rate, the closer the two consecutive multiples of the Nyquist sampling rate. In the case of mixed frequency signal, it will yield incorrect total RMS output if one of the harmonic components is located at a multiple of the Nyquist sampling rate. When a suitable anti-aliasing filter is used, no components will be present equal to the Nyquist sampling rate or its multiples

By checking the frequency response at the frequencies that are not at integer multiple of half the fundamental frequency, it is clear that Y_{RMS} will show fluctuation in output at these frequencies, as in the case for a single frequency signal.

7.5.2 Impact of point-on-wave on total RMS output

As discussed before, the impact of point-on-wave is only at multiples of the Nyquist sampling rate as well as at frequencies that are not integer multiple of half the fundamental frequency. So the terms Y_1^2 and Y_2^2 in (7.5.2) are independent of point-on-wave when the frequency is at the integer multiple of half the fundamental frequencies, except for the multiples of the Nyquist sampling rate. For the other frequencies, the point-on-wave contributes to the fluctuation in total RMS output.

7.5.3 Impact of sampling window size on total RMS output

To study the impact of sampling window size on total RMS output, the terms in (7.5.2) need to be studied.

— The first term Y_1^2

For Y_1^2 , the shortest sampling window size that results in zero error is half the period of the fundamental component.

— The second term Y_2^2

The second term Y_2^2 in (11) can be written as the sum of the RMS values for each of the harmonic terms:

$$Y_2^2 = \sum_{h=2}^H \frac{2}{K} \sum_{k=0}^{K-1} (A_h \cos(2\pi h f_0 k \Delta t + \alpha_{ht}))^2 \quad (7.5.2e)$$

The shortest sampling window size that yields zero error for a given harmonic order is actually half the period for that harmonic order and therefore shorter than half the fundamental component period. However, if all the harmonics show up, the shortest sampling window that can meet the requirement for all the harmonic orders will be

$$T = T_0 / \text{gcd}(2 \times 2, 3 \times 2, \dots, H \times 2) = T_0 / 2 \quad H \in \mathbb{N} \quad (7.5.2f)$$

Where T_0 the period of the fundamental component
gcd the greatest common divisor
H the highest harmonic order in the signal

— The third term Y_3^2

The third term contains cross terms due to the non-linearity in calculating the RMS value. This term can be written as:

$$Y_3^2 = \frac{2}{K} \sum_{k=0}^{K-1} \sum_{m=2}^H (A_m \cos(2\pi f_0 (m+1)k \Delta t + \alpha_t + \alpha_{mt}))$$

$$+ A_m \cos(2\pi f_0 (m-1)k\Delta t - \alpha_t + \alpha_{mt})) \quad (7.5.2g)$$

In (7.5.2g), both terms are sinusoidal waves, but with different frequencies. The summation of a sinusoidal wave is zero over any integer number of periods. The former term has a period equal to $T_0/(m+1)$, with T_0 being the period of the fundamental frequency. The latter term has a period equal to $T_0/(m-1)$.

The inner summation is equal to zero when the summation interval (i.e. the window of the RMS calculation) is equal simultaneously to an integer multiple of $T_0/(m+1)$ and an integer multiple of $T_0/(m-1)$. When the signal contains all harmonics, the shortest sampling window that makes $Y_3^2=0$ is

$$T = T_0/\text{gcd}(2-1, 2+1, 3-1, 3+1, \dots, H-1, H+1) = T_0 \quad (7.5.2h)$$

If the input signal contains no even harmonics, i.e. $H=2n+1$, $n \in \mathbb{N}$, then

$$T = T_0/\text{gcd}(3-1, 3+1, 5-1, 5+1, \dots, H-1, H+1) = T_0/2 \quad (7.5.2i)$$

— The fourth term Y_4^2

The fourth term Y_4^2 in (7.5.2d) can be rewritten as:

$$Y_4^2 = \frac{1}{K} \sum_{k=0}^{K-1} \sum_{l=2}^H \sum_{\substack{m=2 \\ m \neq l}}^H A_l A_m (\cos(2\pi(l+m)f_0 k\Delta t + \alpha_{lt} + \alpha_{mt}) \\ + \cos(2\pi(l-m)f_0 k\Delta t + \alpha_{lt} - \alpha_{mt})) \quad (7.5.2j)$$

Again it is a summation over two sinusoidal waves with different frequencies. To result in a zero summation, the summation interval needs to be an integer multiple of $T_0/(l+m)$ and an integer multiple of $T_0/(l-m)$. The shortest window that makes $Y_4^2 = 0$ is

$$T = T_0 / \gcd(3-2, 3+2, 4-2, 4+2, \dots, l-m, l+m, \dots) = T_0 \quad l, m \in \mathbb{N} \quad (7.5.2k)$$

If no even harmonics are present in the signal, i.e. $l=2p+1, m=2q+1, p, q \in \mathbb{N}$, then the shortest sampling window that makes $Y_4^2 = 0$ is

$$T = T_0 / \gcd(5-3, 5+3, 6-3, 6+3, \dots, l-m, l+m, \dots) = T_0/2$$

$$l=2p+1, m=2q+1, p, q \in \mathbb{N} \quad (7.5.2l)$$

The shortest sampling windows that can result in zero error in (7.5.2) are listed in the table 7.5.1, for each term separately. All the window lengths are referred to one fundamental component cycle

Table 7.5.1 Shortest sampling window size for each term in (7.5.2)

	Independent harmonics	Mutual impact among harmonics *	
		With even harmonics	Without even harmonics
Y_1^2 with zero error	0.5 cycle	—	—
Y_2^2 with zero error**	0.5 cycle	—	—
$Y_3^2 = 0^{**}$	—	1 cycle	0.5 cycle
$Y_4^2 = 0^{**}$	—	1 cycle	0.5 cycle

* Fundamental component is always contained in the input mixed frequency signal

** Assume the signal contains all the harmonic orders

It is clear that using 0.5 cycle sampling window leads to oscillation in RMS output if the input mixed frequency signal contains even harmonics. In case of RMS oscillation, the combined RMS output cannot be calculated as the square root of the sum of the square of each particular component RMS value.

An example of RMS oscillation is shown in Fig. 7.5.1. The input signal in the figure is a mixture of fundamental frequency together with odd and even harmonics. The third oscillating line is obtained by using a half-cycle window, the thin straight line by using a one-cycle window.

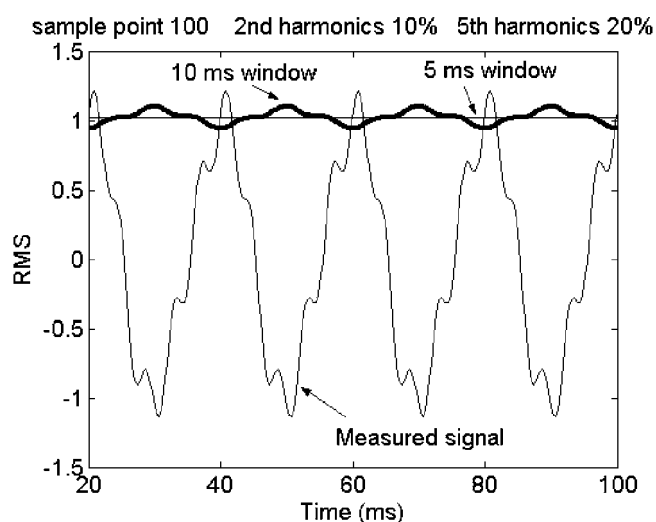


Fig. 7.5.1 RMS fluctuation due to mixture of both even and odd harmonics

In practice, RMS is mainly used to describe a measured voltage. A voltage signal has the following three characteristics:

1. There is always one odd harmonic present: the fundamental frequency.
2. The total harmonic components in voltage signal is relatively low, normally less than 5% of the fundamental magnitude
3. The even harmonic components in voltage signal is relatively low compared with odd ones

These characters can explain why in most cases, 0.5 cycle sampling window can yield an acceptable RMS output. However during voltage dips due to transformer energizing [107] and during transformer saturation after a voltage dip due to a fault [108][109], a large even-harmonic component may occur. This will lead to large oscillations in the RMS value when a half-cycle window is used. This should be avoided when the RMS voltage is used to calculate magnitude and duration of an event [110][111], but could be used as an indicator of transformer saturation when the measurements are used for diagnostic purposes.

7.6 RMS output error for mixed frequency signals

The RMS output error for mixed frequency signal can be estimated by simplifying (7.5.2). For this simplification we assume that the magnitude of the harmonic components is much lower than the fundamental component. This holds for voltage measurements and for most current measurements. However for current measurements close to non-linear load this assumption will not hold. The term Y_4^2 in (7.5.2) contains the product of harmonic amplitudes, and can be omitted. The same holds for the second term. We further assume that we use a half-cycle window, so that the error in the first term of (7.5.2) becomes zero. The resulting expression for the RMS value is:

$$Y_{\text{RMS}(\text{total})} = \sqrt{Y_1^2 + Y_2^2 + Y_3^2 + Y_4^2} \approx \sqrt{1 + Y_3^2} \approx 1 + \frac{1}{2} Y_3^2$$

as

$$\begin{aligned} Y_1^2 &= 1 \\ Y_2^2 &\ll 1 \\ Y_4^2 &\ll 1 \\ Y_3^2 &\text{ is quite small} \end{aligned}$$

Using (7.5.2c) results in the following expression for the error:

$$\Delta Y_{\text{RMS}(\text{total,max})} \approx \left| \frac{2}{K} \sum_{k=0}^{K-1} \sum_{m=2}^H A_m \cos(2\pi f_0 k \Delta t + \alpha_t) \cos(2\pi m f_0 k \Delta t + \alpha_{mt}) \right| \quad (7.6.1)$$

Because we assume a sampling window of half the fundamental period, according to the analysis of equations (7.5.2g) and (7.5.2i) in the previous section, for any odd harmonics order m :

$$\sum_{k=0}^{K-1} A_m \cos(2\pi f_0 k \Delta t + \alpha_t) \cos(2\pi m f_0 k \Delta t + \alpha_{mt}) = 0$$

So the only concerns are with the even harmonics. Since a half fundamental cycle sampling window is applied, $\Delta t = 1/(2Kf_0)$. Only considering even harmonics, we obtain:

$$\begin{aligned} \Delta Y_{\text{RMS}(\text{total})} &= \left| \frac{2}{K} \sum_{k=0}^{K-1} \sum_{\substack{m=2 \\ m \in \text{even}}}^H A_m \cos\left(\frac{\pi}{K}k + \alpha_t\right) \cos\left(\frac{\pi m}{K}k + \alpha_{mt}\right) \right| \\ &= \left| \frac{4}{K} \sum_{\substack{m=2 \\ m \in \text{even}}}^H A_m \frac{e^{j\frac{m+1}{K}\pi} (-\cos \alpha_t \cos(\frac{m}{K}\pi - \alpha_{mt}) + \cos(\frac{\pi}{K} - \alpha_t) \cos \alpha_{mt})}{(e^{j\frac{\pi}{K}} - e^{j\frac{m\pi}{K}})(-1 + e^{j\frac{m+1}{K}\pi})K} \right| \\ &= \left| \frac{2}{K^2} \sum_{\substack{m=2 \\ m \in \text{even}}}^H A_m \frac{(-\cos \alpha_t \cos(\frac{m}{K}\pi - \alpha_{mt}) + \cos(\frac{\pi}{K} - \alpha_t) \cos \alpha_{mt})}{(\cos \frac{\pi}{K} - \cos \frac{m}{K}\pi)} \right| \end{aligned} \quad (7.6.1a)$$

When the sampling rate is high, i.e. K is sufficiently large (e. g. $K=128$), $\cos(\pi/K - \alpha_t) \approx \cos \alpha_t$ and $\cos(\pi/K) \approx 1.0$,

$$\Delta Y_{\text{RMS(total)}} \approx \left| \frac{2}{K^2} \sum_{\substack{m=2 \\ m \in \text{even}}}^H A_m \frac{-\cos \alpha_t (\cos(\frac{m}{K} \pi - \alpha_{mt}) - \cos \alpha_{mt})}{1 - \cos \frac{m}{K} \pi} \right|$$

Let $x = \frac{m}{K} \pi$ then

$$\begin{aligned} \Delta Y_{\text{RMS(total)}} &\approx \left| \frac{2}{K^2} \sum_{\substack{m=2 \\ m \in \text{even}}}^H A_m \frac{-\cos \alpha_t (\cos(x - \alpha_{mt}) - \cos \alpha_{mt})}{1 - \cos x} \right| \\ &= \left| \frac{2}{K^2} \sum_{\substack{m=2 \\ m \in \text{even}}}^H A_m \frac{-\cos \alpha_t (\cos x \cos \alpha_{mt} + \sin x \sin \alpha_{mt} - \cos \alpha_{mt})}{1 - \cos x} \right| \end{aligned} \quad (7.6.1b)$$

As x is small

$$\begin{cases} \cos x \approx 1 - \frac{1}{2} x^2 \\ \sin x \approx x \end{cases}$$

(7.6.1b) can then be simplified as

$$\begin{aligned} \Delta Y_{\text{RMS(total)}} &\approx \left| \frac{2}{K^2} \sum_{\substack{m=2 \\ m \in \text{even}}}^H A_m \frac{-\cos \alpha_t ((1 - \frac{1}{2} x^2) \cos \alpha_{mt} + x \sin \alpha_{mt} - \cos \alpha_{mt})}{\frac{1}{2} x^2} \right| \\ &= \left| \frac{2}{K^2} \sum_{\substack{m=2 \\ m \in \text{even}}}^H A_m \cos \alpha_t (\cos \alpha_{mt} - \frac{2}{x} \sin \alpha_{mt}) \right| \end{aligned} \quad (7.6.1c)$$

Now replace the x in (12c) with $x = m\pi/K$

$$\Delta Y_{\text{RMS(total)}} = \left| \frac{2}{K^2} \sum_{\substack{m=2 \\ m \in \text{even}}}^H A_m \cos \alpha_t \left(\cos \alpha_{mt} - \frac{2K}{m\pi} \sin \alpha_{mt} \right) \right| \quad (7.6.1d)$$

In (7.6.1d), it is the second term that dominates, if the main error contribution is expected from lower order harmonics (note K is much bigger than m), so

$$\begin{aligned} \Delta Y_{\text{RMS(total)}} &\approx \left| \frac{2}{K^2} \sum_{\substack{m=2 \\ m \in \text{even}}}^H A_m \cos \alpha_t \left(-\frac{2K}{m\pi} \sin \alpha_{mt} \right) \right| \\ &= \left| \frac{4}{\pi K} \sum_{\substack{m=2 \\ m \in \text{even}}}^H \frac{1}{m} A_m \cos \alpha_t \sin \alpha_{mt} \right| \end{aligned} \quad (7.6.1e)$$

In case there is a dominant even harmonic M,

$$\begin{aligned} \Delta Y_{\text{RMS(total,max)}} &\approx \frac{4}{\pi KM} \cos \alpha_t \sin \alpha_{Mt} \\ &\leq \frac{4}{\pi KM} = \frac{4}{\pi f_s (T_0/2) M} = \frac{8f_0}{\pi f_s M} \end{aligned} \quad (7.6.1f)$$

This means that in the case that a half-cycle sampling window is applied

- *The lower the order of dominant even harmonics, the larger the RMS error will be*
- *The higher the sampling frequency, the smaller the RMS error will be*

7.7 RMS error of single frequency signals due to frequency deviation

In practical power systems, the frequency of the system will always deviate somewhat from the nominal frequency. In such a case the RMS measurement, which is based on fundamental frequency and harmonics,

cannot yield a magnitude that is identical to the one of the input signal. Such output error is dependent on the factors discussed before.

In normal operation the frequency deviation is small. For a 50 Hz system the variation of power frequency is typically within the range from 49.5 Hz to 50.5 Hz, though in some systems the range in frequency is even wider.

To study the frequency response of RMS method for asynchronous fundamental frequency signals, the derivative of RMS output versus frequency is used. Knowing this derivative, the RMS output error can be estimated.

We will assume a sinusoidal signal and a window length of K.

To deduct the derivative of RMS output versus frequency, starting from (7.3.1):

$$\begin{aligned}
 \frac{dY_{\text{RMS}}(t)}{df} &= \frac{1}{2Y_{\text{RMS}}} \times \frac{1}{K} \left(-4\pi\Delta t \sum_{k=0}^{K-1} k \sin 2(2\pi fk\Delta t + \alpha_t) \right) \\
 &= \frac{-2\pi}{Y_{\text{RMS}} K f_s} \sum_{k=0}^{K-1} k \sin \left(\frac{4fk}{f_s} \pi + 2\alpha_t \right) \\
 &= \frac{\pi}{Y_{\text{RMS}} f_s} \times \frac{\cos \left(\frac{2f}{f_s} \pi - 2\alpha_t \right)}{\sin \left(\frac{2f}{f_s} \pi \right)} \tag{7.7.1}
 \end{aligned}$$

(7.7.1) shows that:

- The variation rate is dependent on sampling rate and point-on-wave

- The variation rate is independent on sampling window size when $f/f_s \neq q/2, q \in \mathbb{N}$
- For any frequency with a fixed sampling rate, the maximum variation rate occurs when the sampling window reaches a position $\alpha_t = f\pi/f_s, f/f_s \neq q/2, q \in \mathbb{N}$. The minimum variation rate happens when $\alpha = (f\pi/f_s \pm 1/4)\pi, f/f_s \neq q/2, q \in \mathbb{N}$. Such values reflect the possible errors in RMS output due to frequency deviation.
- The variation rate is meaningless when $f/f_s \neq q/2, q \in \mathbb{N}$.

Also can be concluded is that when the sampling rate is high enough, $2f\pi/f_s \rightarrow 0$:

$$\Delta Y_{\text{RMS(max)}} \approx \frac{\pi}{Y_{\text{RMS}} f_s} * \frac{1}{2f\pi/f_s} * \Delta f = \frac{\Delta f}{2f} \quad (7.7.1a)$$

(7.7.1a) tells that for a 1% error in fundamental frequency, a 0.5% error will occur in RMS output value. Note here $Y_{\text{RMS}} = 1$, as discussed in the previous section.

7.8 RMS error of mixed frequency signals due to frequency deviation

Similar to the case of single frequency signal, the frequency response of RMS method can be studied for signals of asynchronous fundamental frequency mixed with its harmonics. To do this, derivative is taken on (7.5.2) in the case that terms Y_3^2 and Y_4^2 in (7.5.2) are zero. Bear in mind that here it is assumed that with the fundamental frequency deviates, all the harmonic frequencies change accordingly.

$$\begin{aligned}
 \frac{dY_{\text{RMS}(\text{total})}(t)}{df_0} &= \frac{1}{2Y_{\text{RMS}(\text{total})}(t)} * \frac{1}{K} \left(-4\pi\Delta t \sum_{k=0}^{K-1} k \sin 2(2\pi f_0 k\Delta t + \alpha_t) \right. \\
 &\quad \left. - 4\pi\Delta t \sum_{h=2}^H \sum_{k=0}^{K-1} hkA_h \sin 2(2\pi h f_0 k\Delta t + \alpha_{ht}) \right) \\
 &= \frac{-2\pi}{Y_{\text{RMS}(\text{total})} K f_s} \left(\sum_{k=0}^{K-1} k \sin \left(\frac{4f_0 k}{f_s} \pi + 2\alpha_t \right) + \sum_{h=2}^H \sum_{k=0}^{K-1} hkA_h \sin \left(\frac{4hf_0 k}{f_s} \pi + 2\alpha_{ht} \right) \right) \\
 &= \frac{\pi}{Y_{\text{RMS}(\text{total})}(t) f_s} \left(\frac{\cos \left(\frac{2f_0}{f_s} \pi - 2\alpha_t \right)}{\sin \left(\frac{2f_0}{f_s} \pi \right)} + \sum_{h=2}^H hA_h \frac{\cos \left(\frac{2hf_0}{f_s} \pi - 2\alpha_{ht} \right)}{\sin \left(\frac{2hf_0}{f_s} \pi \right)} \right)
 \end{aligned} \tag{7.8.1}$$

When the sampling rate is high enough, $2f_0 \pi / f_s \rightarrow 0$, the maximum error in total RMS output due to asynchronous fundamental frequency is:

$$\begin{aligned}
 \Delta Y_{\text{RMS}(\text{total}, \text{max})} &\approx \frac{\pi}{Y_{\text{RMS}(\text{total})}(t) f_s} * \left(\frac{f_s}{2\pi f_0} + \sum_{h=2}^H hA_h \frac{f_s}{2\pi h f_0} \right) * \Delta f_0 \\
 &= \left(\frac{1 + \sum_{h=2}^H A_h}{2f_0 Y_{\text{RMS}(\text{total})}(t)} \right) \Delta f_0
 \end{aligned} \tag{7.8.1a}$$

As discussed in the previous sections, in the 1st situation

$$Y_{\text{RMS}(\text{total})}(t) = \sqrt{1 + \sum_{h=2}^H A_h^2}$$

so

$$\begin{aligned}
 \Delta Y_{\text{RMS}(\text{total}, \text{max})} &= \left(\frac{1 + \sum_{h=2}^H A_h}{2f_0 Y_{\text{RMS}(\text{total})}(t)} \right) \Delta f_0 = \left(\frac{1 + \sum_{h=2}^H A_h}{2f_0 \sqrt{1 + \sum_{h=2}^H A_h^2}} \right) \Delta f_0 \\
 &> \frac{\sqrt{1 + \sum_{h=2}^H A_h^2}}{2f_0} \Delta f_0 > \frac{1}{2f_0} \Delta f_0
 \end{aligned} \tag{7.8.1b}$$

Checking both Eqns. (7.8.1b) and (7.7.1a) tells that compared with the case of single frequency signal, a signal of mixed frequencies has larger error in RMS output due to asynchronous fundamental frequency.

Chapter 8 Impact of Frequency Deviation on DFT/DEA-based Relays

As discussed in previous chapters, DFT (Discrete Fourier Transform) algorithm and DEA (Differential Equation) algorithm are the two techniques that are applied in impedance relays in practical industries. To assess the possible impact of frequency deviation on impedance relays, it is necessary to study the frequency responses of these algorithms at frequency deviation.

8.1 Response of DFT for overcurrent relays in case of frequency deviation

To study the response of DFT algorithm for overcurrent relays when there is frequency deviation, we again start from Eqn (3.2.1.9), which reads as follows:

$$I^2 = \left(\frac{2}{K} \sum_{k=0}^{K-1} \cos\left(\frac{2\pi k}{K}\right) A_1 \cos\left(\frac{2\pi k f}{K f_0} + \beta\right) \right)^2 + \left(\frac{2}{K} \sum_{k=0}^{K-1} \sin\left(\frac{2\pi k}{K}\right) A_1 \cos\left(\frac{2\pi k f}{K f_0} + \beta\right) \right)^2 \quad (8.1.1)$$

where	K	Sampling points in one fundamental cycle
	f	Signal frequency
	f ₀	fundamental frequency
	β	point-on-wave of measurement (initial phase)

The above equation calculates the square of the detected value after DFT processing. As can be seen later, such a detected value is equal to A_I if the input signal is of standard sinusoidal waveform.

This expression can be expanded as follows:

$$I^2 = G_1^2 + G_2^2$$

with

$$G_1^2 = \left(\frac{2}{K} \sum_{k=0}^{K-1} \cos\left(\frac{2\pi k}{K}\right) A_I \cos\left(\frac{2\pi k f}{K f_0} + \beta\right) \right)^2$$

$$G_2^2 = \left(\frac{2}{K} \sum_{k=0}^{K-1} \sin\left(\frac{2\pi k}{K}\right) A_I \cos\left(\frac{2\pi k f}{K f_0} + \beta\right) \right)^2$$

To know the impact of frequency deviation on the DFT output in (8.1.1), one can take the derivative of the above equation at $f=f_0$.

$$\begin{aligned} \frac{d}{df} G_1^2 &= -2G_1 \frac{2}{K} \times \frac{2\pi A_I}{K f_0} \sum_{k=0}^{K-1} k \cos\left(\frac{2\pi k}{K}\right) \sin\left(\frac{2\pi k f}{K f_0} + \beta\right) \\ &= -8G_1 \times \frac{\pi A_I}{K^2 f_0} \sum_{k=0}^{K-1} k \cos\left(\frac{2\pi k}{K}\right) \sin\left(\frac{2\pi k f}{K f_0} + \beta\right) \end{aligned}$$

at $f=f_0$, we write G_1 as

$$\begin{aligned} G_1 &= \frac{2}{K} \sum_{k=0}^{K-1} \cos\left(\frac{2\pi k}{K}\right) A_I \cos\left(\frac{2\pi k}{K} + \beta\right) \\ &= A_I \cos \beta \end{aligned}$$

resulting in the following expression for the derivate:

$$\begin{aligned} \left. \frac{d}{df} G_1^2 \right|_{f=f_0} &= -8A_I \cos \beta \times \frac{\pi A_I}{K^2 f_0} \sum_{k=0}^{K-1} k \cos\left(\frac{2\pi k}{K}\right) \sin\left(\frac{2\pi k f_0}{K f_0} + \beta\right) \\ &= -8A_I^2 \cos \beta \times \frac{\pi}{K^2 f_0} \times \left(\frac{K}{8}\right) \times \left(-4 \sin \beta + 2K \sin \beta - 2 \cos \beta \operatorname{ctg} \frac{2\pi}{K}\right) \end{aligned}$$

$$= -A_1^2 \cos \beta \times \frac{\pi}{Kf_0} \times \left(-4 \sin \beta + 2K \sin \beta - 2 \cos \beta \operatorname{ctg} \frac{2\pi}{K} \right) \quad (8.1.2)$$

Similarly for the derivative of G_2^2 over frequency f

$$\begin{aligned} \frac{d}{df} G_2^2 &= -2G_2 \frac{2}{K} \times \frac{2\pi A_1}{Kf_0} \sum_{k=0}^{K-1} k \sin\left(\frac{2\pi k}{K}\right) \sin\left(\frac{2\pi kf}{Kf_0} + \beta\right) \\ &= -8G_2 \times \frac{\pi A_1}{K^2 f_0} \sum_{k=0}^{K-1} k \sin\left(\frac{2\pi k}{K}\right) \sin\left(\frac{2\pi kf}{Kf_0} + \beta\right) \end{aligned}$$

at $f=f_0$, we get:

$$\begin{aligned} G_2 &= \frac{2}{K} \sum_{k=0}^{K-1} \sin\left(\frac{2\pi k}{K}\right) A_1 \cos\left(\frac{2\pi k}{K} + \beta\right) \\ &= -A_1 \sin \beta \end{aligned}$$

So that

$$\begin{aligned} \left. \frac{d}{df} G_2^2 \right|_{f=f_0} &= 8A_1 \sin \beta \times \frac{\pi A_1}{K^2 f_0} \sum_{k=0}^{K-1} k \sin\left(\frac{2\pi k}{K}\right) \sin\left(\frac{2\pi kf_0}{Kf_0} + \beta\right) \\ &= A_1^2 \sin \beta \times \frac{\pi}{Kf_0} \times \left(2K \cos \beta - 2 \sin \beta \operatorname{ctg} \frac{2\pi}{K} \right) \quad (8.1.3) \end{aligned}$$

Combining (8.1.2) and (8.1.3) gives the following expression for the slope of the estimated current versus frequency, around the fundamental frequency.

$$\begin{aligned} \left. \frac{d}{df} I \right|_{f=f_0} &= \left(\left. \frac{d}{df} (G_1^2 + G_2^2)^{\frac{1}{2}} \right) \right|_{f=f_0} \\ &= \left(\frac{1}{2} \times \frac{1}{\sqrt{G_1^2 + G_2^2}} \times \left(\frac{d}{df} G_1^2 + \frac{d}{df} G_2^2 \right) \right) \Big|_{f=f_0} \end{aligned}$$

$$\begin{aligned}
 &= \frac{1}{2} \times \frac{1}{A_1} \times A_1^2 \times \frac{\pi}{Kf_0} \times (4 \sin \beta \cos \beta - 2K \sin \beta \cos \beta \\
 &+ 2 \cos^2 \beta \operatorname{ctg} \frac{2\pi}{K} + 2K \sin \beta \cos \beta - 2 \sin^2 \beta \operatorname{ctg} \frac{2\pi}{K}) \\
 &= A_1 \times \frac{\pi}{Kf_0} \times \left(\sin 2\beta + \cos 2\beta \operatorname{ctg} \frac{2\pi}{K} \right) \quad (8.1.4)
 \end{aligned}$$

Note that K is the number of sampling points per fundamental cycle. Typical values in protection relays are 16 and 32. For increasing value of K we can use that

$$\operatorname{ctg} \frac{2\pi}{K} \approx \frac{K}{2\pi}$$

so that
$$\lim_{K \rightarrow \infty} \frac{1}{K} \operatorname{ctg} \frac{2\pi}{K} = \frac{1}{2\pi}$$

For $K=16$, the error is about 5% while for $K=32$ the error is about 1%

Using this approximation in (8.1.4) yields

$$\left. \frac{d}{df} I \right|_{f=f_0} = A_1 \times \frac{\pi}{Kf_0} \times \sin 2\beta + A_1 \times \cos 2\beta \times \frac{1}{2f_0} \quad (8.1.5)$$

The slope (and thus the error) is a function of the initial phase β . The maximum of (8.1.5) is:

$$\max \left(\left. \frac{d}{df} I \right|_{f=f_0} \right) = \sqrt{\left(\frac{\pi}{K} \times \frac{A_1}{f_0} \right)^2 + \left(\frac{1}{2} \times \frac{A_1}{f_0} \right)^2} = \frac{A_1}{f_0} \sqrt{\frac{\pi^2}{K^2} + \frac{1}{4}}$$

For practical value of K we can approximate $K^2 \gg \pi^2$, so that

$$\max \left(\left. \frac{d}{df} I \right|_{f=f_0} \right) \approx \frac{A_1}{2f_0}$$

For $f_0 = 50$ Hz, the error in current estimate is 1% of the frequency deviation.

8.2 Response of DFT for impedance relays in case of frequency deviation

To study the response of DFT algorithm for impedance relays when there is frequency deviation around fundamental power frequency f_0 , it is necessary to take derivative for the expressions of resistance R and reactance X in equations (3.3.1.2) and (3.3.1.3):

$$\begin{aligned}
 \left. \frac{dR}{df} \right|_{f=f_0} &= \left. \frac{d}{df} \left(\frac{U_C I_C + U_S I_S}{I_C^2 + I_S^2} \right) \right|_{f=f_0} \\
 &= \left. \left(\frac{(U_C I_C + U_S I_S)'}{I_C^2 + I_S^2} - \frac{(U_C I_C + U_S I_S)(I_C^2 + I_S^2)'}{(I_C^2 + I_S^2)^2} \right) \right|_{f=f_0} \\
 &= \left. \left(\frac{U_C' I_C + U_C I_C' + U_S' I_S + U_S I_S'}{I_C^2 + I_S^2} - \frac{(U_C I_C + U_S I_S)(2I_C I_C' + 2I_S I_S')}{(I_C^2 + I_S^2)^2} \right) \right|_{f=f_0}
 \end{aligned} \tag{8.2.1}$$

$$\begin{aligned}
 \left. \frac{dX}{df} \right|_{f=f_0} &= \left. \frac{d}{df} \left(\frac{U_S I_C - U_C I_S}{I_C^2 + I_S^2} \right) \right|_{f=f_0} \\
 &= \left. \left(\frac{(U_S I_C - U_C I_S)'}{I_C^2 + I_S^2} - \frac{(U_S I_C - U_C I_S)(I_C^2 + I_S^2)'}{(I_C^2 + I_S^2)^2} \right) \right|_{f=f_0} \\
 &= \left. \left(\frac{U_S' I_C + U_S I_C' - U_C' I_S - U_C I_S'}{I_C^2 + I_S^2} - \frac{(U_S I_C - U_C I_S)(2I_C I_C' + 2I_S I_S')}{(I_C^2 + I_S^2)^2} \right) \right|_{f=f_0}
 \end{aligned} \tag{8.2.2}$$

$$\text{Let } U(k\Delta t) = A_v \cos(2\pi f k \Delta t + \alpha) \tag{8.2.3a}$$

$$I(k\Delta t) = A_I \cos(2\pi f k \Delta t + \beta) \quad (8.2.3b)$$

$$\text{As } \Delta t = \frac{1}{Kf_0}$$

Then

$$\begin{aligned} U_C|_{f=f_0} &= \frac{2}{K} \sum_{k=0}^{K-1} \cos\left(\frac{2\pi k}{K}\right) A_V \cos\left(\frac{2\pi f_0 k}{Kf_0} + \alpha\right) \\ &= A_V \cos \alpha \end{aligned} \quad (8.2.3c)$$

$$\begin{aligned} U_S|_{f=f_0} &= \frac{2}{K} \sum_{k=0}^{K-1} \sin\left(\frac{2\pi k}{K}\right) A_V \cos\left(\frac{2\pi f_0 k}{Kf_0} + \alpha\right) \\ &= -A_V \sin \alpha \end{aligned} \quad (8.2.3d)$$

$$\begin{aligned} I_C|_{f=f_0} &= \frac{2}{K} \sum_{k=0}^{K-1} \cos\left(\frac{2\pi k}{K}\right) A_I \cos\left(\frac{2\pi f_0 k}{Kf_0} + \beta\right) \\ &= A_I \cos \beta \end{aligned} \quad (8.2.3e)$$

$$\begin{aligned} I_S|_{f=f_0} &= \frac{2}{K} \sum_{k=0}^{K-1} \sin\left(\frac{2\pi k}{K}\right) A_I \cos\left(\frac{2\pi f_0 k}{Kf_0} + \beta\right) \\ &= -A_I \sin \beta \end{aligned} \quad (8.2.3f)$$

$$I_C^2 + I_S^2 = A_I^2 \quad (8.2.3g)$$

Similarly as in the case of section 8.1

$$(U_C)' = \frac{d}{df} U_C \Big|_{f=f_0}$$

$$= -A_V \times \frac{\pi}{2Kf_0} \times \left(-4\sin\alpha + 2K\sin\alpha - 2\cos\alpha \operatorname{ctg} \frac{2\pi}{K} \right) \quad (8.2.3h)$$

$$(U_S)' = \frac{d}{df} U_S \Big|_{f=f_0}$$

$$= -A_V \times \frac{\pi}{2Kf_0} \times \left(2K\cos\alpha - 2\sin\alpha \operatorname{ctg} \frac{2\pi}{K} \right) \quad (8.2.3i)$$

$$(I_C)' = \frac{d}{df} I_C \Big|_{f=f_0}$$

$$= -A_I \times \frac{\pi}{2Kf_0} \times \left(-4\sin\beta + 2K\sin\beta - 2\cos\beta \operatorname{ctg} \frac{2\pi}{K} \right) \quad (8.2.3j)$$

$$(I_S)' = \frac{d}{df} I_S \Big|_{f=f_0}$$

$$= -A_I \times \frac{\pi}{2Kf_0} \times \left(2K\cos\beta - 2\sin\beta \operatorname{ctg} \frac{2\pi}{K} \right) \quad (8.2.3k)$$

Eqn. (8.2.1) can then be expanded as

$$\frac{d}{df} R \Big|_{f=f_0} = \left(\frac{U'_C I_C + U_C I'_C + U'_S I_S + U_S I'_S}{A_I^2} - \frac{(U_C I_C + U_S I_S)(2I'_C + 2I'_S)}{(A_I^2)^2} \right) \Big|_{f=f_0}$$

$$\begin{aligned}
 &= \frac{\cos \beta}{A_I} U'_C + \frac{A_V \cos \alpha}{A_I^2} I'_C - \frac{\sin \beta}{A_I} U'_S - \frac{A_V \sin \alpha}{A_I^2} I'_S \\
 &\quad - \frac{2A_V \cos \alpha \cos^2 \beta}{A_I^2} I'_C + \frac{2A_V \cos \alpha \cos \beta \sin \beta}{A_I^2} I'_S \\
 &\quad - \frac{2A_V \sin \alpha \cos \beta \sin \beta}{A_I^2} I'_C + \frac{2A_V \sin \alpha \sin^2 \beta}{A_I^2} I'_S \\
 &= \frac{\cos \beta}{A_I} U'_C - \frac{A_V \cos \alpha \cos 2\beta}{A_I^2} I'_C - \frac{\sin \beta}{A_I} U'_S - \frac{A_V \sin \alpha \cos 2\beta}{A_I^2} I'_S \\
 &\quad + \frac{A_V \cos \alpha \sin 2\beta}{A_I^2} I'_S - \frac{A_V \sin \alpha \sin 2\beta}{A_I^2} I'_C \\
 &= \frac{\cos \beta}{A_I} U'_C - \frac{\sin \beta}{A_I} U'_S - \frac{A_V \cos(\alpha - 2\beta)}{A_I^2} I'_C - \frac{A_V \sin(\alpha - 2\beta)}{A_I^2} I'_S
 \end{aligned} \tag{8.2.3l}$$

Substituting the Eqns (8.2.3h), (8.2.3i), (8.2.3j) and (8.2.3k) into (8.2.3l) and letting $K \rightarrow \infty$ (same principle as in section 8.1) yields

$$\left. \frac{d}{df} R \right|_{f=f_0} = \frac{A_V}{A_I} \times \frac{1}{2f_0} (\cos(\alpha + \beta) - \cos(\alpha - 3\beta)) \tag{8.2.3m}$$

In practice, $\beta \in [0 \quad 360^\circ]$, α leads β at a fixed angle θ , which stands for the transmission line/cable characteristics. In normal case, the value of θ is within the range between 45° (for cables) and 85° (for transmission lines).

Let $\alpha = \beta + \theta$, then

$$\begin{aligned}
 &\cos(\alpha + \beta) - \cos(\alpha - 3\beta) \\
 &= \cos(\beta + \theta + \beta) - \cos(\beta + \theta - 3\beta) \\
 &= -2 \sin \theta \sin 2\beta
 \end{aligned}$$

$$\text{So } \max \left(\left. \frac{d}{df} R \right|_{f=f_0} \right) = \frac{A_V}{A_I} \times \frac{1}{2f_0} \times 2 \sin \theta \quad (8.2.3n)$$

In case of $f_0 = 50$ Hz, the value of this expression is less than 2% of $\frac{A_V}{A_I}$.

Similarly for X

$$\begin{aligned} \left. \frac{d}{df} X \right|_{f=f_0} &= \left(\frac{U'_S I_C + U_S I'_C - U'_C I_S - U_C I'_S}{A_I^2} \right. \\ &\quad \left. - \frac{(U_S I_C - U_C I_S)(2I_C I'_C + 2I_S I'_S)}{(A_I^2)^2} \right) \Big|_{f=f_0} \\ &= \frac{\cos \beta}{A_I} U'_S - \frac{A_V \sin \alpha}{A_I^2} I'_C + \frac{\sin \beta}{A_I} U'_C - \frac{A_V \cos \alpha}{A_I^2} I'_S \\ &\quad + \frac{2A_V \sin \alpha \cos^2 \beta}{A_I^2} I'_C - \frac{2A_V \sin \alpha \cos \beta \sin \beta}{A_I^2} I'_S \\ &\quad - \frac{2A_V \cos \alpha \cos \beta \sin \beta}{A_I^2} I'_C + \frac{2A_V \cos \alpha \sin^2 \beta}{A_I^2} I'_S \\ &= \frac{\cos \beta}{A_I} U'_S + \frac{A_V \sin \alpha \cos 2\beta}{A_I^2} I'_C + \frac{\sin \beta}{A_I} U'_C - \frac{A_V \cos \alpha \cos 2\beta}{A_I^2} I'_S \\ &\quad - \frac{A_V \sin \alpha \sin 2\beta}{A_I^2} I'_S - \frac{A_V \cos \alpha \sin 2\beta}{A_I^2} I'_C \\ &= \frac{\cos \beta}{A_I} U'_S + \frac{\sin \beta}{A_I} U'_C + \frac{A_V \sin(\alpha - 2\beta)}{A_I^2} I'_C - \frac{A_V \cos(\alpha - 2\beta)}{A_I^2} I'_S \end{aligned} \quad (8.2.3o)$$

Substituting the Eqns (8.2.3h), (8.2.3i), (8.2.3j) and (8.2.3k) into (8.2.3o) and letting $K \rightarrow \infty$ yields

$$\begin{aligned} \left. \frac{d}{df} X \right|_{f=f_0} &= \frac{A_V}{A_I} \times \frac{1}{2f_0} (\sin(\alpha + \beta) + \sin(\alpha - 3\beta)) \\ &= \frac{A_V}{A_I} \times \frac{1}{f_0} \sin \theta \cos 2\beta \end{aligned} \quad (8.2.3p)$$

$$\max \left(\left. \frac{d}{df} X \right|_{f=f_0} \right) = \frac{A_V}{A_I} \times \frac{1}{f_0} \times \sin \theta \quad (8.2.3q)$$

Similar as in the case of R, the value of this expression is less than 2% of $\frac{A_V}{A_I}$.

Comparing Eqns. (8.2.3n) and (8.2.3p) tells that the max error due to frequency deviation cannot happen simultaneously on both R and X. The maximum errors of R and X appear in turn with the time passes by.

In both cases for overcurrent relays and impedance relays, the variation of signal initial angle β reflects the process of sampling window moving. The fluctuation of the deviation value in the diagrams tells the fact that the measured parameters are not fixed in time domain, in case of fundamental frequency deviation. Since such impact on the measured parameters is so small (1% to 2%), it can be concluded that frequency deviation impact can be negligible for overcurrent relays and impedance relays that are based on DFT algorithms.

8.3 Response of DEA for impedance relays in case of frequency deviation

Unlike DFT algorithms that are based on the characteristics of the measured signals, DEA algorithms are based on the characteristics of the simplified system model. As long as the approximation of the system model holds, the output of the DEA algorithms will not be affected.

In the case of frequency deviation, the system model is unchanged. Therefore the output of DEA algorithms will still yield correct measurement as in normal case.

Chapter 9 Conclusions and Future Work

9.1 Main contributions in this work

The main contributions in this work consist of two parts: quantification of component switching in the viewpoint of protective relays; analysis of frequency deviation impact on protective relays.

— Quantification of component switching in the viewpoint of protective relays

A new approach is proposed to quantify the severity of component switching transients. Unlike the traditional way based on the transient signal waveform, the new approach starts with the signals after relay filtering and evaluates the filtered signals according to different relay algorithms. Impact severity curves are developed for overcurrent and impedance relays to quantify the potential risk of mal-trip due to a component switching transient. The method of quantification is not limited to component switching transients, but can be applied to any event for which sufficient waveform data is available.

The impact severity curves can be used to compare two different switching transients. They can also be used in coordinating the trade-off between relay setting threshold and relay response speed.

— Analysis of frequency deviation impact on protective relays

Detailed analysis is made of the impact of frequency deviation on protective relays that are based on RMS, DFT and DEA. The maximum errors that might arise due to frequency deviation around the nominal frequency can be estimated.

Also the frequency response characteristics of RMS relays are extensively studied. The results will interest meter manufacturers as well as laboratory engineers that use modern data acquisition equipment, PICs, controllers and PCs.

9.2 Summary of conclusions in this work

—Quantification of impact on different relays due to component switching

A novel way of structuring power system transient data is proposed in this thesis for assessing the impact of switching transients on protective relays and algorithms. The methodology for application is similar to the use of the voltage-tolerance curve for end-user equipment, which is sensitive to voltage dips (the CBEMA curve and its derivatives). The switching transient is compared with the setting curve of the relay. The approach is further developed for overcurrent-time relays and impedance relays with a mho-characteristic.

Non-fault switching of some power system components can cause large transient currents, which might affect the operation of overcurrent relays, including time-delayed overcurrent relays and thermal relays.

Knowing the overcurrent relay type, it is possible to determine an impact severity curve for each transient current. Such a curve demonstrates the

border for the coordination between the two overcurrent relay setting parameters (time and current). Comparison among different impact severity curves tells the relative impact severities in different cases on a particular type of overcurrent relay.

Collection of impact severity curves for transient currents paves the way to database setup for non-fault switching impact on overcurrent relays.

Switching transients associated with energizing of unloaded long-distance transmission lines can lead to inaccuracy in the apparent impedance seen by digital impedance relays. The presence of the traveling wave component in voltage and current signals can cause the calculated impedance point to enter the relay characteristic, thus forming a potential risk of mal-trip for some fast detection algorithms. The longer the line, the more apparent impedance points are close to or inside the relay characteristic, thus the higher the probability that mal-trip occurs.

The apparent impedance at the beginning and at the end of the line switching transient is determined by the line parameters only, while the impedance calculated during the transient is dependent on the relay algorithm, the point-on-wave at the switching instant and the relay sampling frequency.

For impedance relays, the switching severity is dependent on the apparent impedance measured by the relay. The relay trip counter value is the other parameter that helps describe the characteristics of switching transients, from the viewpoint of impedance relays. An impact-severity/trip-counter diagram is formed, in which a ‘mal-trip zone’ can be set.

Starting from the principles of fault evaluation techniques, the maximum reach of the trip counter is useful in quantifying the potential risk of mal-trip by an impedance relay.

—Output errors on different relays due to frequency deviation

The accuracy of presenting the effective magnitude using the RMS method is dependent on sampling rate, point-on-wave and sampling window size.

The sampling rate determines the location of the harmonic frequencies at which RMS might yield incorrect output. The higher the sampling rate, the wider the frequency band between two multiples of the Nyquist sampling rate will be. For sampling rate f_s , the incorrect RMS output occurs at frequencies of $f = qf_s / 2$, $q \in \mathbb{N}$. Thus the minimum sampling rate for fundamental frequency is calculated to be 3 samples per cycle. For the harmonics that are not of triple order, 3 sampling points also yields the desired RMS output.

Point-on-wave determines the fluctuation of RMS output along the time axis. It has no impact on the accuracy of RMS at the frequencies whose periods are an integer multiple of twice the sampling window size, except at the multiples of the Nyquist sampling rate. However it will affect the frequency responses at all other frequencies as well as the multiples of the Nyquist sampling rate. The consequence of such impact is the fluctuation of RMS output, whose period is half the studied frequency cycle and independent on sampling rate or sampling window size.

Sampling window size determines at which frequencies the desired RMS unity output will be obtained, or in another word, the RMS output error is zero. A longer sampling window size can ensure that there are more

frequencies that can yield the correct effective magnitude of the signal by RMS calculation.

The RMS output fluctuates around the exact value as the sampling window moves through the signal. Of interest for error analysis is the amplitude of the oscillation. In the case of a single frequency signal, the error in RMS output is approximately inverse proportional to the signal frequency.

If the studied signal is a mixture of fundamental component and odd harmonics, a proper sampling rate should be chosen so that no harmonic component is at the multiples of the Nyquist sampling rate.

A 0.5 cycle sampling window is the shortest possible window to yield accurate total RMS output if the mixed frequency signal contains no even harmonics. If the mixed frequency signal contains both odd (including the fundamental) and even harmonics, a 0.5 cycle sampling window can cause fluctuation in total RMS output. The higher the even harmonic order, the smaller the fluctuation magnitude is. The higher the sampling frequency, the smaller the fluctuation magnitude is. In this case, a 1 cycle sampling window is needed to yield accurate total RMS output.

When the actual frequency of the input signal deviates from the nominal frequency, the RMS output is not identical to the actual magnitude of the input signal. In power systems the frequency deviation is relatively small. Therefore such output error can be studied by calculating the derivative of the RMS to signal frequency. For a nominal frequency of 50 Hz, 1% frequency variation near 50 Hz can yield a maximum error in RMS output of 0.5%, if the input signal is of single frequency. For the signals that are mixed with

fundamental and harmonic frequencies, the maximum error in total RMS output can be higher.

The relative output error due to frequency deviation is less than 1% of the relative frequency error for DFT overcurrent relays, and less than 2% in the case of DFT impedance relays. There will be no output error due to frequency deviation in the case of DEA impedance relays.

9.3 Directions for future research

The methodology developed in this thesis cannot replace the testing of individual relays for individual events. But it is an instrument in the development and setting of protective relays and algorithms.

In this thesis the testing is on relays installed on the line where a switching occurs. To assess the impact of component switching on the relays at other locations in a system, it is necessary to study the propagation of the component switching events in the system before applying the techniques developed in this study. In some cases, the component switching disturbances might attenuate with the increase of electrical distance from the disturbance source. However the disturbances can be magnified at some locations where certain resonance conditions are met. It will therefore be beneficial to develop a new approach to detect the location of the most severe resonance in terms of the severity indicators developed in this thesis. Locating such disturbance-magnifying network configuration leads to assessment of the maximum propagated impact severity throughout the studied system.

The research described in this thesis is focused on some of the existing relay algorithms. In such cases, the disturbance signals after relay processing are

predictable, which makes it possible to quantify the impact severity by checking against pre-set relay characteristics. In practical engineering however, the algorithms of a relay are not open to the public. When in the future a new ultra-high-speed protection algorithm is proposed and implemented, what a researcher might get is merely a blackbox with input/output interfaces, with the output being either of the two status: trip or non-trip. To test the immunity of a relay (actually the relay algorithms), it is necessary to study the impact severity in another way. The new set of testing procedures should involve playing with not only various input disturbance signals, but also various relay characteristics. The same problem holds to some extent during the development of completely new algorithm when its performance has to be evaluated for non-fault disturbances.

Also the setting-up and filling of the disturbance database remains to be studied. Quantification of the impact severity of a particular disturbance is the first step to database set-up. However, more work needs to be done to coordinate the collection of disturbance data from different sources, either simulation, local recorders or protective relays. Criteria need to be set to reject the non severe disturbances so as to avoid oversize of the database.

References

- [1] **H. H. Kajihara**, *Quality power for electronics*, Electro-Technology, Vol. 82, No. 5, November 1968, p. 46
- [2] **D. L. Plette**, “The effects of improved power quality on utilization equipment”, *Proceedings of the IEEE National Aerospace Electronics Conference*, May 1969, Dayton, OH, pp. 243 – 250
- [3] **P. M. Knoller** and **L. Lonnstam**, “Voltage quality and voltage tendency recorders”, *Siemens Review*, Vol. 36, No. 8, August 1969, pp. 302 – 303
- [4] **M. H. J. Bollen**, *Understanding power quality problems: voltage sags and interruptions*, New York: IEEE Press, 1999
- [5] **F. Wang**, “*On power quality and protection*”, Licentiate Thesis, Chalmers University of Technology, 2001
- [6] **D. S. Baker** et al., “Application Considerations of Static Overcurrent Relays: A Working Group Report”, *IEEE Trans. on Industry Applications*, Vol. 33, No. 6, pp. 1493-1500, Nov./Dec. 1997
- [7] **M.A. Chapman** et al., “Switching and Fault Caused Transients in Electric Power Systems”, IEEE Power Engineering Society 1999 Winter Meeting, Vol. 2, pp. 1015 –1021, 1999
- [8] **V. E. Wagner** et al., ”Effects of harmonics on equipment — Report of the IEEE Task Force on the Effects of Harmonics on Equipment”, *IEEE Transactions on Power Delivery*, Vol. 8, No. 2, April 1993, pp. 672-680
- [9] **C.F. Henville**, “Power quality impacts on protective relays - and vice versa”, *2001 IEEE Power Engineering Society Summer Meeting*, Vol. 1, 2001, pp. 587 -592

- [10] **J. P. Brozek**, “The effects of harmonics on overcurrent protection devices”, *Conference Record of the 1990 IEEE Industry Applications Society Annual Meeting*, Seattle, U. S. A., October 1990, Vol. 2, pp. 1965-1967
- [11] **W. F. Horton** and **S. Goldberg**, “The effect of harmonics on the operating points of electromechanical relays”, *IEEE Transactions on Power Apparatus and Systems*, Vol. PAS-104, No. 5, May 1985, pp. 1178-1186
- [12] **B. Bozoki** et al., “The effects of GIC on protective relaying”, *IEEE Transactions on Power Delivery*, Vol. 11 Issue 2, Apr 1996, pp. 725 –739
- [13] **J.F. Fuller**, **E.F. Fuchs** and **D.J. Roesler**, “Influence of harmonics on power distribution system protection”, *IEEE Transactions on Power Delivery*, Vol. 3 Issue: 2 , April 1988, pp. 549 –557
- [14] **A.A. Girgis**, **J.W. Nims**, **J. Jacamino**, **J.G. Dalton** and **A. Bishop**, “Effect of voltage harmonics on the operation of solid state relays in industrial applications”, *Conference Record of the 1990 IEEE Industry Applications Society Annual Meeting*, 7-12 Oct 1990, Vol.2, pp. 1821 -1828
- [15] **S. E. Zocholl** and **G. Benmouyal**, “How microprocessor relays respond to harmonics, saturation, and other wave distortions”, *24th Annual Western Protective Relay Conference*, Spokane, U. S. A., October 1997
- [16] **R.A. Rob** and **W.T. Jewell**, “Computer based harmonic simulation and testing for microprocessor-based phase impedance relay with phase locator”, *Conference Record of 1993 Industrial and Commercial Power Systems Technical Conference*, 2-6 May 1993, pp. 70 –77

- [17] **W.A. Elmore, S.E. Zocholl and C.A. Kramer**, “Effect of waveform distortion on protective relays”, *IEEE Transactions on Industry Applications*, Vol. 29, Issue: 2 , March/April 1993, pp. 404 – 411
- [18] **M. Zielichowski and M. Fulczyk**, “Influence of load on operating conditions of third harmonic ground-fault protection system of unit connected generators”, *IEE proceedings – Generation, transmission and distribution*, Vol. 146, No. 3, May 1999, pp. 241-248
- [19] **N.T. Stringer, L. Lawhead, T. Wilkerson, J. Biggs and G.D. Rockefeller**, “Testing and performance of transformer differential relays”, *IEEE Industry Applications Magazine*, Vol. 3 Issue: 4, Jul/Aug 1997, pp. 36 –42
- [20] **A.W. Sharaf, L.A. Snider and K. Debnath**, “A third harmonic sequence ANN based detection scheme for high impedance faults”, *1993 Canadian Conference on Electrical and Computer Engineering*, 14-17 Sep 1993, vol.2, pp. 802 -806
- [21] **T. Segui et al.**, ”Fundamental basis for impedance relaying with parametrical estimation”, *IEEE Transactions on Power Delivery*, Vol. 15, No. 2, April 2000, pp. 659-664
- [22] **B. Kasztenny and E. Rosolowski**, “Two new measurement algorithms for Generator and transformer relaying”, *IEEE Transactions on Power Delivery*, Vol. 13, No. 4, October 1998, pp. 1053-1059
- [23] **Liancheng Wang**, “Frequency responses of phasor-based microprocessor relaying algorithms”, *IEEE Transactions on Power Delivery*, Vol. 14, No. 1, January 1998, pp. 98-105
- [24] **P. J. Moore, R. D. Carranza and A. T. Johns**, “Model system tests on a new numeric method of power system frequency

- measurement”, *IEEE Transactions on Power Delivery*, Vol. 11, No. 2, April 1996, pp. 696-701
- [25] **I. Kamwa** and **R. Grondin**, “Fast adaptive schemes for tracking voltage phasor and local frequency in power transmission and distribution systems”, *Proceedings of the 1991 IEEE Power Engineering Society Transmission and Distribution Conference*, September 1991, pp. 930-936
- [26] **T. Sezi**, “A new method for measuring power system frequency”, *Proceedings of the 1999 IEEE Transmission and Distribution Conference*, April 1999, pp. 400-405
- [27] **A. Koksal Hocaoglu** and **M.J. Devaney**, “A new quadratic form based frequency measurement algorithm”, *Conference Proceedings of 1996 IEEE Instrumentation and Measurement Technology Conference (IMTC-96)*, Vol. 2 , 4-6 Jun 1996, pp. 1065 – 1070
- [28] **L. A. Shankland**, **J. W. Feltes** and **J. J. Burke**, “The effect of switching surges on 34.5 kV system design and equipment”, *IEEE Transactions on Power Delivery*, Vol. 5 No. 2, April 1990, pp. 1106-1112
- [29] **R. A. Walling**, **R. D. Melchior** and **B. A. McDermott**, “Measurement of cable switching transients in underground distribution systems”, *IEEE Transactions on Power Delivery*, Vol. 10 No. 1, January 1995, pp. 534-539
- [30] **J. F. Witte**, **F. P. DeCesaro** and **S. R. Mendis**, “Damaging long-term overvoltages on industrial capacitor banks due to transformer energization inrush currents”, *IEEE Transactions on Industry Applications*, Vol. 30 No. 4, July-August 1994, pp. 1107-1115
- [31] **C. E. McCoy** and **B. L. Floryancic**, “Characteristics and measurement of capacitor switching at medium voltage distribution

- level”, *IEEE Transactions on Industry Applications*, Vol. 30 No. 6, November 1994, pp. 1480-1489
- [32] **M.R. Yenchek, J.C. Cawley, A.L. Brautigain and J.S. Peterson**, “Distinguishing motor starts from short circuits through phase-angle measurements”, *IEEE Transactions on Industry Applications*, Vol. 38 Issue: 1, Jan/Feb 2002, pp. 195 –202
- [33] **C.M. Wiggins, F.S. Nickel, J. Haney and S.E. Wright**, “Measurement of switching transients in 115 kV substation” *IEEE Transactions on Power Delivery*, Vol. 4, Issue: 1, Jan 1989, pp. 756 - 769
- [34] **P.C. Fernandez**, et al., “Mitigation of power system switching transients to improve power quality”, *Proceedings of 8th International Conference on Harmonics And Quality of Power*, 1998, Vol. 2, Oct. 1998, pp. 988 –993
- [35] **T.E. Grebe**, “Application of distribution system capacitor banks and their impact on power quality”, *Proceedings of 39th Annual Conference on Rural Electric Power*, April/May 1995, pp. C3/1 -C3/6
- [36] **R. Borlotti, C. Gemme and R. Tinggren**, “Integrated power quality in distribution equipment”, *CIREC. 16th International Conference and Exhibition on Electricity Distribution, 2001*. Part 1: Contributions. (IEE Conf. Publ No. 482), Vol. 2, June 2001, pp. 6
- [37] **R. Rüdénberg**, *Transient Performance of Electric Power Systems*, The M.I.T. Press, 1969
- [38] **A. Greenwood**, *Electrical Transients in Power Systems*, John Wiley & Sons Inc. 1991
- [39] **L. van der Sluis**, *Transients in Power Systems*, John Wiley & Sons Ltd, 2001

- [40] **L. G. Perez, A. J. Flechsig and V. Venkatasubramanian**, “Modeling the protective system for power system dynamic analysis”, *IEEE Transactions on Power Systems*, Vol. 9 No. 4 November 1994, pp. 1963-1973
- [41] **D.V. Coury, P.G. Campos and M.C. Tavares**, “Modeling a power transformer for investigation of digital protection schemes”, *Proceedings of 8th International Conference on Harmonics And Quality of Power*, Vol. 2, 14-18 Oct 1998, pp. 1041 -1046
- [42] **A. Kulidjian, B. Kasztenny and B. Campbell**, “New magnetizing inrush restraining algorithm for power transformer protection”, *Proceedings of Seventh International Conference on (IEE) Developments in Power System Protection*, April 2001, pp. 181-184
- [43] **B. Kasztenny, E. Rosolowski, M.M. Saha and B. Hillstrom**, “A self-organizing fuzzy logic based protective relay-an application to power transformer protection”, *IEEE Transactions on Power Delivery*, Vol. 12 Issue: 3, July 1997, pp. 1119 –1127
- [44] **J. H. Brunke and K. J. Frohlich**, “Elimination of transformer inrush currents by controlled switching”, *IEEE Transactions on Power Delivery*, Vol. 16, Issue: 2, Apr 2001 pp. 276 –285
- [45] **L. Cipcigan, W. Xu and V. Dinavahi**, “A new technique to mitigate inrush current caused by transformer energization”, *Proceedings of 2002 IEEE Power Engineering Society Summer Meeting*, Vol. 1, 2002 pp. 570 -574
- [46] **IEEE PES Power System Engineering Committee, Power System Restoration Working Group**, “Overvoltage control during restoration”, *IEEE Transactions on Power Systems*, Vol. 7, Issue: 4, Nov 1992, pp. 1464-1470
- [47] **S. H. Horowitz and A. G. Phadke**, *Power System Relaying*, England: RSP Ltd, 1995

- [48] **James Ward Brown** and **Ruel Vance Churchill**, *Fourier series and boundary values problems*, New York: McGraw-Hill, 1993
- [49] **A. G. Phadke** and **J. S. Thorp**, *Computer relaying for power systems*, England: RSP Ltd, 1998
- [50] **S. M. Bozic**, *Digital and Kalman filtering*, Edward Arnold, Great Britain, 1994
- [51] **C. K. Chui** and **G. Chen**, *Kalman Filtering*, Springer 1999
- [52] **Y.V.V.S. Murty** and **W.J. Smolinski**, “A Kalman filter based digital percentage differential and ground fault relay for a 3-phase power transformer”, *IEEE Transactions on Power Delivery*, Vol. 5 Issue: 3, July 1990, pp. 1299 –1308
- [53] **A. A. Girgis** and **E. B. Makram**, “Application of adaptive Kalman filtering in fault classification, distance protection, and fault location using microprocessors”, *IEEE Transactions on Power Systems*, Vol. 3, Issue: 1, Feb. 1988, pp. 301 –309
- [54] **T. Segui**, **P. Bertrand**, **M. Guillot**, **P. Hanchin** and **P. Bastard**, “Fundamental basis for distance relaying with parametrical estimation”, *IEEE Transactions on Power Delivery*, Vol. 15, No. 2, April 2000, pp. 659 – 664
- [55] **E.O. III. Schweitzer** and **D. Hou**, “Filtering for protective relays”, Proceedings of IEEE Conference ‘Communications, Computers and Power in the Modern Environment’ (WESCANEX 93), 17-18 May 1993, pp. 15 –23
- [56] **M. Kezunovic**, **S. Kreso**, **J.T. Cain** and **B. Perunicic**, “Digital protective relaying algorithm sensitivity study and evaluation”, *IEEE Transactions on Power Delivery*, Vol. 3 Issue: 3, July 1988, pp. 912 - 922

- [57] **E.H. Shehab-Eldin** and **P.G. McLaren**, “Travelling wave distance protection-problem areas and solutions”, *IEEE Transactions on Power Delivery*, Vol. 3 Issue: 3, July 1988, pp. 894 –902
- [58] **V. Pathirana**, **P.G. McLaren** and **E. Dirks**, “Investigation of a hybrid travelling wave/impedance relay principle”, IEEE Canadian Conference on Electrical and Computer Engineering, 2002 (CCECE 2002), Vol. 1, May 2002, pp. 48 -53
- [59] **W. J. Smolinski**, “An algorithm for digital impedance calculation using a single pi section”, IEEE Transactions on PAS, Vol. 99, No. 6, November/December 1980, pp. 2251-2252
- [60] **M. Vitins**, “A correlation method for transmission line protection”, *IEEE Transactions on Power Apparatus and Systems*, Vol, PAS-97, 1998, page(s): 1607-1617
- [61] **P. A. Crossley** and **P. G. McLaren**, “Distance protection based on traveling waves”, *IEEE Transactions on Power Apparatus and Systems*, Vol. PAS-102, 1983, page(s): 2971-2983
- [62] **J. Kohlas**, “Estimation of fault locations on power lines”, *Proceeding of the 3rd IFAC Symposium*, 1973, page(s): 393-402
- [63] **C. Christopoulos**, **D. W. P. Thomas** and **A. Wright**, “Scheme based on travelling-waves for the protection of major transmission lines”, *IEE Proceedings-Pt. C.*, Vol. 135, 1988, page(s): 63-73
- [64] **M. H. J. Bollen**, “Travelling-wave-based protection of double-circuit lines”, *IEE Proceedings C-Generation, Transmission and Distribution*, Vol. 140, Issue: 1, Jan. 1993, pp. 37 -47
- [65] **Rongxiang Yuan**, **Deshu Chen**, **Zhe Zhang**, **Xianggen Yin** and **Tianhao Ma**, “A new algorithm of the ultra-high-speed directional relay”, 2000 IEEE Power Engineering Society Winter Meeting, Vol. 3, 23-27, Jan. 2000, pp. 1961 -1966 vol.3

- [66] **M. H. J. Bollen**, “On travelling-wave-based protection of high-voltage networks”, Ph. D. Thesis, Eindhoven University of Technology, 1989
- [67] **A. W. A. Van Dongen**, “Een distantiebeveiligings-algorithme voor hoogspanningslijnen”, Master Thesis, Eindhoven University of Technology, 1988
- [68] **M. P. Ransick**, “Numeric protective relay basics”, *Proceedings of the 33rd IAS Annual Meeting (The IEEE 1998 Industry Applications Conference)*, 1998. Vol. 3, 12-15 Oct 1998, pp(s): 2342 -2347
- [69] **P.K. Dutta** and **P.B. Dutta Gupta**, “Microprocessor-based UHS relaying for distance protection using advanced generation signal processing”, *IEEE Transactions on Power Delivery*, Vol. 7, Issue: 3, July 1992, pp. 1121 –1128
- [70] **D. S. Baker** et al., “Application Considerations of Static Overcurrent Relays: A Working Group Report”, *IEEE Trans. on Industry Applications*, Vol. 33, No. 6, pp. 1493-1500, Nov./Dec. 1997
- [71] **J. F. Witte**, **F. P. DeCesaro**, and **S. R. Mendis**, “Damaging Long-term Overvoltages on Industrial Capacitor Banks due to Transformer Energization Inrush Currents”, *IEEE Trans. on Industry Applications*, Vol. 30 4, pp. 1107-1115, Jul./Aug. 1994
- [72] **D. A. Woodford** and **L. M. Wedepohl**, “Transmission Line Energization with Breaker Pre-Strike”, *Proceedings of the IEEE Conference on Communications, Power and Computing (WESCANEX' 97)*, Winnipeg, MB, May 1997, pp. 105-108
- [73] **R. P. P. Smeets** and **A. G. A. Lathouwers**, “Capacitive Current Switching Duties of High-Voltage Circuit Breakers: Background and Practice of New IEC Requirements”, *Proceedings of the IEEE Power Engineering Society Winter Meeting*, Singapore, Jan. 2000, Vol. 3, pp. 2123-2128

- [74] **F. Wang** and **M. H. J. Bollen**, “Disturbance Database Setup for Protective Relay Testing”, *Proceedings of 9th International Conference on Harmonics and Quality of Power (ICHQP)*, Orlando, Oct. 2000, Vol. 3, pp. 1059-1064
- [75] **M. H. J. Bollen**, “Voltage sags in three-phase systems”, *IEEE Power Engineering Review*, Sep. 2001, pp. 8-15
- [76] **E. Styvaktakis**, “On feature extraction of voltage disturbance signals”, Licentiate Thesis, Chalmers University of Technology, 2000
- [77] *IEC Standard Electrical Relays*, IEC 255-03, 1989
- [78] *IEEE Standard Inverse-Time Characteristic Equations for Overcurrent Relays*, IEEE Std C37.112-1996
- [79] *IEC Standard Thermal Electrical Relays*, IEC 255-8
- [80] *Protective Relays Application Guide*, GEC Alstom T & D, 1987
- [81] **A. Wright** and **C. Christopoulos**, *Electrical Power System Protection*, Chapman & Hall, 1993
- [82] *Advancements in Microprocessor Based Protection and Communication*, IEEE tutorial course, 1997
- [83] **R. Natarajan**, **V. K. Misra**, **M. Oommen**, "Time domain analysis of induction motor starting transients", *Proceedings of the Twenty-First Annual North-American Power Symposium*, 1989, pp. 120-128
- [84] **E. Styvaktakis**, *Automating Power Quality Analysis*, Ph. D. thesis, Chalmers University of Technology, Sweden, 2002
- [85] **J. Lewis Blackburn**, *Protective Relaying — Principles and Applications*, Marcel Dekker, Inc., 1998
- [86] **Y. G. Paithankar**, *Transmission Network Protection — Theory and Practice*, Marcel Dekker, Inc., 1998

- [87] GEC ALSTHOM T & D, *Protective Relays Application Guide*, 1987
- [88] **M.A. Date, B. Oza and N. C. Nair**, *Power System Protection*, Bharti Prakashan, 1999
- [89] **M. Akke and J. S. Thorp**, “Some improvements in the three-phase differential equation algorithm for fast transmission line protection”, *IEEE Transactions on Power Delivery*, Vol. 143, Jul. 1999, pp. 851-856
- [90] **C. Fernández and F. L. Pagola**, “Total least squares and discrete-time line models in HV distance protection”, *IEEE Transactions on Power Delivery*, Vol. 14, No. 1, Jan. 1999, pp. 504 - 515
- [91] **A. O. Schweitzer and Daqing Hou**, “Filtering the protective relays”, *19th Annual Western Protective Relay Conference*, Spokane, Washington, Oct. 1992
- [92] **M. M. Saha et al.**, “First zone algorithm for protection of series compensated lines”, *IEEE Transactions on Power Delivery*, Vol. 16, No.2, Apr. 2001, pp. 200 – 207
- [93] **D. A. Keeling and S. D. A. Pickering**, “High speed numeric techniques for transmission line protection”, *Proceedings of the Sixth International Conference on Developments in Power System Protection (DPSP)*, 1997, pp. 14 - 17
- [94] **P. J. Moore et al.**, *Power system protection*, United Kingdom: Electricity association Services Limited, 1995
- [95] ABB Power T & D Company Inc., *Descriptive bulletin for REL 300 (MDAR) numeric transmission line protection*, 1996
- [96] GE Power Management, *MLP microprocessor based distance protection*, GEK-98846A

- [97] SIEMENS AG, *SIPROTEC4-7SA6 distance protection relay for all voltage levels*, Protection system catalog SIP 4.3.2001
- [98] ALSTOM T & D Protection & Control Ltd, *Type LFZR high-speed numerical distance relays*, Publication R4117G, 1998
- [99] **L. Pottonen, P. Martinole and O. Huet**, “Selecting protective relays with digital test methods”, *IEEE Computer Applications in Power*, October 2001, pp. 47 –52
- [100] **P. J. Moore and A. T. Johns**, “New method of power swing blocking for digital distance protection”, *IEE Proceedings – Generation, Transmission and Distribution*, Vol. 143, No. 1, January 1996, pp. 19-26
- [101] **L. D. Zhang, M.H.J. Bollen**, "Characteristics of voltage dips (sags) in power systems", *IEEE Transactions on Power Delivery*, Vol.15, no.2, April 2000, pp.827-832.
- [102] **Lin Yin, Ruikang Yang, M. Gabbouj and Y. Neuvo**, “Weighted median filters: a tutorial”, *IEEE Transactions on Circuits and Systems II: Analog and Digital Signal Processing*, Vol. 43 Issue: 3 , Mar 1996, pp: 157 –192
- [103] **W. K. Yong and M. J. Devaney**, “Power measurement using the wavelet transform”, *IEEE Transactions on Instrumentation and Measurement*, Vol. 47, No. 5, 1998, pp. 1205-1210
- [104] **E. Y. Hamid and Z. I. Kawasaki**, “Wavelet packet transform for RMS values and power measurements”, *IEEE Power Engineering Review*, Sep. 2001, pp. 49-51
- [105] **E. Kamen**, *Introduction to Signals and Systems*, Macmillan Publishing Company, 1987
- [106] **Z. Q. Wang, S. Z. Zhou and Y. J. Guo**, “Comparisons on ways of magnitude characterization of power quality disturbances”,

- Proceedings of the 2002 Large Engineering Systems Conference on Power Engineering*, pp. 178-183, 2002
- [107] **E. Styvaktakis, M. H. J. Bollen and I. Y. H. Gu**, “Transformer saturation after a voltage dip”, *IEEE Power Engineering Review*, Vol. 20, No. 4, April 2000, pp. 60-62.
- [108] **E. Styvaktakis and M. H. J. Bollen**, ”Signatures of voltage dips: transformer saturation and multistage dips”, *IEEE Transactions on Power Delivery*, Vol. 18 No.1, 2003, pp. 265-270
- [109] **J. Pedra, L. Sainz, R. Lopez and S. Bogarra**, “Transformer saturation model for the harmonic analysis on power systems”, *Proceedings of the 8th International Conference on Harmonics and Quality of Power*, Vol. 2, Oct 1998, pp. 1053-1058
- [110] *IEC Standard Electromagnetic compatibility (EMC) - Part 4-30: Testing and measurement techniques - Power quality measurement methods*, IEC-61000-4-30
- [111] *IEEE Standard Recommended Practice for the Establishment of Voltage Sag Indices*, IEEE Std. P1564